ASSESSMENT OF TWO CONE PENETRATION TEST BASED METHODS FOR EVALUATING THE LIQUEFACTION POTENTIAL OF TAILINGS DAMS

Luis Alberto Torres Cruz

Interim research report.
University of the Witwatersrand.
Faculty of Engineering and the Built Environment.

Johannesburg, 2011

I, Luis Alberto Torres Cruz, declare that this dissertation is my own unaided work. It is being submitted to the Degree of Master of Science to the University of the Witwatersrand, Johannesburg. It has not been submitted before for any degree or examination to any other University.

....

...... day of .... year....................

Abstract

The stability of tailings dams is of great importance to the mining industry. It is well known that soil liquefaction is one of the mechanisms that can compromise the stability of such structures. Given the difficulty of extracting undisturbed samples of any cohesionless material, the use of *in situ* tests to assess liquefaction potential has been intensely researched. The purpose of this work was to assess the applicability to tailings dams of two CPT-based liquefaction assessment methodologies, namely, the Robertson-based and the Olson and Stark methodologies. Ten case histories were evaluated. When considering triggering of liquefaction, the Robertson-based and Olson and Stark methodologies correctly predicted the behaviour of four out of five and seven out of ten case histories, respectively. When considering the onset of flow failure, the Olson and Stark methodology correctly predicted the behaviour in four of seven case histories for which a post-triggering analysis was made. The results are useful in understanding the shortcomings of implementing these methodologies on TSFs and the limits of their predictive power.

Acknowledgements

I would like to express my gratitude to:

My family for their unwavering support.

My supervisor Prof. Geoffrey Blight and co-supervisor Dr. Irvin Luker for their patient guidance.

My colleagues Prof. Chris James and Mr. Valentine Katte for their availability to engage in productive discussions.

The School of Civil and Environmental Engineering of the University of the Witwatersrand for providing me with the time and resources to work on my research.

Fraser F. Alexander Tailings for granting me access to their report on GMTS and Mooifontein.

The Digital Library of the International Development Research Centre for digitising several of the references corresponding to the Dashihe Tailings Dam.

Jones & Wagener Consulting Civil Engineers for granting me access to their files on the Merriespruit Tailings Dam.

Prof. Eben Rust from the University of Pretoria for providing digitised versions of the CPT soundings made at the Merriespruit Tailings Dam.

Contents

List of figures

List of tables

List of frequently used symbols and abbreviations

γ_t	*Total unit weight*
Γ	Value of the critical void ratio when p' = 1 kPa
λ_{ln}	Slope of the critical state locus
v	Poisson's ratio
σ_1, σ_3	Major and minor principal stress, respectively
σ'_v	Vertical effective stress
σ'_{vo}	Effective overburden stress
σ_{vo}	Total overburden stress
τ_{av}	Average cyclic shear stress
$\tau_{ave,seismic}$	Average seismic load in the Olson and Stark methodology
$\tau_{driving}$	Static shear stress acting on a slope in the Olson and Stark methodology
τ_h	Horizontal shear stress
τ_{other}	Other shear stresses acting on a slope in the Olson and Stark methodology
τ_s	Static shear stress
φ'	Effective friction angle
ψ	State parameter

a_{max}	Peak horizontal acceleration
c	Cohesion
c'	Effective cohesion
CPT	Cone penetration test
CRR	Cyclic resistance ratio
$CRR_{7.5}$	Cyclic resistance ratio for an earthquake M_w = 7.5
CRR_{α}	Cyclic resistance ratio considering horizontal shear stresses
CSL	Critical state locus
CSR	Cyclic stress ratio
$CSR_{7.5}$	Cyclic stress ratio for an earthquake M_w = 7.5
CU	Compression undrained (triaxial test)
D_r	Relative density
e	Void ratio
E	Young's modulus
e_c	Critical void ratio
FC	Fines content
F_r	Friction ratio
f_s	Sleeve friction
FS	Factor of safety

FS_{Flow}	Factor of safety against flow failure
$FS_{Triggering}$	Factor of safety against triggering of liquefaction
g	Acceleration due to gravity
GDP	Gross domestic product
I_c	Soil behaviour type index
K_0	Coefficient of lateral stress at rest
K_α	Static shear stress correction factor
K_c	Clean sand correction factor
LSR	Liquefied strength ratio
M_L	Richter earthquake magnitude
MSF	Magnitude scaling factor
M_w	Moment earthquake magnitude
N/A	Not applicable
$(N_1)_{60}$	SPT count normalised to a 60% energy ratio and atmospheric pressure
N_{60}	SPT count normalised to a 60% energy ratio
N_{kt}	Empirical cone factor
p'	Mean effective stress
p_a	Atmospheric pressure
PI	Plasticity index
q_c	Cone penetration resistance
q_{c1}	Normalized cone tip resistance
q_t	Total cone penetration resistance
Q_{tn}	Normalised cone penetration parameter
$Q_{tn,CS}$	Clean sand equivalent of Q_{tn}
r_d	Depth reduction factor
SPT	Standard penetration test
S_u	Undrained shear strength
$S_u(LIQ)$	Liquefied shear strength
$S_u(yield)$	Undrained yield shear strength
u	Pore water pressure
V_s	Shear wave velocity
V_{s1}	Normalized shear wave velocity
WT	Water table
YSR	Yield strength ratio

1 Introduction

Several well documented disasters serve to confirm the destructive potential of improperly managed mining activities. Tailings dams are associated with only a fraction of these disasters, but the failure of these man-made earth structures is usually quite catastrophic and widely publicized in the media. Davies et al. (2000) reviewed the database of tailings dams' instabilities from 1970 to 1999 and estimated an annual probability of failure rate between 1 in 700 to 1 in 1,750. They further pointed out the negative comparison of this rate against the estimated 1 in 10,000 probability of failure of conventional dams. These figures leave little doubt about the role played by tailings dams' failures in fostering a negative image around the mining industry. As an example of how relevant this issue remains, one has to look no further back than October 4, 2010 for news of the latest catastrophic tailings dam failure to feature in international media. On that day, an aluminium tailings pond located in Ajka, Hungary suffered a breach that released approximately 700,000 m^3 of sludge. The incident killed ten people and caused considerable destruction in two nearby towns.

Although not the cause of failure of the Ajka aluminium tailings dam, soil liquefaction has in several instances been associated with catastrophic tailings dam failures. The topic has been the subject of intense research, especially after the 1964 earthquake of Niigata, Japan when the devastating consequences of soil liquefaction on structures in general, not only tailings dams, were recognized worldwide. The Niigata earthquake was a major precursor of the simplified procedure to evaluate liquefaction potential originally proposed by Seed and Idriss (1971). Essentially, the simplified procedure relies on the results of standard penetration tests (*SPT*) to estimate the maximum seismic load that a level ground soil deposit can withstand without the development of liquefaction. The concept of using an *in situ* test to estimate the liquefaction potential of cohesionless soils is very convenient, given the difficulty of extracting undisturbed samples. Therefore procedures to evaluate liquefaction potential were also developed around other suitable *in situ* tests, primarily cone penetration test (*CPT*) and shear wave velocity (V_s). Some of these methods were also extended to consider the possibility of liquefaction under static loads only and sloping ground (e.g. Olson, 2001). Due to the low time and cost involved in their implementation, these field-test-based methods can be of great utility when studying the stability of tailings dams. This is particularly true during the initial stages of design or when performing a screening to determine which are the critical sections of a tailings dam from the liquefaction point of view. As generally acknowledged by their authors, the inherent simplifications of these field-test-based methods do not make them suitable tools for final designs or ultimate decision making.

The purpose of this research is to investigate the performance of two *CPT*-based simplified procedures to evaluate liquefaction potential in tailings dams. One of the methodologies is a slightly modified version of the procedures outlined by Robertson (2009a). The modifications were incorporated with the purpose of making it applicable to the sloping ground conditions characteristic of tailings dams' outer walls. The methodology only addresses cases involving seismic loading. The other methodology is described in Olson and Stark (2002 and 2003) and is readily applicable to sloping ground conditions with seismic or static loading. Both methodologies were conceived by their authors to be applicable to soil deposits in general and both have been applied to several case histories previously (e.g. Robertson and Wride 1998a, Zhang et al. 2002, Olson 2006 and Neto 2009). What is novel about this study is that the applicability of the methodologies is being considered for the specific case of tailings dams and their unique set of features (e.g. mostly non-plastic material, high water table, typically unaged/uncemented soil and considerable outer slopes). As will be discussed in Chapter 2, an important distinction between the Robertson-based and the Olson and Stark methodologies is that the former is limited to the assessment of liquefaction (loss of shear strength), whereas the latter assesses the potential for flow failure (loss of shear strength conducive to large tailings displacements). Nonetheless, although the Robertson-based methodology does not provide a means of assessing whether a tailings dam is prone to flow failure, it has been considered in this study because predicting triggering of liquefaction alone is a matter of great interest when analysing the stability of tailings dams and a necessary step to assess the potential of flow failure.

The procedure outlined by Robertson (2009a) was chosen for study because it has been widely cited in the technical literature. Furthermore, the basis of the method was endorsed by the participants of the Workshop on Evaluation of Liquefaction Resistance of Soils, organized by the National Center for Earthquake Engineering Research in 1996 (Youd et al., 2001). The methodology proposed by Olson and Stark (2002 and 2003) was considered for study because, given that it considers sloping ground and static and seismic loading, it is readily applicable to tailings dams. *SPT*-based methodologies were not chosen for study because of the lower repeatability of this test when compared to the CPT. V_s-based methodologies were not chosen either because the database for V_s results in tailings dams is still rather limited worldwide in general and almost nonexistent in South Africa in particular.

In order to assess the performance of the two methodologies when applied to tailings dams, they were both applied to flow failure and non flow failure case histories. A database of ten case histories was compiled, consisting of five flow failure and five non flow failure cases. Likewise, five of the case histories involved seismic loads, whereas the other five only involved static loads. The Robertson-based methodology was only applied to the five seismic case histories and the Olson and Stark methodology was applied to all ten case histories. The work has been organized in six chapters as follows. Chapter 2 explains the conditions that lead to the flow failure of a soil mass, and points out which of these conditions are addressed by the two liquefaction assessment methods considered in this research. Chapter 3 is a review of the Robertson-based and Olson and Stark methodologies. The details of the way in which the two methods were implemented in this study are also covered in this chapter. Chapter 4 describes the ten case histories considered for study. Chapter 5 presents the results of the implementation of both methodologies and Chapter 6 presents a discussion of the results and major conclusions. Additionally, two appendices provide detailed information regarding the analysis of the case histories. Appendix A contains the profiles of different parameters calculated for the implementation of the Robertson-based methodology and Appendix B illustrates the different slope stability scenarios considered for the implementation of the Olson and Stark methodology.

2 Theoretical considerations

Soil liquefaction is a process by which a tendency for undrained volumetric contraction of a soil mass causes an increase in pore water pressure that in turn leads to a sudden loss of shear strength. Depending on the prevalent site conditions, this loss of shear strength can be manifested in a variety of ways which include sand boils, sudden collapse of foundations, vertical settlements and flow failure of slopes such as the ones in tailings dams. Given that the increase in pore water pressure that leads to liquefaction affects only the frictional component of soil strength, soils with considerable amounts of cohesive fines are less vulnerable to the destructive effects of liquefaction. Conversely, soils that derive their shear strength mostly from the frictional contacts between particles, i.e. exhibit sandlike behaviour, can be more severely affected by liquefaction. Ishihara (1993) noted that a good example of this second type of soil is mining tailings, given that the fines contained in tailings are typically cohesionless.

When sheared under undrained conditions, a contractive saturated soil will experience an increase in pore water pressure and, if the increase is high enough, might exhibit liquefaction. Conversely, when sheared undrained, a dilative soil will experience a reduction of pore water pressure and is therefore not susceptible to liquefaction. Thus, central to the concept of liquefaction is the question of whether a soil will tend to contract or dilate when sheared. Casagrande (1936) addressed this issue and found that, when sheared, loose sands contracted and dense sands dilated until reaching approximately the same ultimate void ratio (e). Casagrade referred to this ultimate void ratio as the critical void ratio (e_c). Upon shearing, a soil sample will contract if its e is greater than the critical value, and will dilate if its e is lower than the critical value. Casagrande also noticed that e_c was inversely proportional to the mean effective stress (p') acting on the sand. That is, a large p' inhibits soils' tendency to dilate and therefore the resulting e_c is small. Conversely, a small p' will offer little resistance to a soil's tendency to dilate and therefore the resulting e_c is large. The curve that relates e_c to the p' for a given soil can be approximated as a straight line when a logarithmic scale is used to plot p' (Figure 2.1). This line is an intrinsic characteristic that varies from one soil type to another and is referred to as the critical state locus (*CSL*). The *CSL* can be expressed mathematically as:

$$e_c = \Gamma - \lambda_{ln} \cdot \ln(p') \qquad \text{Eq. 2.1}$$

where λ_{ln} is the slope of the *CSL* and Γ is the value of e_c when p' = 1 kPa. It is usual for the *CSL* to be plotted with a base 10 logarithmic scale in the p' axis, in this case a factor of 2.303 correlates the slope of the plot to λ_{ln}. It follows that, in principle, soils that plot above their *CSL* are contractive and thus liquefiable, whereas soils that plot below their *CSL* are dilative and thus not liquefiable. Additionally, it is also known that upon shearing a soil that plots slightly above its *CSL*, it will initially exhibit a contractive behaviour and therefore lose shear strength, but at larger strains will exhibit dilation and therefore recover shear strength. Ishihara (1993) and Robertson and Wride (1998a) explain in greater detail the behaviours just described.

Casagrande also observed that the further away a sand plotted from its *CSL*, the greater the contraction or dilation it would exhibit. In order to characterise sand behaviour based on this deviation, Been and Jefferies (1985) introduced the state parameter (ψ) defined as:

$$\psi = e - e_c \qquad \text{Eq. 2.2}$$

where e is the current void ratio of the soil and e_c is the critical void ratio at the same mean stress (Figure 2.1). Equation 2.2 implies that when $\psi > 0$ the soil is contractive and when $\psi < 0$ the soil is dilative.

Based on the previous observations, it is clear that in order for liquefaction to lead to a flow failure in a tailings dam the first condition that must be met is that the tailings must exist in a contractive state, i.e. be susceptible to the development of high pore water pressures and consequent loss of frictional shear strength. Secondly, there must be a shearing stress big enough to make the tailings contract and therefore develop a significant increase in pore water pressure. This second consideration has been referred to by several authors as the triggering condition for liquefaction (e.g. Poulos et al. 1985, Ishihara et al. 1990, and Olson and Stark 2003). Several reported cases of flow failures in tailings dams (e.g. Blight 2010) serve to confirm that both static and dynamic loads can generate shear stresses that can trigger liquefaction. Thirdly, once liquefaction is triggered and the shear strength of a soil is reduced to a residual value, there must be a permanent load inducing shear stresses greater than the residual shear strength of the soil. If such a condition is met, e.g. in sloping ground or on level ground bearing foundations, large displacements of the soil mass (flow failure) can be expected to occur (Ishihara et al. 1990, Olson 2001). Evaluation of this third condition is usually referred to as a post-triggering analysis. In the case of sloping ground, liquefaction can lead to flow failures such as those experienced by tailings dams; whereas in the case of level ground, liquefaction can lead to a sudden collapse of foundations. In the case of permanent stresses not being larger than the residual shear strength, such as in level ground subjected only to self weight, the consequences of liquefaction will be less severe and can be manifested as sand boils accompanied by vertical settlement due to densification, or lateral displacements.

Having recognized that the prediction of a flow failure in a soil deposit entails a three-step analysis: susceptibility, triggering, and post-triggering; it is convenient to determine which of these three steps are addressed by the two liquefaction assessment methods considered in the present study. For the Robertson-based methodology, adapted here from Robertson (2009a), it is important to recognize that this methodology follows the same rationale as the simplified procedure presented by Seed et al. (1985): Liquefaction and non-liquefaction case histories on level ground are plotted on a two dimensional graph that has a measure of penetration resistance on the horizontal axis and of shear stress on the vertical axis (Figure 2.2). A curve is then traced to divide the liquefaction and non-liquefaction case histories. This curve is used to correlate penetration resistance to the shear stress required to trigger liquefaction. Beyond a certain penetration value, the curve rises steeply suggesting that the soil deposit is not susceptible to liquefaction. This procedure does not provide an estimation of the residual strength of the soil. Based on these observations, it is apparent that the Robertson-based methodology addresses only the susceptibility and triggering steps of a liquefaction analysis. If a soil exhibits a penetration resistance value lower than the value beyond which the curve rises steeply, then the procedure indicates that liquefaction can occur. This can be interpreted as the soil being in a contractive state. Once it has been determined that liquefaction is a possibility, the curve separating liquefaction and non-liquefaction case histories is used to estimate the triggering shear stress. Given that the methodology is not intended to provide a means of estimating the residual strength of the liquefied soil, a post-triggering analysis is not possible. As for the Olson and Stark (2002 and 2003) methodology, it is explicitly divided by its authors into three parts that correspond to the three steps of a flow failure analysis. Cone penetration resistance (q_c) is used during the three steps of the analysis to determine in turn: whether a soil is contractive or dilative, the triggering shear stress and the residual shear strength. Therefore the methodology is intended to predict not only whether a sloping soil deposit will exhibit liquefaction, but also whether the permanent loads and residual strength are such that a flow failure will occur. The Robertson-based and Olson and Stark methodologies are described with further detail in Chapter 3.

2.1 Tables and Figures

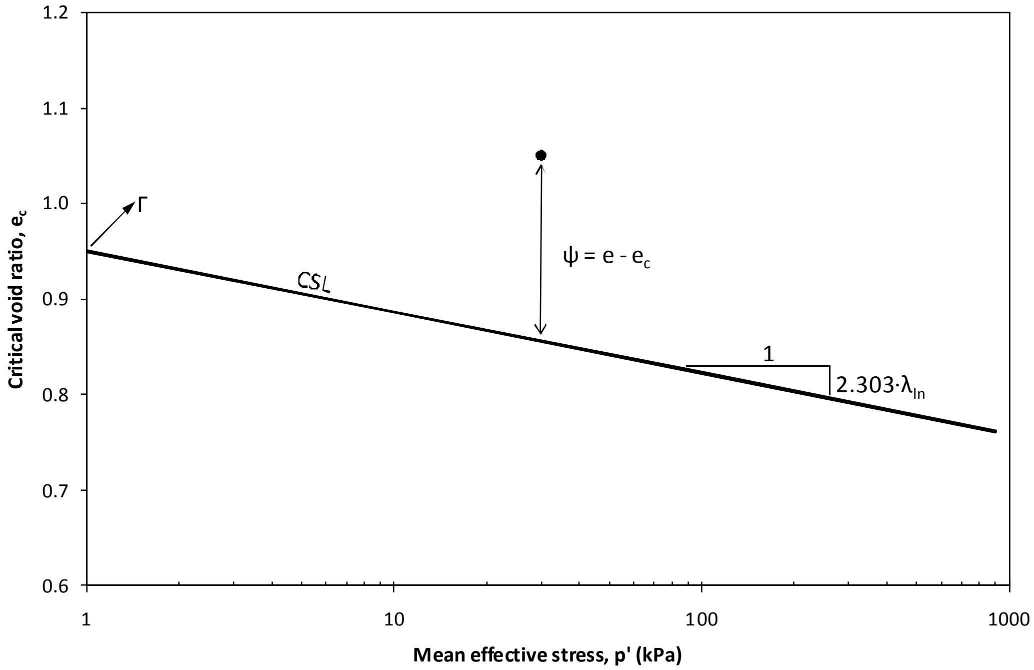

Figure 2.1 Critical state locus (*CSL*) and meaning of parameters *Γ*, λ_{ln}, and *ψ*.

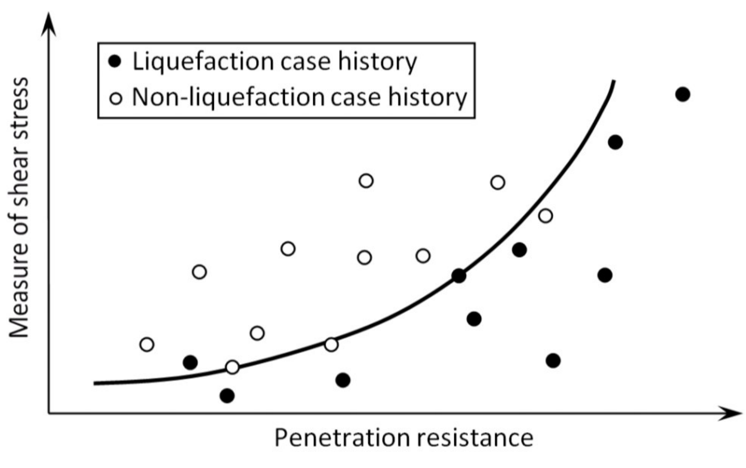

Figure 2.2 Schematic form of the diagram used in the Robertson-based methodology to correlate liquefaction resistance and penetration resistance.

3 Review of the *CPT*-based liquefaction assessment methodologies

3.1 Introduction

The two *CPT*-based liquefaction potential methodologies used in this research are reviewed in this chapter. The first methodology is based on the procedures outlined by Robertson (2009a). This methodology is intended for use in level ground and therefore some modifications have been included here to account for the slope of the outer walls of tailings dams. This methodology will be referred to here as the 'Robertson-based methodology'. The second methodology is described in Olson (2001) and Olson and Stark (2002, 2003). This methodology will be referred to here as the 'Olson and Stark methodology'. Two main differences exist between the two methodologies. First, the Robertson-based methodology is intended for use with cyclic loading only, whereas the Olson and Stark methodology is intended for use with both cyclic and monotonic loading. Therefore, the former was applied only to the five seismic case histories and the latter was applied to all ten case histories. It is worth noticing that Robertson and his co-workers have also investigated the correlation between cone penetration resistance and monotonic undrained strength (Yoshimine et al. 1999). However, their results suggest that the correlation is dependent on the mode of shearing and therefore no general correlation has been proposed. Second, as discussed in Chapter 2, the Robertson-based methodology is concerned only with the triggering of liquefaction and therefore does not include a post-triggering analysis, whereas the Olson and Stark methodology also includes a post-triggering analysis.

3.2 Commonalities between the methodologies

Prior to examining the details of the two methodologies and the different approaches the authors use, the commonalities between the two methods will be discussed. The two methodologies were developed by their authors as simple tools to evaluate the liquefaction potential of soil deposits. Due to their inherent simplicity, the authors of both methodologies recommend their use only in small projects or during the initial stages of large projects. In principle, neither methodology requires soil samples for their implementation, only the results of *CPT* tests. Further similarities are discussed in sections 3.2.1 and 3.2.2 .

3.2.1 Stress normalization of CPT data

Given that it is widely known that cone penetration resistance (q_c) values are strongly affected by the initial, undisturbed stress level, a logical first step when analyzing *CPT* data is to remove such effect. The two methodologies account for the effect of stress level by using the reference stress approach. In this approach, the penetration data measured at the *in situ* stress condition is converted to the penetration resistance that would have been measured at a reference stress level and the same *in situ* relative density. Jefferies and Been (2006) use published experimental data to make several objections to this approach. The data show how a soil's relative density alone is not a good indicator of its behaviour, i.e. different soils do not behave in the same way at the same relative density. They also point out that the conversion functions used in the reference stress approach are not clearly established and that the approach neglects the known effect of horizontal stress. These last two objections will be made clear in the current review, where the two methodologies use different conversion functions and neither of them requires estimation of horizontal stresses.

3.2.2 Assessment of the Cyclic Stress Ratio

To quantify the effect of the seismic loads that might trigger liquefaction in a soil deposit, the methodologies adopt the approach of the simplified procedure proposed by

Seed and Idriss (1971). In this procedure the seismic effect induced on a soil profile by any earthquake is quantified as:

$$CSR = \frac{\tau_{av}}{\sigma'_{vo}} = 0.65 \left(\frac{a_{max}}{g}\right) \left(\frac{\sigma_{vo}}{\sigma'_{vo}}\right) r_d \quad \text{Eq. 3.1}$$

where *CSR* stands for cyclic shear stress ratio, τ_{av} is the average cyclic shear stress induced by seismic action, σ'_{vo} and σ_{vo} are the effective and total overburden stress respectively before the earthquake, a_{max} is the maximum horizontal acceleration at ground surface, g is the acceleration due to gravity, and r_d is a depth reduction factor that accounts for the flexibility of the soil deposit.

Estimation of both a_{max} and r_d for application of Eq. 3.1 to tailings dams' case histories involves considerable uncertainty. For instance, in none of the five seismic case histories considered in this research, were acceleration readings available at the location of the dam. Thus, attenuation relationships or other means described in Chapter 4 were used to estimate a_{max} at the natural ground level of the site being analysed. Furthermore, the "ground surface" at a tailings dam is not the natural ground level, but the surface of the tailings beach. Therefore the relevant a_{max} is the maximum horizontal acceleration at the top of the tailings deposit. Given that a tailings dam is not a rigid object, the maximum acceleration at its base can be different from the acceleration at its crest. This difference is dependent on the specific ground motion and site and materials characteristics of each case history. However, as a working simplification, a_{max} in the present work was taken as equal to the maximum acceleration estimated for the natural ground level.

The depth reduction factor r_d, has a maximum value of one at ground surface and reduces with depth to account for soil flexibility. One of the first attempts to provide a range of values for r_d was made by Seed and Idriss (1971). Although their proposed range was based on only a limited number of site response analyses, it is widely used in simplified empirical estimations of *CSR*.

In 1996, a panel of experts participated in a Workshop on Evaluation of Liquefaction Resistance of Soils, organized by the National Center for Earthquake Engineering Research (NCEER). The purpose of the workshop was to review a series of developments and augmentations that had been made to the original simplified liquefaction assessment procedure proposed by Seed and Idriss (1971). Amongst the issues reviewed, was the determination of r_d. The NCEER workshop participants recommended that determination of r_d be done as presented by Robertson and Wride (1998b), namely:

$r_d = 1.0 - 0.00765z$	for $z \leq 9.15m$	Eq. 3.2a
$r_d = 1.174 - 0.0267z$	for $9.15m < z \leq 23m$	Eq. 3.2b
$r_d = 0.744 - 0.008z$	for $23 < z \leq 30m$	Eq. 3.2c
$r_d = 0.50$	for $z > 30m$	Eq. 3.2d

where z is depth in meters below ground surface.

The Olson methodology suggests the use of a formula proposed by Kayen et al. (1992) to estimate r_d:

$$r_d = 1 - 0.012z \quad \text{Eq. 3.3}$$

Considering that: a) Eq. 3.3 is a simpler approximation to r_d than Eq. 3.2; b) contrary to Eq. 3.3, the variation of r_d with depth is known to be non-linear (e.g. Seed and Idriss 1971, Cetin and Seed 2004); and c) Eq. 3.2 was endorsed by the panel of experts participating in the NCEER workshop; Eq. 3.2 was used in this research to estimate r_d in both the Robertson-based and Olson and Stark methodologies.

Despite its slightly greater complexity when compared with Eq. 3.3, Eq. 3.2 is still a very approximate way of estimating r_d based only on depth. As pointed out by Cetin and Seed (2004), several authors have conducted studies showing that r_d is nonlinearly dependent on a suite of variables such as depth, ground motion frequency, maximum acceleration, earthquake magnitude and site stiffness. To illustrate this dependence, Cetin and Seed (2004) performed 2153 site response analyses to study the variation of r_d profiles with different values of the variables affecting r_d. Their results show the extent to which r_d profiles can vary depending on site conditions and ground motion characteristics. Figure 3.1 compares Eqs. 3.2 and 3.3 with the r_d profile obtained by Cetin and Seed (2004). The lines corresponding to the ±1 standard deviation highlight the uncertainty involved in estimating r_d. It is also apparent that Eq. 3.2 yields considerably higher values of r_d than those predicted by the mean r_d profile of Cetin and Seed (2004), especially between depths of 5 to 20m. This indicates a high degree of conservatism in Eq. 3.2.

3.3 The Robertson-based methodology

3.3.1 Horizontal shear stresses (τ_h) generated by sloping ground

Robertson (2009a) outlines a methodology to assess the liquefaction potential of sandlike and claylike soils in level to gently sloping ground subjected to seismic forces. In this research, an addition was made to the methodology to account for the horizontal shear stresses (τ_h) generated by the outer walls of the tailings dams in four of the five seismic case histories. This addition required the estimation of τ_h profiles under the walls. To this purpose, drained *in situ* stress analyses with a 2-dimensional, linear-elastic, isotropic finite element model were performed for the four seismic case histories involving an outer wall. The module Sigma/W of the GeoStudio 2007 (Geo-Slope International Ltd.) software was employed to build the finite element models. Triangular and quadrilateral elements, of three and four nodes respectively, were used in the meshes. In all cases both horizontal and vertical displacements were constrained at the base of the models, whereas only horizontal displacements were constrained on the lateral borders. Figure 3.2 shows the meshes, boundary conditions and location of the water table used to model each case history. For each case history the mesh was refined until further refinements did not result in significant changes in τ_h values. The dashed lines are the vertical profiles along which the τ_h values were calculated.

The resulting τ_h profiles predicted by the models depend on two material properties: total unit weight (γ_t) and Poisson's ratio (v). The adopted values are reported in Table 3.1. For simplicity, each case history was modelled with a single soil type, since including additional soil types did not significantly alter the resulting τ_h profiles. The γ_t values were taken as the average value of the unit weight of the different soil types involved in each case history as reported by several references. There were no reported v values for any of the case histories so it was taken as 0.3 for all cases. This is similar to v values adopted in other finite element models of tailings dams. E.g. Zardari (2011) used 0.33, Zandarín et al. (2009) used 0.35, and Psarropoulos and Tsompanakis (2008) used 0.3.

The profiles of τ_h were used to calculate a static shear stress correction factor (K_α). Seed (1983) introduced the K_α factor to account for the reduction of a soil's resistance to cyclic loading due to initial static shear stresses. Based on experiments done on silts and clays exhibiting a wide range of plasticity indices Boulanger and Idriss (2007) suggested the following expression for K_α in claylike soils:

$$K_\alpha = 1.344 - \frac{0.344}{\left(1 - \frac{\tau_s}{S_u}\right)^{0.638}} \qquad \text{for } 0 \leq \tau_s/S_u \leq 0.88 \qquad \text{Eq. 3.4a}$$

$$K_\alpha = 0 \qquad \text{for } \tau_s/S_u > 0.88 \qquad \text{Eq. 3.4b}$$

where τ_s is the initial static shear stress acting on the plane of interest (horizontal in this case), and S_u is the peak undrained shear strength. Robertson (2009a) noted that for claylike soils S_u can be expressed as:

$$S_u = \frac{q_t - \sigma_{vo}}{N_{kt}} \qquad \text{Eq. 3.5}$$

where N_{kt} is an empirical cone factor with an average value of 15 recommended by Robertson (2009a). Therefore in this research K_α was calculated in terms of penetration resistance as:

$$K_\alpha = 1.344 - \frac{0.344}{\left(1 - \frac{15 \cdot \tau_h}{q_t - \sigma_{vo}}\right)^{0.638}} \qquad \text{for } 0 \leq \tau_s/S_u \leq 0.88 \qquad \text{Eq. 3.6a}$$

$$K_\alpha = 0 \qquad \text{for } \tau_s/S_u > 0.88 \qquad \text{Eq. 3.6b}$$

Eq. 3.6 was used in this study for all the soil types (as opposed to claylike soils only as recommended by Robertson, 2009a) encountered in the four seismic case histories involving an outer wall: Hokkaido, Mochikoshi dykes 1 and 2, and Dashihe outer wall. Of these four case histories, only the Mochikoshi dykes were classified by the method as being entirely claylike (Ic > 2.6, see Section 5.1.2). Nonetheless, this approach was employed here because there is no widely accepted method to account for the effect of horizontal static shear stresses on the liquefaction potential of sandlike soils (Youd et al. 2001). The role of K_{α} in assessing the liquefaction potential of sands and clays is explained in later sections.

3.3.2 Distinction between sandlike and claylike soils

The first step of the methodology is to establish whether the soil exhibits sandlike or claylike behaviour. This classification is done through the Soil Behaviour Type Index (I_c) which was determined in this research in one of three ways described here in order of decreasing preference. The first approach is used in Robertson (2009a) and relies on total cone penetration resistance corrected for unequal area effects (q_t) and sleeve friction (f_s) *CPT* readings used together with a soil behaviour type chart. The following equations are given in Robertson (2009a) to define I_c:

$$I_c = ((3.47 - \log Q_{tn})^2 + (\log F_r + 1.22)^2)^{0.5} \quad \text{Eq. 3.7}$$

$$Q_{tn} = \left(\frac{q_t - \sigma_{vo}}{p_a}\right)\left(\frac{p_a}{\sigma'_{vo}}\right)^n \quad \text{Eq. 3.8}$$

$$F_r = \left(\frac{f_s}{q_t - \sigma_{vo}}\right) \cdot 100\% \quad \text{Eq. 3.9}$$

$$n = 0.381 \cdot (I_c) + 0.05 \cdot (\sigma'_{vo}/p_a) - 0.15 \quad \text{Eq. 3.10}$$
$$where\ n \leq 1.0$$

where Q_{tn} is the normalised cone penetration parameter, F_r is the friction ratio, p_a is the atmospheric pressure, and n is a stress exponent part of the conversion function used to remove the effect of the stress level on q_t measurements. In this case, the q_t measurements are being converted to the reference stress level p_a. It should be noted that this research has been made under the assumption that the cone penetration resistance values (q_c) reported in the different references have been corrected for unequal area effects and can therefore be taken as equal to q_t. Equation 3.10 was initially proposed by Robertson (2009b) and is supported mostly on qualitative observations. In general, Eq. 3.10 yields n values close to 0.5 for sandlike soils or low effective stress conditions, and close to 1.0 for claylike soils or high effective stress conditions (σ'_v > 1 MPa). Given the interdependence between I_c, n, and Q_{tn}, an iteration process is required to find their final values.

Equation 3.7 is given by Robertson and Wride (1998a) as a means of approximating the boundaries between the different regions in a soil behaviour type chart that was originally proposed by Robertson (1990). In this chart, referred to here as the Q_{tn} vs. F_r chart, the different regions represent different soil behaviour types. Figure 3.3 shows the Q_{tn} vs. F_r chart but instead of using the original boundaries between regions 2 through 7, actual I_c contours are shown. The boundaries that define regions 1, 8 and 9 are shown unchanged with respect to Robertson (1990). Soil behaviour type can be established in terms of I_c as shown in Table 3.2 proposed by Robertson and Wride (1998a).

Besides I_c and Table 3.2, the following criteria mentioned by Robertson and Wride (1998a) should also be considered when using the Q_{tn} vs. F_r chart to determine soil behaviour type:

1. I_c does not apply to regions 1, 8 or 9.
2. Very loose clean sands may be confused with denser sands containing fines in the region defined by $1.64 < I_c < 2.36$ and $F_r < 0.5\%$ (Figure 3.3). Therefore, any soil plotting in this zone should be conservatively treated as clean sand.
3. Soils that fall in the region defined by $I_c > 2.6$ and $F_r \leq 1.0\%$ (Figure 3.3) can be very sensitive and susceptible to liquefaction. Soils in this region require additional testing to determine their liquefaction potential.

The second approach to determine I_c was based on the correlation given in Robertson and Wride (1998a) between I_c, fines content (*FC*), and plasticity index (*PI*) (Figure 3.4). *FC* and *PI* values reported in the literature were used to make an estimation of I_c based on one of the two correlations shown in Figure 3.4. In the correlations given by Robertson and Wride (1998a), the line for non-plastic fines is only defined up to an apparent fines content of 50%. In this study, this line has been extrapolated up to 85% to allow for the estimation of an I_c value of the Mochikoshi tailings. This second approach to determine I_c was used in case histories for which f_s readings were not available.

A third approach based only on soil description had to be used for one of the case histories (Hokkaido). This approach relies on the qualitative soil description available in the literature and the corresponding I_c range given in Table 3.2. Due to the greater uncertainty of this third approach, the upper and lower bound values of the I_c range were used to assess liquefaction potential.

Once I_c had been calculated using one of the approaches mentioned above, the soil was classified into sandlike ($I_c \leq 2.6$) or claylike ($I_c > 2.6$). The *CSR* calculated with Eq. 3.1 is applicable to both sandlike and claylike soils. However, the estimation of the resistance to liquefaction follows different procedures for sandlike and claylike soils. The following two sections describe these procedures.

3.3.3 Sandlike soils ($I_c \leq 2.6$)

Estimation of *CRR* for sand-like soils is based on the $CRR_{7.5}$ curve proposed by Robertson and Wride (1998a) (Figure 3.5), where $CRR_{7.5}$ is the cyclic resistance ratio for an earthquake with moment magnitude $M_w = 7.5$[1]. The $CRR_{7.5}$ curve is basically a boundary between liquefaction and non-liquefaction level ground case histories on $Q_{tn,cs} - CSR_{7.5}$ space. $Q_{tn,cs}$ (Eq. 3.12) is a clean sand equivalent of Q_{tn}, and $CSR_{7.5}$ is *CSR* (Eq. 3.1) calculated for an $M_w = 7.5$ earthquake. This curve was obtained from the clean sand *SPT*-based liquefaction boundary proposed by Seed et al. (1985), *SPT-CPT* conversions, and a slight adjustment made during the 1996 NCEER workshop (Youd et al. 2001). Robertson and Wride (1998a) proposed the following equations to approximate the $CRR_{7.5}$ boundary line:

---

[1] The moment magnitude (M_w) is equal to $2/3 \cdot log_{10}(M_0) - 10.7$, where M_0 is the magnitude of the seismic moment in dyne-centimetre (Hanks and Kanamori 1979).

$$if\ Q_{tn,cs} < 50, \quad CRR_{7.5} = 0.833\left[\frac{Q_{tn,cs}}{1000}\right]^3 + 0.05 \quad \text{Eq. 3.11a}$$

$$if\ 50 \leq Q_{tn,cs} \leq 160, \quad CRR_{7.5} = 93\left[\frac{Q_{tn,cs}}{1000}\right]^3 + 0.08 \quad \text{Eq. 3.11b}$$

Conservatively, $CRR_{7.5}$ was taken as 0.5 for $Q_{tn,cs} > 160$. $Q_{tn,cs}$ is calculated as:

$$Q_{tn,cs} = Q_{tn} \cdot K_c \quad \text{Eq. 3.12}$$

where K_c is a correction factor that depends on I_c. In general, K_c is equal to 1 for clean sands and has greater values for claylike soils to account for their greater liquefaction resistance. K_c is defined by Robertson and Wride (1998a) as:

$$if\ I_c \leq 1.64, \quad K_c = 1.0 \quad \text{Eq. 3.13a}$$

$$if\ I_c > 1.64,$$
$$K_c = -0.403 \cdot I_c^4 + 5.581 \cdot I_c^3 - 21.63 \cdot I_c^2 + 33.75 \cdot I_c - 17.88 \quad \text{Eq. 3.13b}$$

The literature reviewed in this research does not provide an explanation of how Eq. 3.13 was arrived at. Once $CRR_{7.5}$ has been determined from Eq. 3.11 or Figure 3.5, it must be adjusted by a magnitude scaling factor (*MSF*). This allows comparisons with the *CSR* calculated with Eq. 3.1 which does not necessarily correspond to an M_w = 7.5 earthquake. Robertson and Wride (1998a) suggest that *MSF* for sandlike soils be calculated according to the recommendations contained in Youd et al. (2001). These recommendations provide a range of *MSF* values for $M_w < 7.5$ and a set of single values for $M_w > 7.5$ (Table 3.3). Four of the five seismic case histories analysed in this research had $M_w > 7.5$, and the remaining one had $M_w = 7.5$ (Table 4.1). Their *MSF* values were calculated from an exponential interpolation of the values presented in Table 3.3 for $5.5 < M_w < 8.5$. In calculating the interpolating exponential equation, the lower bound values were used for $M_w < 7.5$. Once *MSF* has been determined, *CRR* of sandlike soils was computed as:

$$CRR = CRR_{7.5} \cdot MSF \quad \text{Eq. 3.14}$$

To account for the initial static horizontal shear stresses induced by the outer walls, *CRR* was multiplied by K_α (Eq. 3.6) and the resulting product is referred to as CRR_α. The factor of safety against the triggering of liquefaction was then determined as:

$$FS = \frac{CRR_\alpha}{CSR} \quad \text{Eq. 3.15}$$

3.3.4 Claylike soils (I_c > 2.6)

In order to calculate the $CRR_{7.5}$ of claylike soils, Robertson (2009a) uses the expression suggested by Boulanger and Idriss (2007) who state that the $CRR_{7.5}$ for level ground natural deposits of claylike fine grained soils can be estimated as:

$$CRR_{7.5} = 0.8\frac{S_u}{\sigma'_{vo}} \quad \text{Eq. 3.16}$$

However, Boulanger and Idriss (2007) also suggest that for tailing slimes, Eq. 3.16 should be reduced by approximately 20%, thus yielding the expression that was used in this study:

$$CRR_{7.5} = 0.64\frac{S_u}{\sigma'_{vo}} \quad \text{Eq. 3.17}$$

Following the same procedure used by Robertson (2009a), Eq. 3.5 can be used to replace S_u in Eq. 3.17, and considering that for claylike soils $n \approx 1$, $CRR_{7.5}$ can be expressed in terms of tip resistance as:

$$CRR_{7.5} = 0.043 \cdot Q_{tn} \quad \text{Eq. 3.18}$$

$CRR_{7.5}$ must be adjusted by a *MSF* to allow comparisons to the *CSR* calculated with Eq. 3.1 which does not necessarily correspond to an M_w = 7.5 earthquake. Such adjustment was done by Eq. 3.14, but in this case *MSF* values were determined from Eq. 3.19 proposed by Boulanger and Idriss (2007) specifically for claylike soils:

$$MSF = 1.12 \cdot exp\left(\frac{-M_w}{4}\right) + 0.828 \quad \text{Eq. 3.19}$$

The initial static horizontal shear stresses induced by the outer walls were accounted for in the same way as for sandlike soils, i.e. computing the product of *CRR* and K_α to obtain CRR_α. The factor of safety against the triggering of liquefaction was then determined by Eq. 3.15.

3.4 The Olson and Stark methodology

Olson and Stark (2002, 2003), proposed a methodology to assess the potential of flow failure liquefactions in sloping ground conditions subjected to static and seismic stresses. The methodology uses only the cone tip resistance reading of the *CPT* and is based on the back analyses of flow failure liquefaction case histories. It is divided into three steps: liquefaction susceptibility, triggering of liquefaction, and post-triggering/flow failure stability.

3.4.1 Step 1 – Liquefaction susceptibility analysis

This step determines whether a soil is in a contractive or dilative state. Several authors have proposed penetration resistance vs. vertical effective stress relationships to define an empirical contractive-dilative boundary. Olson and Stark (2003) recommend the boundary relationship proposed by Fear and Robertson (1995) and state that it can be approximated as:

$$(\sigma'_{vo})_{boundary} = 1.10 \times 10^{-2}(q_{c1})^{4.79} \quad \text{Eq. 3.20}$$

where σ'_{vo} and q_{c1} have units of kPa and MPa, respectively and σ'_{vo} has an upper bound value of about 350 kPa. q_{c1} is the cone tip resistance, q_c, normalized to a reference vertical effective stress equal to the atmospheric pressure:

$$q_{c1} = q_c \cdot \frac{1.8}{0.8 + (\sigma'_{vo}/p_a)} \quad \text{Eq. 3.21}$$

Equation 3.20 does not appear as such in Fear and Robertson (1995) and it is unclear how Olson and Stark (2003) arrived at this approximation, although it appears that their procedure was as follows. Fear and Robertson (1995) present in their Eq. 8:

$$\psi = \left(\frac{A}{B} - \Gamma\right) - \left\{\frac{V_{s1}}{B(K_o)^{na}} - \lambda_{ln} \ln\left[\frac{\sigma'_{vo}}{3}(1 + 2K_o)\right]\right\} \quad \text{Eq. 3.22}$$

where ψ is the state parameter; A and B are constants that correlate a soil's shear wave velocity to its void ratio; Γ and λ_{ln} are constants that define a soil's steady state line; V_{s1} is a normalized measure of shear wave velocity; K_o is the horizontal stress ratio; and *na* is a stress exponent typically taken as 0.125. Further, Fear and Robertson (1995) also suggest that V_{s1} and q_{c1} are correlated as follows:

$$V_{s1} = C1 \cdot {q_{c1}}^{C2} \quad \text{Eq. 3.23}$$

where *C1* and *C2* are constants whose specific value will vary from one type of soil to another. Substituting V_{s1} in Eq. 3.22 by Eq. 3.23, taking ψ = 0 to reproduce the contractive-dilative boundary, and solving for σ'_{vo} yields:

$$(\sigma'_{vo})_{boundary} = \frac{3}{1 + 2K_o} \cdot exp\left[\frac{\frac{C1 \cdot q_{c1}^{C2}}{B \cdot K_o^{0.125}} - \left(\frac{A}{B} - \Gamma\right)}{\lambda_{ln}}\right] \quad \text{Eq. 3.24}$$

Reducing Eq. 3.24 to an expression in which $(\sigma'_{vo})_{boundary}$ is dependent only on q_{c1} (e.g. Eq. 3.20) implies making assumptions of the values of seven constants that are dependent on soil type and site conditions. Olson and Stark (2003) may have made assumptions regarding these seven constants to arrive at Eq. 3.20, but even if this were not their approach, it is clear from Fear and Robertson (1995) that it is not possible to establish a single contractive-dilative boundary in q_{c1}-σ'_{vo} space that is applicable to all soils and site conditions. Figure 3.6 further illustrates this concept by using Eq. 3.24 to plot contractive-dilative boundaries for the different soils whose characteristics are given in Table 3.4. The boundary recommended by Olson and Stark (2003) (Eq. 3.20) is also included. The non-uniqueness of the contractive dilative boundary is evident.

Further insight into the contractive dilative boundary proposed by Olson and Stark can be obtained by considering the mobilised friction angles implied by Eq. 3.20. In order to do this, the q_{c1} values in Eq. 3.20 were converted to undrained shear strength (S_u) and subsequently, the friction angle required to mobilise each combination of $(\sigma'_{vo})_{boundary}$ and S_u was determined. The procedure to convert q_{c1} to S_u was as follows. Initially, q_{c1} was converted to q_c using Eq. 3.21. In doing this, the σ'_{vo} value used in Eq. 3.21 was $(\sigma'_{vo})_{boundary}$. Subsequently, q_c was converted into an S_u value by using Eq. 3.5. The σ_{vo} value in Eq. 3.5 was taken as $(\sigma'_{vo})_{boundary}$. Given that both σ_{vo} and $(\sigma'_{vo})_{boundary}$ are generally very small when compared to q_c, choosing one or the other has only a small effect on the computed S_u value. Of much greater significance is the value chosen for N_{kt}, therefore the calculations were made with N_{kt} = 15 and N_{kt} = 20. Finally, the corresponding friction angle was calculated as:

$$\varphi_{cu} = \text{atan}(S_u/\sigma'_{vo}) \quad \text{Eq. 3.25}$$

Since it is reasonable to expect that the in situ tailings have had enough time to consolidate before the CPT sounding and that the loading of the CPT is fast enough to induce undrained conditions, the sub index *cu* has been used to denote that this is a consolidated undrained friction angle.

The results (Figure 3.7) show that, regardless of the N_{kt} value used in Eq. 3.5, ϕ_{cu} values initially decrease rapidly as σ'_{vo} increases, and then stabilises at around σ'_{vo} = 150 kPa. The curves stabilise at ϕ_{cu} values of 75˚ and 71˚ for N_{kt} values of 15 and 20 respectively. The implication that a soil is expected to exhibit a ϕ_{cu} value close to 70˚ in order to be considered dilative seems overly conservative.

3.4.2 Step 2 – Triggering of liquefaction analysis

For this step Olson and Stark (2003) proposed a relationship between yield strength ratio (*YSR*) and q_{c1} that was based on liquefaction case histories on sloping ground. The *YSR* is defined as the undrained yield shear strength [$S_u(yield)$] normalized by σ'_{vo} (Eq. 3.26). Given that a liquefiable soil will suffer a considerable loss of strength if it is loaded beyond $S_u(yield)$, this strength defines the maximum allowable stress if triggering of liquefaction is to be averted. Both permanent (e.g. static) and temporary loads (e.g. seismic) contribute to the stresses that can trigger liquefaction, thus both are considered in this step.

In order to allow the estimation of $S_u(yield)$ from *CPT* results, Olson and Stark (2003) considered eight liquefaction case histories in which the average mobilised shear stress along the slip surface shortly before the failure was deemed to be equal or very close to $S_u(yield)$. Through back analyses using pre-failure geometry, they estimated the values of mobilised shear stress acting along various possible slip surfaces for each case history. The average σ'_{vo} acting on these slip surfaces was also estimated. Due to the uncertainties involved, Olson and Stark (2003) computed a range of *YSR* values for each case history. Published penetration resistance values were used to estimate characteristic q_{c1} values for the eight case histories. Due to uncertainties, a range of possible q_{c1} values was established for seven case histories. Two of the q_{c1} values were based on *CPT* readings. For the other six case histories q_{c1} values were inferred from *SPT* results, relative density measurements, or otherwise estimated.

Figure 3.8 shows the plot of mean q_{c1} vs. best estimate of *YSR* as reported by Olson and Stark (2003) for the eight case histories. Due to overlap at (3 MPa; 0.265), only seven points are visible in the figure. The error bars are based on the upper and lower bound values for *YSR* and q_{c1}. Referring to the data points in Figure 3.8 Olson and Stark (2003) state that "*despite the uncertainties, a trend of increasing yield strength ratio with increasing penetration resistance is observed.*" The equation they proposed to describe this trend is:

$$YSR = \frac{S_u(yield)}{\sigma'_{vo}} = 0.205 + 0.0143(q_{c1}) \pm 0.04 \quad for \quad q_{c1} \leq 6.5\ MPa \qquad \text{Eq. 3.26}$$

where q_{c1} has units of MPa. The term ±0.04 represents the upper and lower boundary lines suggested to account for data scatter. The mean line and the upper and lower bounds of Eq. 3.26 are plotted in Figure 3.8 with dashed lines. A linear regression was performed in the current research using the eight mean data points of (q_{c1}, *YSR*) and is plotted as a solid line in Figure 3.8. A poor fit was achieved (R^2 = 0.15), indicating that the conclusion of a trend of direct proportionality between *YSR* and q_{c1} can hardly be reached considering only the data in Figure 3.8. It is also evident that the linear regression line differs from the mean line of Eq. 3.26, the latter having a slope three times higher. No explanation is given by Olson and Stark (2003) or Olson (2001) as to how exactly Eq. 3.26 was arrived at.

The *YSR* values calculated with Eq. 3.26 are used in the triggering of liquefaction analysis together with the steps described by Olson and Stark (2003) and which were adhered to in the current research. The following description of these steps is mostly an excerpt from Olson and Stark (2003):

1. Conduct a slope stability back analysis of the pre-failure geometry to estimate the static shear stress ($\tau_{driving}$) in the contractive (liquefiable) soil(s). A trial value of shear strength is assumed for the liquefiable soils, and this value is modified until a factor of safety of unity is achieved. Fully mobilised drained or undrained shear strengths are assigned to the non-liquefiable soils. The slope stability search should consider both circular and non-circular potential failure surfaces.
2. Divide the critical failure surface into a number of segments. Ten to fifteen segments are satisfactory.
3. Determine the weighted average value of σ'_{vo} (defined by Eq. 3.27) along the critical failure surface and calculate the average static shear stress ratio, $\tau_{driving}/\sigma'_{vo}(ave)$.

$$\sigma'_{vo}(ave) = \frac{\sum_{i=1}^{n} \sigma'_{v,i} \cdot L_i}{\sum_{i=1}^{n} L_i} \qquad \text{Eq. 3.27}$$

Where n is the number of segments into which the slip surface has been divided; $\sigma'_{v,i}$ is the σ'_{vo} acting on segment i; and L_i is the length of segment i.

4. Estimate the average seismic shear stress ($\tau_{ave,seismic}$) applied to each segment of the critical failure surface using Eq. 3.1 and divide it by the appropriate *MSF* to account for earthquake magnitude.
5. If applicable, estimate other shear stresses (τ_{other}) applied to each segment of the critical failure surface using appropriate analyses.
6. Determine the value of *YSR* from Eq. 3.26. The desired level of conservatism can be incorporated by using a q_{c1} value larger or smaller than the mean, or by selecting a *YSR* higher or lower than the mean value. In this research the characteristic q_{c1} value was taken as the 66th percentile of the q_{c1} values found to be contractive in Step 1, i.e. the characteristic q_{c1} was smaller than 66% of the contractive q_{c1} values. This approach to determining a characteristic q_{c1} was recommended by Anderson et al. (2007). The same characteristic q_{c1} value was used for the post-triggering analysis.
7. Calculate the values of $S_u(yield)$ and $\tau_{driving}$ for each segment of the critical failure surface by multiplying the values of *YSR* and $\tau_{driving}/\sigma'_{vo}(ave)$ by the σ'_{vo} for the segment.
8. The factor of safety against the triggering of liquefaction in each segment is then estimated as

$$FS_{Triggering} \approx \frac{S_u(yield)}{\tau_{driving} + \tau_{ave,seismic} + \tau_{other}} \qquad \text{Eq. 3.28}$$

- Segments with $FS_{Triggering} \leq 1$ are likely to liquefy and they should be assigned the liquefied shear strength for the post-triggering analysis that is described in the following section.
- Segments with $FS_{Triggering} > 1$ should be assigned their $S_u(yield)$ value in a post-triggering analysis.
- If all segments have $FS_{Triggering} > 1$, a post-triggering analysis is not needed.
- The analysis must consider circular and non-circular failure surfaces that cross the liquefiable soils at different locations and depth.

3.4.3 Step 3 – Post –triggering/flow failure stability analysis

For this step Olson and Stark (2002) proposed a relationship between liquefied strength ratio (*LSR*) and q_{c1} that was based on liquefaction case histories on sloping ground. The *LSR* is defined as the liquefied shear strength [$S_u(LIQ)$] normalized by σ'_{vo} (Eq. 3.29). $S_u(LIQ)$ is the shear strength of a soil after liquefaction has triggered. This step considers that if the permanent (e.g. static) loads to which a soil is subjected after the triggering of liquefaction are bigger than $S_u(LIQ)$, then a flow failure can be expected to occur. Thus, only static loads are considered in the flow failure analysis.

In order to allow the estimation of $S_u(LIQ)$ from *CPT* results, Olson and Stark (2002) considered 21 liquefaction case histories for which enough information was available to perform a rigorous stability analysis of the post-failure geometry. For 10 of these 21 cases, the available information also allowed performance of a kinetic analysis. Olson and Stark (2002) state that the kinetic analysis allows the best estimate of $S_u(LIQ)$ mobilised during failure because it considers inertial forces. They also present experimental data showing that the kinetic analysis is particularly important when the height of the embankment is greater than 10 m. Only 1 of the 11 case histories on which a kinetic analysis was not performed involved an embankment with height greater than 10 m, therefore it can be assumed that performing a kinetic analysis on these 11 case histories would not significantly alter their $S_u(LIQ)$ estimates. Average values of σ'_{vo} considering the pre-failure geometry were also calculated for each case history. Due to the uncertainties involved, Olson and Stark (2002) computed a range of values of *LSR* for 19 of the 21 case histories. Published penetration resistance values were used to estimate characteristic q_{c1} values for the 21 case histories. Due to uncertainties, a range of possible q_{c1} values was established for 19 case histories. Seven of the q_{c1} values were based on *CPT* readings. For the other 14 case histories q_{c1} values were inferred from *SPT* results, relative density measurements, or otherwise estimated.

Figure 3.9 shows the plot of mean q_{c1} vs. best estimate of *LSR* as reported by Olson and Stark (2002) for the 21 case histories. Upper and lower bound values for *LSR* and q_{c1} were also reported by Olson and Stark (2002) but error bars were not included in Figure 3.9 to avoid clutter. Referring to the data points in Figure 3.9 Olson and Stark (2002) state that "*despite the uncertainties for each case, a reasonable trend in the data is apparent...*" The equation they proposed to describe this trend is:

$$LSR = \frac{S_u(LIQ)}{\sigma'_{vo}} = 0.03 + 0.0143(q_{c1}) \pm 0.03 \quad for \quad q_{c1} \leq 6.5\ MPa \qquad \text{Eq. 3.29}$$

where q_{c1} has units of MPa. The term ±0.03 represents the upper and lower boundary lines suggested to account for data scatter. The mean line and the upper and lower bounds of Eq. 3.29 are plotted in Figure 3.9 with dashed lines. A linear regression was performed in the current research using the 21 mean data points of (q_{c1}, *YSR*) and is plotted as a solid line in Figure 3.9. A poor fit was achieved (R^2 = 0.21), indicating that the conclusion of a trend of direct proportionality between *LSR* and q_{c1} can hardly be reached considering only the data in Figure 3.9. Given that a linear regression was reported by Olson and Stark (2002) as the means of developing Eq. 3.29, it is an unexpected finding that this work's linear regression yields a different equation with a slope 35% lower than that of Eq. 3.29.

Olson (2001) explains that the *LSR* values computed from Eq. 3.29 can be multiplied by appropriate σ'_{vo} values to compute $S_u(LIQ)$ for those segments of the slip surface that yielded $FS_{triggering}$ < 1 in step two. Once $S_u(LIQ)$ have been assigned to these segments, new factors of safety can be computed for all segments as:

$$FS_{Flow} = \frac{S_u}{\tau_{static}} \qquad \text{Eq. 3.30}$$

where S_u may be equal to $S_u(yield)$ or $S_u(LIQ)$ depending on whether or not the segment was predicted to liquefy in step 2; and τ_{static} are all static shear stresses acting along the slip surface. If the average FS_{Flow} is smaller than 1, flow failure is expected to occur; if the average FS_{Flow} is greater than 1.1, flow failure is unlikely; and if the average FS_{Flow} is between 1 and 1.1, some deformation is expected to occur and the analysis must be repeated assigning $S_u(LIQ)$ to all segments with $FS_{Triggering}$ between 1 and 1.1.

3.5 Concluding Remarks

Both of the *CPT*-based methodologies reviewed in this chapter are intended as simplified procedures to be used only in small projects or as a screening tool in large projects. It is worth noting that one of the conclusions of the NCEER 1996 workshop (Youd et al. 2001) was that simplified procedures for assessing liquefaction potential, are not recommended for routine use in soil deposits subjected to considerable static stresses (e.g. sloping ground in tailings dams). Nonetheless, the usefulness of these simplified procedures is such that it is considered here that it is worthwhile to explore their suitability to predict flow failures in tailings dams.

Shortcomings or questionable aspects of the methods that may affect their performance have been highlighted in the review. In general, the Robertson-based methodology seems to make better use of *CPT* results by incorporating both cone tip resistance and sleeve friction into its calculations, unlike the Olson and Stark methodology which only uses cone tip resistance. However, neither of the methods uses pore water pressure readings. The Robertson-based methodology might also benefit from the fact that both liquefaction and non-liquefaction case histories were considered in its formulation, whereas the Olson and Stark methodology is based on the back analyses of exclusively liquefaction case histories. Nonetheless, when being applied to tailings dams, the Olson and Stark methodology has the advantage of having been designed specifically for sloping ground where static shear stresses are considerable. A modification was included in this research to the procedures outlined by Robertson and his co-workers to enable analysis of liquefaction of sand-like soils in sloping ground.

3.6 Tables and Figures

Table 3.1 Total unit weight (γ_t) and Poisson's ratio (v) values used in the finite element models.

Case history	γ_t (kN/m^3)	v
Hokkaido	19.8	0.3
Mochikoshi dyke 1	17.1	
Mochikoshi dyke 2	16.4	
Dashihe outer wall	17.8	

Table 3.2 Boundaries of soil behaviour type in terms of I_c (after Robertson and Wride, 1998a).

Soil behaviour type index, I_c	Zone (Figure 3.3)	Soil behaviour type
$I_c < 1.31$	7	Gravelly sand to dense sand
$1.31 < I_c < 2.05$	6	Sands: clean sand to silty sand
$2.05 < I_c < 2.60$	5	Sand mixtures: silty sand to sandy silt
$2.60 < I_c < 2.95$	4	Silt mixtures: clayey silt to silty clay
$2.95 < I_c < 3.60$	3	Clays: silty clay to clay
$I_c > 3.60$	2	Organic soils: peats

Table 3.3 Magnitude scaling factors (Youd et al. 2001).

Earthquake Magnitude, M_w	Magnitude scaling factor	
	Lower bound	Upper bound
5.5	2.20	2.8
6.0	1.76	2.1
6.5	1.44	1.6
7.0	1.19	1.25
7.5	1.00	
8.0	0.84	
8.5	0.72	

Table 3.4 Soil parameters of the three sands used in Figure 3.6.

Soil	**K_o (--)**	**C1[a] [m /(s·kPa)]**	**C2[a] (--)**	**A[b] (m/s)**	**B[b] (m/s)**	**Γ[b] (--)**	**λ_{ln}[b] [1/ln(kpa)]**
Ottawa Sand	0.5	102	0.23	381	259	0.926	0.032
Alaska Sand				307	167	1.485	0.117
Syncrude Sand				311	188	0.950	0.027

a. Values taken from a general $V_{s1} - q_{c1}$ correlation proposed by Fear and Robertson, 1995.

b. Values taken from Cunning et al., 1995.

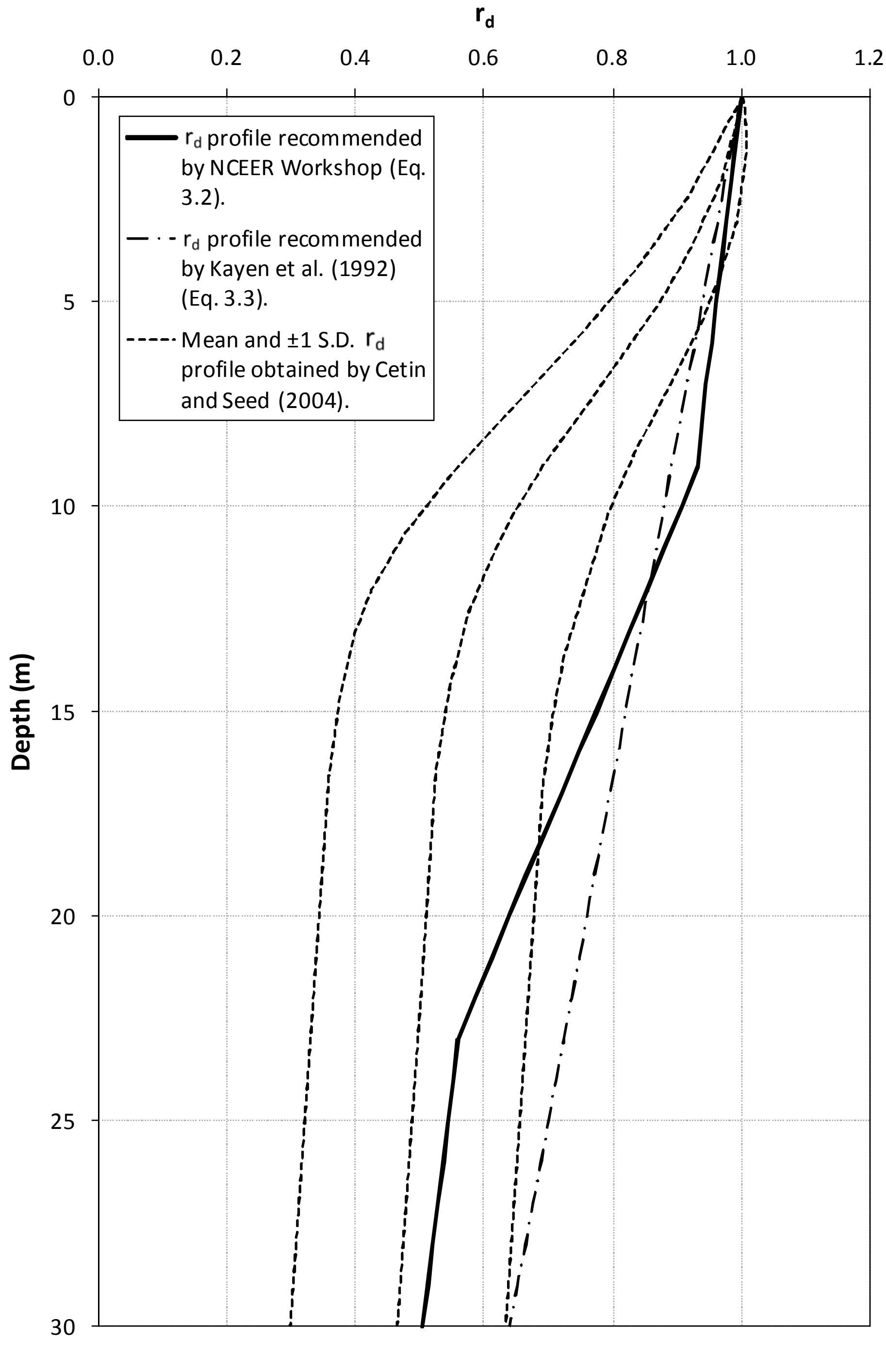

Figure 3.1 Comparison of r_d profiles suggested by different authors.

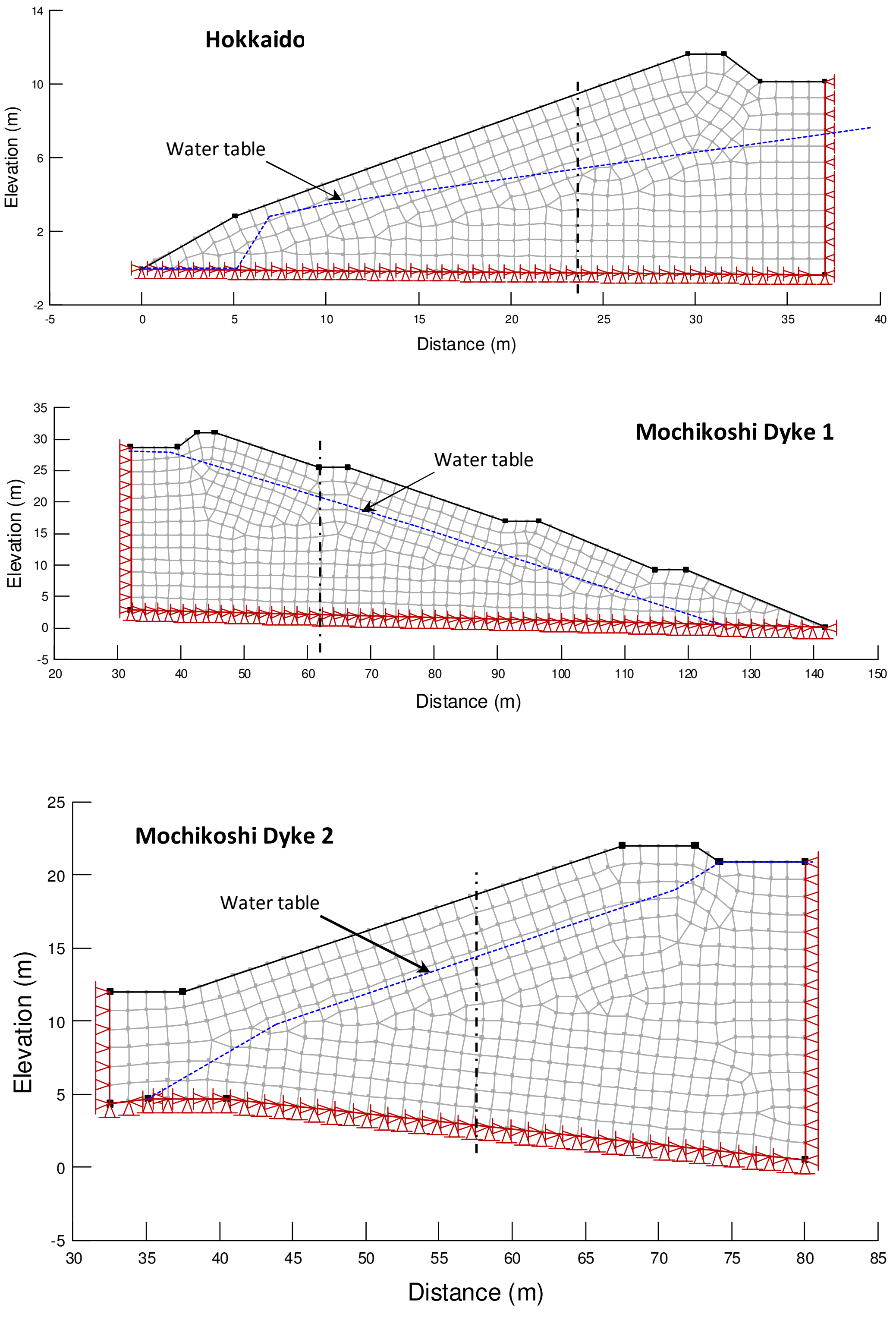

Figure 3.2 Meshes, boundary conditions and soil types of four seismic case-histories. Dashed vertical line indicates approximate profile along which horizontal static shear stresses (τ_h) were calculated.

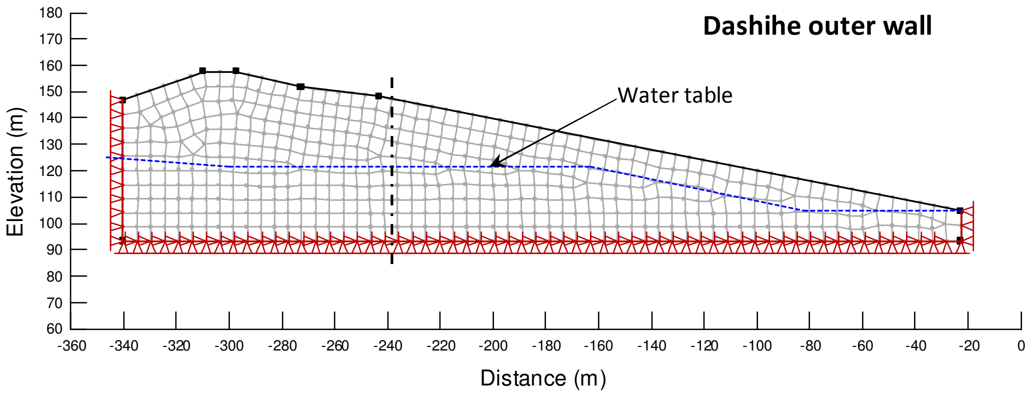

Figure 3.2 Continued.

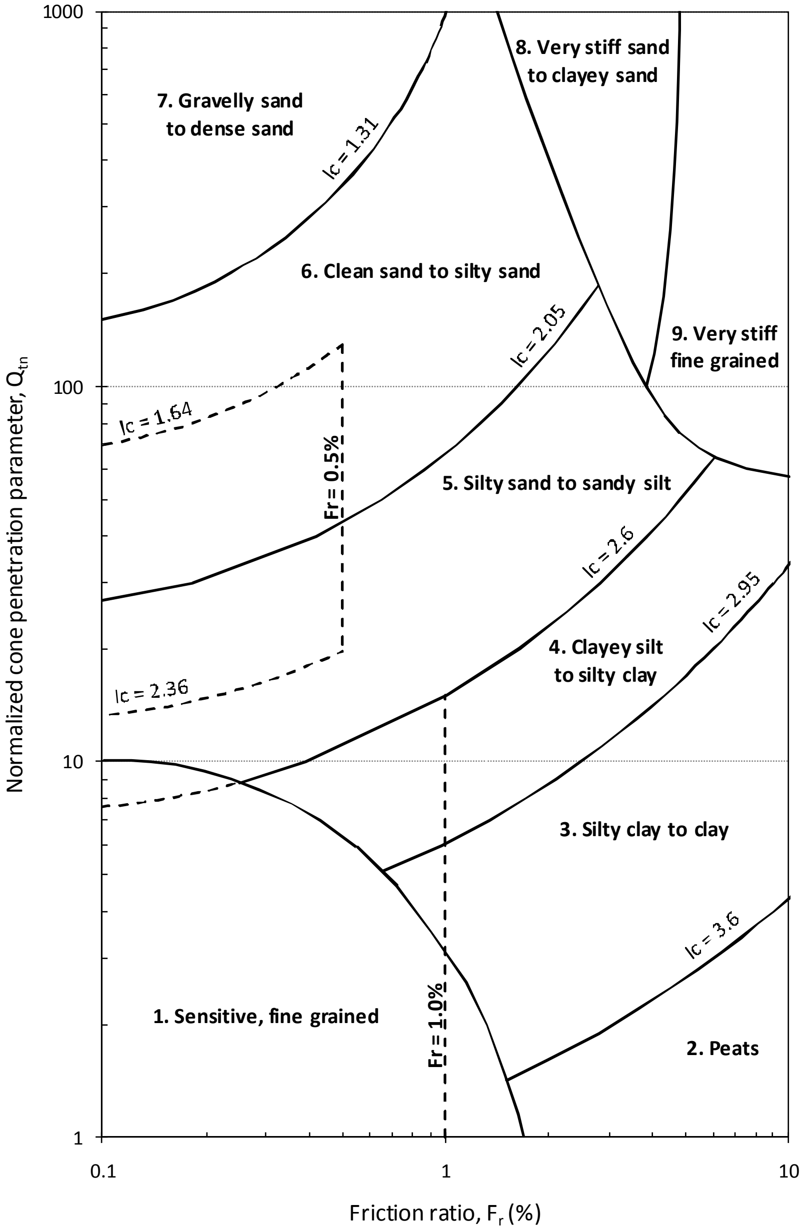

Figure 3.3 Soil behaviour type chart using I_c contours as region boundaries (after Robertson, 2009a.)

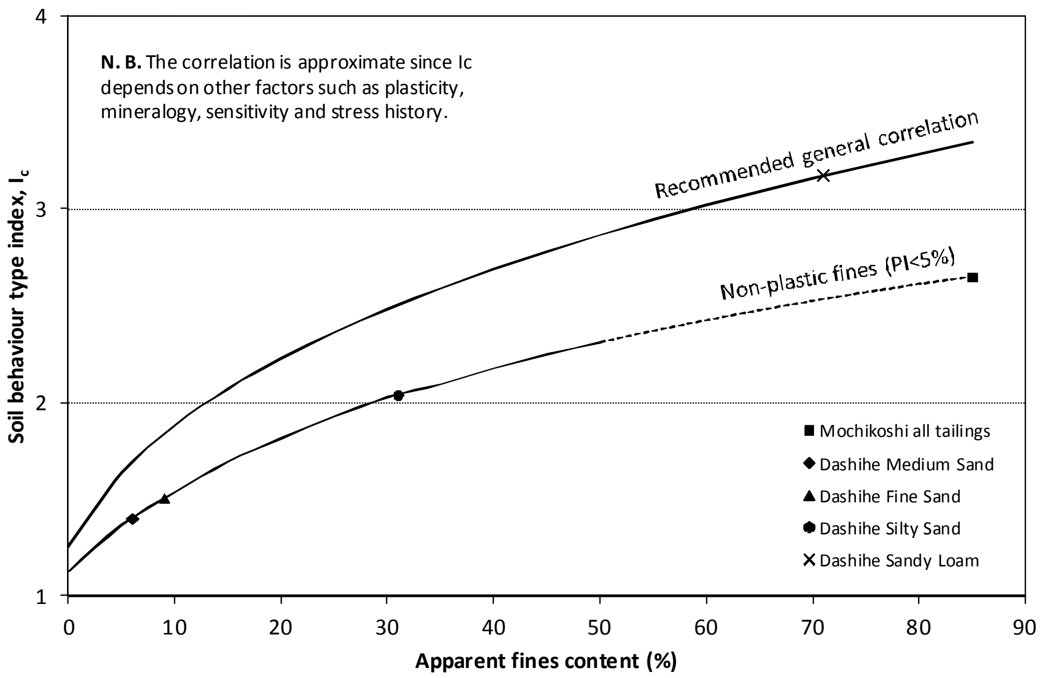

Figure 3.4 Correlations between I_c, *FC*, and *PI* used in this research (after Robertson and Wride, 1998a). Dashed curve indicates the extrapolation made in this study.

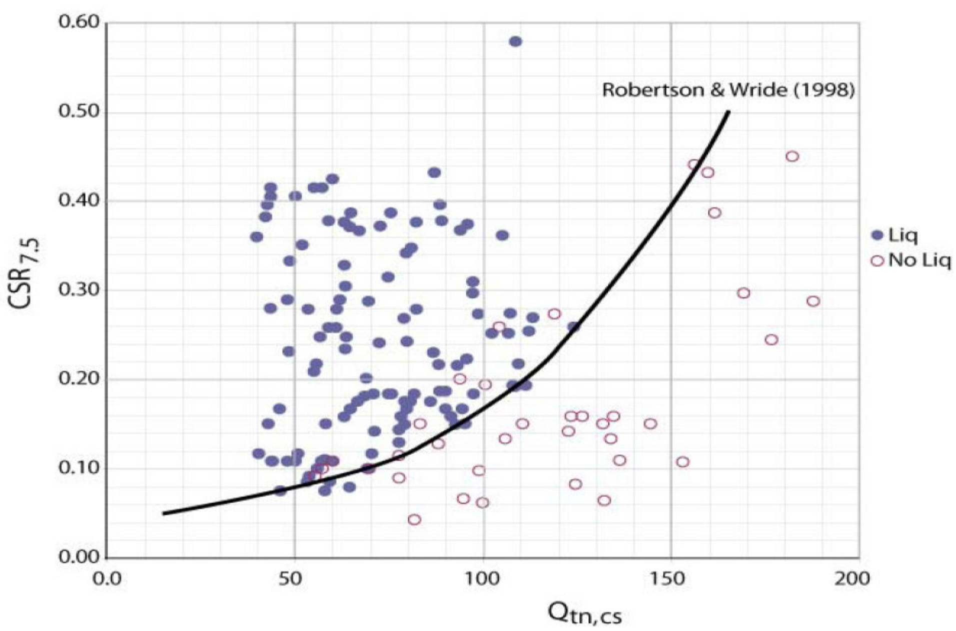

Figure 3.5 *CPT*-based liquefaction boundary curve (from Robertson 2009a.)

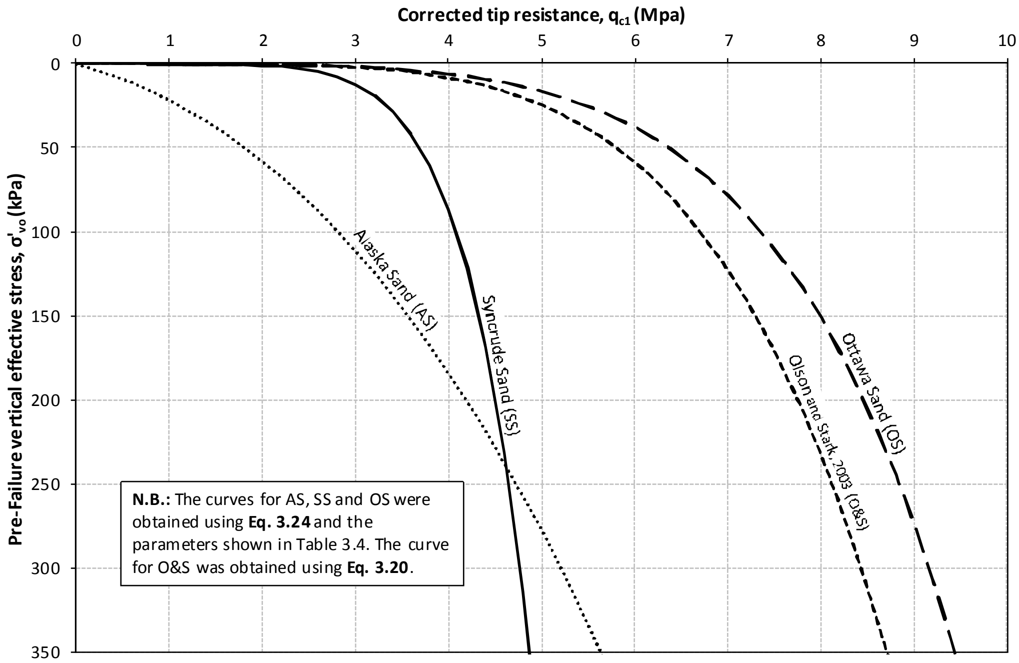

Figure 3.6 Comparison between Eqs. 3.20 and 3.24.

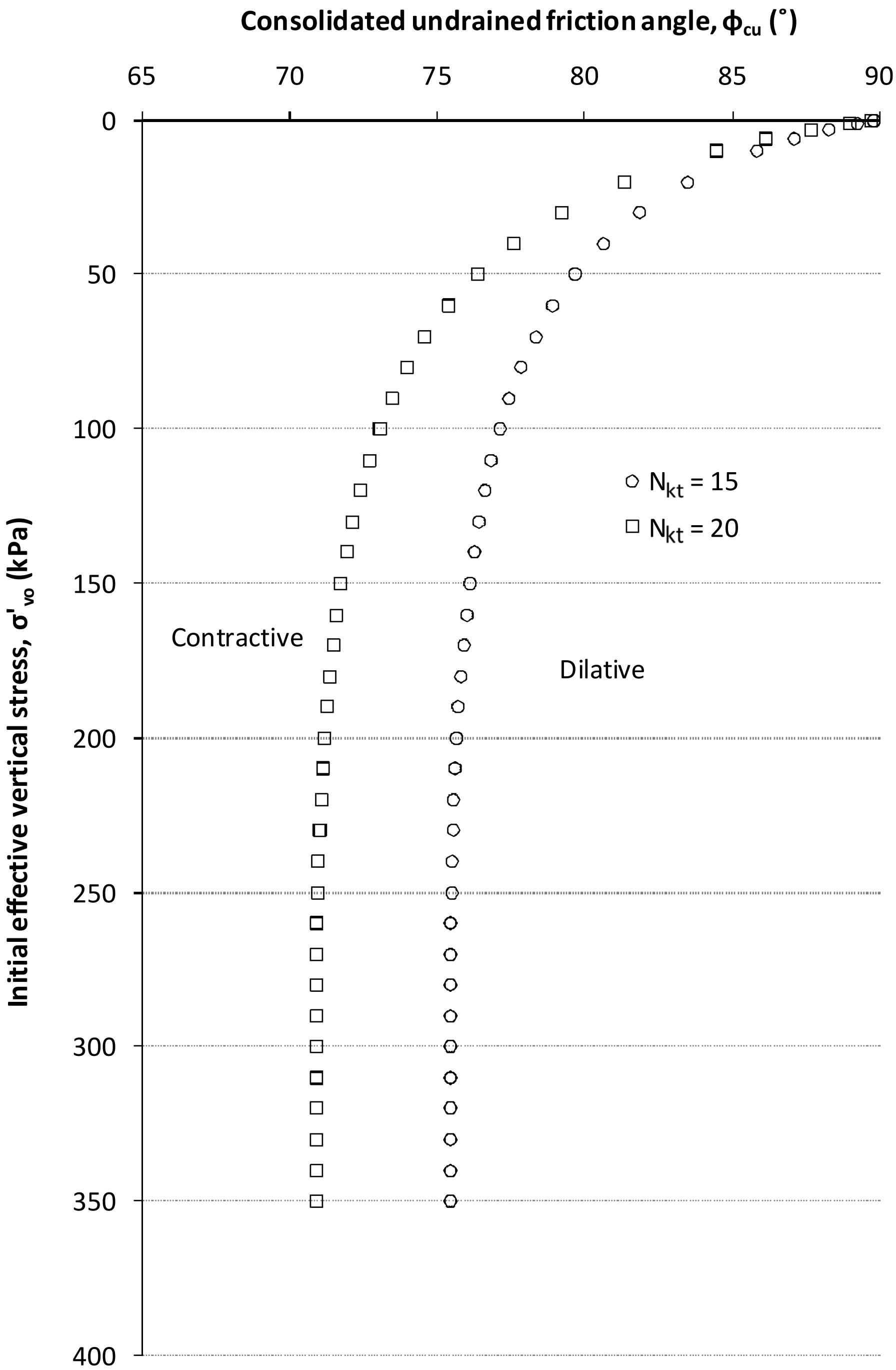

Figure 3.7 Contractive dilative boundary (Eq. 3.20) with q_{c1} converted into consolidated undrained friction angle (φ_{cu}).

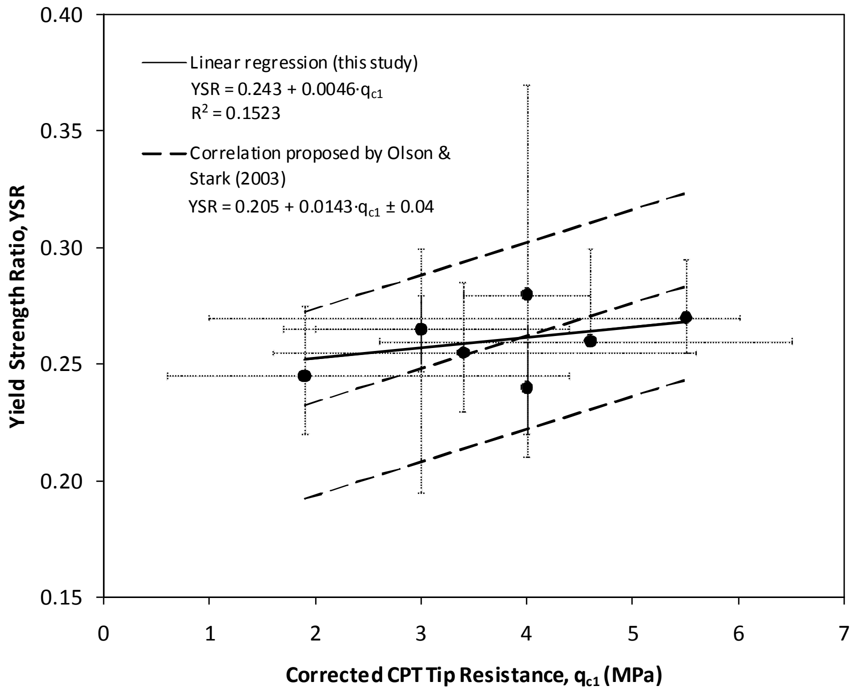

Figure 3.8 *YSR* vs. q_{c1} relationship suggested by Olson and Stark (2003) and linear regression obtained in this study.

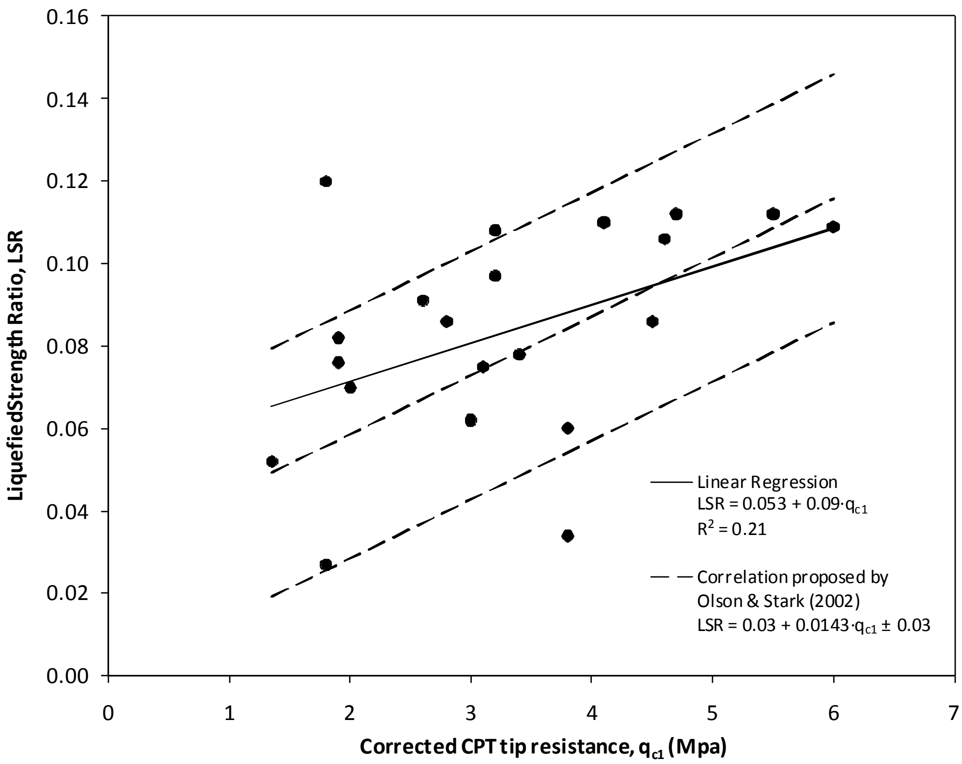

Figure 3.9 *LSR* vs. q_{c1} relationship suggested by Olson and Stark (2002) and linear regression obtained in this study.

4 Case Histories

4.1 Introduction

In order to assess the applicability of the two *CPT*-based liquefaction potential assessment methods to tailings dams, ten case histories (five of which exhibited flow failure) were analysed. Information on each of the following aspects was collected for each case history:

- *Loading characteristics:* For all case histories this implied knowledge of the pre-failure geometry of the tailings dam, unit weights of the soils involved and location of the water table. Additionally, for seismic case histories, earthquake moment magnitude (M_w) and peak acceleration (a_{max}) were also estimated.
- *CPT profiles:* Both the cone penetration resistance (q_c) and the sleeve friction (f_s) are of interest when applying the Robertson-based methodology, whereas only q_c is required to apply the Olson and Stark methodology. f_s readings have been reproduced here when available and necessary for the implementation of the methodologies. For instance, f_s readings are available in the literature for case histories Sullivan, Mooifontein and GMTS. However, since these case histories only involve static loads and thus the Robertson-based methodology was not applied to them, their f_s profiles have not been reproduced.
- *Grain size and plasticity:* For some case histories this was done through reported values of fines content (*FC*) and plasticity index (*PI*), but in other cases only a qualitative description was available.
- *Strength properties:* Effective friction angle (ϕ') and effective cohesion (c') are also reported.

A brief description of the case histories is presented in the following sections. Table 4.1 summarizes part of the information.

4.2 Hokkaido Dam – Japan, 1968

The Tokachi-Oki earthquake struck the northern Pacific coast of Japan on May 16, 1968. With a magnitude M_w = 8.0 (Kanamori, 2004) and a_{max} of 2.3 m/s^2, it caused 50 deaths, collapsed 676 buildings, and triggered 78 slope failures (Yoshimi and Akagi, 1968).

Liquefaction triggered a flow failure at a tailings dam in Hokkaido (Figure 4.1 and Figure 4.2). The events are described by Ishihara et al. (1990). Results of two *CPT* soundings performed at an intact location near the slide after the failure are shown in Figure 4.3. In accordance with the high water table shown in Figure 4.2 the water table was assumed to be at a depth of 1 m for both *CPT* soundings. No f_s readings were available for this case history.

Ishihara et al. (1990) describe the tailings as silty sand. Based on this description, Olson (2001) assumes *FC* = 50%. However, Jefferies and Been (2006) state that the low q_c values seem more representative of silt-sized grains than of a silty sand. The latter description was adopted in this research. No reports of actual *FC* or *PI* measurements were found in the literature.

A total unit weight (γ_t) of 19.8 kN/m^3 was reported for the tailings by Ishihara et al. (1990) and is adopted here. The location of the water table was taken as suggested by Ishihara et al. (1990) (Figure 4.2). Olson (2001) assumes that φ' of the tailings is between 30˚ to 35˚, and this same range was used in the current study. The starter dyke was not affected by the failure, so it was taken as impenetrable bedrock.

4.3 Mochikoshi Dam – Japan, 1978

The Izu-Ohshima-Kinkai earthquake struck the Izu peninsula of Japan on 14 January 1978. With a Richter scale magnitude M_L = 7.0[2], it caused 25 deaths and caused

[2] The Richter magnitude (M_L) is equal to $log_{10}(A)$, where A is the maximum amplitude (in µm) recorded by a standard seismometer at 100 km on the surface from the epicentre (Blight 2010).

extensive material damage (Okusa and Anma, 1980). In accordance with the M_L – M_w correlation suggested by Youd et al. (2001), an equivalent moment magnitude M_w = 7.7 was used here for this case history.

About 40 km away from the epicentre, a flow failure was triggered at the Mochikoshi tailings dam where three dykes had been built. Accounts are provided by Okusa and Anma (1980) and Ishihara et al. (1990). Dyke No. 1, the tallest, failed almost immediately after the earthquake struck, developing a breach 73 m wide and 14 m high through which approximately 80,000 m^3 of liquefied silver and gold tailings flowed between 7 km to 8 km down the valley and killed one person. Dyke No. 2, the second tallest, withstood the main shock but subsequently failed due to an aftershock on 15 January. Plan views and cross sections of both dikes are shown in Figure 4.4 and Figure 4.5, respectively. Given that acceleration estimates are only available for the main shock, and that there is great uncertainty on the prevailing pore water pressure conditions at the tailings dams when the aftershock struck, only the main shock was considered in this study.

Okusa and Anma (1980), report a_{max} values recorded at different locations around the epicentre. The maximum recorded horizontal acceleration was of 1 m/s^2, measured in the City of Ito, 26 km away from the epicentre. However, Okusa and Anma (1980) state that due to local amplification along the activated faults, horizontal accelerations as high as 4 m/s^2 could have occurred closer to the epicentre. Ishihara and Nagao (1983) report approximate contours of maximum horizontal acceleration derived from the analyses of overturned tombstones in cemeteries in the region. From these contours, maximum horizontal accelerations for Ito and Mochikoshi can be estimated as 2 m/s^2 and 2.5 m/s^2, respectively. Ishihara and Nagao (1983) hypothesize that the difference between these contours and the recorded accelerations is due to the different soil conditions of cemeteries and seismic stations. Most cemeteries were located on firm competent ground, whereas the Ito recording station was located on an alluvial deposit. Given that the Mochikoshi tailings dam was founded on volcanic rock (Okusa and Anma, 1980), i.e. similar foundation conditions to those of the cemeteries, a_{max} was taken as 2.5 m/s^2.

Ishihara et al. (1990) report q_c results of two soundings performed with a portable cone penetrometer on the intact part of the tailings impoundment adjacent to the failure scar

(Figure 4.6). Ishihara et al. (1990) and Okusa and Anma (1980) agree in that the depth where liquefaction occurred was between 6 m to 7 m. No f_s readings were available for this case study.

Okusa and Anma (1980) described the tailings as alternating layers of silt and sandy silt of 3 cm to 7 cm in thickness. They analysed a sample of tailings recovered from the valley below Dike No. 1 and determined *FC* = 85%. Since the tailings in the valley were composed of the intermixed layers of silt and sandy silt, this *FC* value was taken here as representative of the liquefied tailings involved in both dykes. The *PI* of the silt was reported as 10% and the sandy silt was described as non plastic. An average *PI* = 5% was used in this research as representative of the whole tailings deposit.

Ishihara et al. (1990) report that the tailings had an approximate γ_t of 17.6 kN/m^3. Okusa and Anma (1980) report that the γ_t of the dyke material for dykes 1 and 2 was 16.6 kN/m^3 and 15.1 kN/m^3, respectively. Jefferies and Been (2006) point out that no information is given in the literature regarding the position of the phreatic surface, however they suggest that it can be taken as near ground surface. Given that the Mochikoshi tailings dam was in operation when it failed, and that Okusa and Anma (1980) reported degrees of saturation of 100% for tailings recovered from both slides; the near ground surface assumption seems reasonable. Water table depths of 0 m and 2 m were considered in this research when performing the slope stability analyses for the Olson and Stark methodology and an average water table depth of 1 m was considered when implementing the Robertson-based methodology. As for shear strength parameters, Olson (2001) assumes that, due to their likely angular particle shape, the effective friction angle of the dyke material is 35˚; this value is adopted in the current study. No shear strength parameters for the impounded tailings are reported in the literature, thus a range of φ' of 30˚ to 35˚ was assumed here and the tailings were taken as cohesionless.

4.4 Dashihe Iron Tailings Dam – China, 1990

Amante (1993) presents a synthetic case history in which the finite element (FE) models TARA-3 and TARA-3FL are used to predict the performance of the major tailings dam at the Dashihe iron mine in China (Figure 4.7) in its 1990 configuration, subjected to the Tangshan earthquake of 28 July, 1976. Kanamori (1977) estimated the moment magnitude of the earthquake to be M_w = 7.5. Amante (1993), using an attenuation relationship, estimated the peak acceleration at the dam site to be around 1.2 m/s^2.

Admittedly, the reliability of a synthetic case history is not as good as that of a real one. However, two considerations have led to conclude that Amante's modelling of the problem was suitable for inclusion in this study. First, the main FE programme used by Amante, TARA-3 (Finn et al. 1986), had already been used by other researchers to successfully model the response of the Dashihe tailings dam, in its 1976 configuration, to the Tangshan earthquake and its Luanxian aftershock. And second, the input parameters of the FE model were of high quality, as they were drawn from comprehensive field and laboratory studies made on the Dashihe tailings, e.g. Gao et al. (1991) and Lee et al. (1992).

Amante performed both a triggering and post-triggering analysis to study the stability of the beach and outer wall of the Dashihe dam. His triggering analysis, which Amante refers to as 'seismic response analysis' and is implemented with the aid of the TARA-3 FE code, predicts that liquefaction can be expected to occur in the tailings that lie under the pond and in the beach area near the pond. As for the outer wall, the analysis only predicts the triggering of liquefaction in a very limited portion close to the crest of the starter dyke. The post-triggering analysis, which Amante refers to as 'post-liquefaction analysis' and is implemented with the aid of the TARA-3FL FE code, predicts that the tailings in the beach would exhibit flow failure and estimates deformations of 2 m to 13.5 m, i.e. a rather small flow. Since these tailings would flow downslope, deeper into the pond, the only consequence predicted is extensive cracking in the beach due to loss of support. The post-triggering analysis did not predict significant displacements in any portion of the outer wall.

Amante confirmed the results of the post-triggering analysis with a detailed pseudo-static analysis of the beach and outer wall. The pseudo-static analysis confirmed the occurrence of a flow failure in the beach tailings. As for the outer wall, given the more serious consequences that a flow failure of this portion of the dam would imply, the pseudo-static analysis considered the uncertainties in the response acceleration of the outer wall and the reduction in strength of a thin clay layer underlying the tailings. From the triggering analysis, Amante determined that the response acceleration of the tailings in the outer wall varied from 0.08 g to 0.24 g with an average of 0.13 g. Based on previously published experimental data he determined that the lower bound of the cyclic yield strength of clay could be taken as 80% of the static undrained strength. This last assumption is also consistent with more recent experimental data published by Boulanger and Idriss (2007). Considering these value ranges for response acceleration and clay weakening, Amante performed the pseudo static analysis for response accelerations ranging from 0.10 g to 0.17 g with increments of 0.01 g, and strength reductions of the clay layer of 5%, 10%, 15% and 20%. The resulting factors of safety varied from 0.87 to 1.3. The lowest response acceleration that led to a factor of safety smaller than 1.0 was 0.14 g and it occurred when considering a strength reduction of the clay layer of 20%. Given that the average response acceleration expected in the outer wall is 0.13 g and that the FE-based post-triggering analysis did not predict significant displacements in the outer wall, Amante concluded that flow failure of the outer wall was unlikely to occur.

Three *CPT* soundings were used in this research to characterize the beach tailings. Henian et al. (1990) present average f_s values of these three *CPT* soundings and Lee et al. (1992) present the corresponding continuous q_c profiles (Figure 4.9 and Table 4.2). Four *CPT* soundings were used in this research to characterize the tailings on and underneath the outer wall. Continuous q_c profiles of the four soundings are presented by Lee et al. (1992) (Figure 4.10). No f_s readings are available for the outer wall.

FC and *PI* information for the tailings on the outer wall zone was collected to enable calculation of the soil type index (I_c). Amante (1993) shows a cross sectional cut of the outer wall illustrating the location of the different soil layers as inferred from collected samples. The four *CPT* outer wall soundings were approximately located on this cut to determine the types of soils penetrated during each test. The *FC* and *PI* of each one of these types of soils was reported by Lee et al. (1992) and were used in this research. Table 4.3 shows the different soil types that were involved in each outer wall sounding and Table 4.4 shows the characteristic *FC* and *PI* values of the different soil types.

Average values of γ_t of 19.6 kN/m^3 and 15.9 kN/m^3 are reported for the tailings below and above the water table, respectively. Figure 4.8 shows the location of the phreatic surface adopted in this research based on Amante (1993). Lee et al. (1992) also reported the location of the water table for the different *CPT* soundings. For the beach soundings I8, I9 and II6, the water table was located at depths of 27 m, 17.5 m, and 23.5 m respectively. For the outer wall soundings I4, I5, II2, and II4, the water table was located at depths of 12.5 m, 16 m, 4 m, and 16 m respectively. Average values of φ' of 37˚ and 39˚ were reported for the tailings below and above the water table, respectively. All tailings were reported as cohesionless. Amante (1993) reports that the tailings are underlain by clay with γ_t = 18.9 kN/m^3 and a total strength parameter *c* = 164 kPa.

4.5 Sullivan Tailings Dam – Canada, 1991

Accounts for this case history have been obtained from Davies (1999) and Jefferies and Been (2006). Due to the overlap in the information presented by these authors, references will only be provided when specific information is reported by only one of the sources. The Sullivan tailings dam is located in the Canadian province of British Columbia. On 23 August 1991 a 300 m section of the 21 m high dyke slumped suddenly, causing a predominantly horizontal displacement of up to 45 m in the toe region. Despite these downstream movements, and the involvement of 75,000 m^3 of tailings, the failure did not have major economic or environmental consequences, nor did it cause loss of human lives because the involved tailings slid into an adjacent siliceous pond. Given that: the failure occurred as a 2.4 m raise was being placed, it happened quickly, and sand boils were observed after the failure; it was concluded that this was a case of static liquefaction. Figure 4.12 illustrates the pre- and post-failure geometry of the tailings dam. Davies (1999) states that although the 2.4 m rise and dynamic loads due to construction equipment may have contributed to trigger liquefaction, there is stronger evidence indicating that failure would have occurred even if the raise had not been built nor dynamic loads been present. Consequently, the 2.4 m raise was not included in the slope stability analyses made in this research.

Jefferies and Been (2006) published q_c results of six *CPT* soundings (Figure 4.11) made through the failed soil mass beneath the original location of the dykes. Three of these soundings were made on the crest of the dam, at the location marked as CP91-29 on Figure 4.12, and the other three were made on the toe of the dam, at the location marked as CP91-31 on Figure 4.12. These six q_c profiles were used in this research to characterise the tailings. Reports in the literature indicate that liquefaction took place on the old iron tailings on which the dyke was founded, at an approximate depth of 10 m to 12 m of the soundings performed on the crest (Figure 4.12).

The tailings are described as fine-grained, with *FC* = 50% or more, classified as non-plastic silt or silty fine sand. Jefferies and Been (2006) reported γ_t of 22.4 kN/m^3 and 24.0 kN/m^3 for the compacted fill (dyke material) and iron tailings respectively. They also report that standpipe piezometers that had been operating at the site before the failure indicate that the water table was 'generally within a few feet of ground surface' and 'above ground level at the dyke toe', but that a declining trend had been detected a month before the failure. Accordingly, a rather high water table was used here in the slope stability models (Appendix B). As for the position of the water table after the failure when the *CPT* soundings were performed, Jefferies and Been (2006) show data indicating that for the sounding CP91-29, the water table was located 2 m below ground surface. No information was found in the literature regarding the location of the water table for the other five soundings, therefore a water depth of 2 m was assumed throughout the six soundings. The references do not provide any estimation of the shear strength parameters of the soils involved in the failure, therefore strength parameters had to be assumed in the slope stability models. The tailings were taken as cohesionless and with φ' varying between 30˚ to 35˚. The dyke material was assumed to have either c' = 5 kPa and φ' = 30˚, or c' = 15 kPa and φ' = 35˚.

4.6 Merriespruit gold tailings dam – South Africa, 1994

The failure of the 31 m high northern outer wall of a gold tailings dam upslope of Merriespruit, a suburb of the town of Virginia, South Africa, took place in 22 February 1994. The failure resulted in a breach of approximately 600,000 m^3 of gold tailings that caused the death of 17 people, extensive destruction of property and environmental damage (Wagener et al. 1997). The conditions leading to the failure have been studied in detail by several authors. Fourie and Papageorgiou (2001) performed a series of *CU* triaxial compression loading tests on re-constituted Merriespruit tailings to determine the steady state line of four different particle size distributions. Comparing these steady state lines and the behaviour of undisturbed samples, Fourie et al. (2001) concluded that the failure had occurred due to static liquefaction of the impounded tailings. Wagener et al. (1997), Wagener et al. (1998), and Strydom and Williams (1999) present conclusive evidence pointing at overtopping during rainfall, and the resulting erosion, as the triggering mechanism of the failure. The accepted sequence of events (Figure 4.13) is that overtopping at a section of the dam caused considerable erosion of the outer wall, and triggered a series of retrogressive slope failures that left the impounded tailings without confinement. Under this scenario, the impounded tailings were subjected to a static shear stress large enough to trigger liquefaction.

The cone penetration resistance results of five *CPT* soundings (Figure 4.14) made on the beach, close to the failure scar, between 22 and 35 days after the failure were obtained from the files of Jones and Wagener Consulting Civil Engineers (J&W), a firm that conducted an investigation to determine the causes of the failure. For one of the soundings (J&WWEST1 - Figure 4.14), the entirety of the tailings penetrated was above the water table. The implication for this sounding is that, despite possible capillary effects, these tailings were probably not saturated and therefore were not prone to liquefaction. However, the results of this sounding have been included here to help characterize the penetration resistance of the tailings.

Fourie et al. (2001) reported that the grain size distribution of the tailings varied considerably throughout the impoundment. They determined the grain size distribution of 41 samples obtained from different locations around the failure scar and found that the *FC* varied from 40% to 100%. Regarding plasticity, Wagener et al. (1998) reported the existence of distinct layers of non-plastic and moderately plastic slimes with *PI* varying between 1% and 8%. Papageorgiou (2004) described the Merriespruit tailings as a non plastic cohesionless material. His description is consistent with the low plasticity indices reported by Wagener et al. (1998).

Strydom and Williams (1999) indicate that the *in situ* γ_t of the impounded tailings was close to 20 kN/m^3. They also use a satellite image to show that at least three weeks before the failure, the pond was already lying against the section of the outer wall that eventually failed. Based on this observation, high water table conditions (Figure 4.15) were assumed in this research for the slope stability analyses. Shear strength parameters of the tailings were determined by J&W through a series of stability back analyses. The tailings were found to be cohesionless and with φ' = 39˚. The natural soil was reported to have c' = 40 kPa and φ' = 40˚.

4.7 GMTS and Mooifontein dams at the Crown Tailings Complex – South Africa, 2001

The Crown Tailings Complex is located in Johannesburg, South Africa and is comprised of four tailings dams (Figure 4.17). The stability of these tailings dams is of great relevance due to their proximity to large residential areas, major highways and a stadium with a capacity of up to 90,000 spectators. In 2001, a study (WM&B, 2001) was made to assess the stability, and general state of the tailings, of two of the dams of the Crown Complex, namely GMTS dam and Mooifontein dam. This study is the sole reference for this case history. To date, none of the tailings dams of the Crown Complex have exhibited any indications of being near failure or any manifestation of liquefaction.

Two *CPT* soundings were available for each dam. The resulting q_c profiles are shown in Figure 4.16. The soundings were made on the outer wall along cross sections G5 and M4 (Figure 4.17, Figure 4.18, and Figure 4.19). These cross sections were selected for study by WM&B (2001) because in previous investigations the state of the tailings in these sections had been identified as being of concern.

The tailings of both dams are broadly divided into historic and recent. The former were deposited between the 1930s and 1960s and the latter between the 1980s until current date. Mining activities ceased between the 1960s and 1980s. The post 1980 tailings originate from remining and reprocessing other nearby tailings deposits. Grain size distribution analyses were available for the historic and recent tailings of both dams. *FC* varied broadly from 35% to 83%. No information regarding the plasticity of the tailings was available.

Total unit weight was estimated from samples retrieved from different depths from both tailings dams. An average value of γ_t = 19 kN/m^3 was adopted in this research. The γ_t of the natural soil in the foundation was reported as 18 kN/m^3. The location of the water table (Figure 4.18 and Figure 4.19) was determined for both dams from standpipe piezometer and *CPT* pore pressure measurements. Shear strength parameters were determined from *CU* triaxial loading tests made on disturbed samples retrieved from different depths. The samples were tested at void ratios similar to the *in situ* void ratios as determined from shear wave velocity measurements. All tailings were reported to be cohesionless, the recent tailings exhibited φ' = 39˚, and the historic tailings exhibited φ' = 40˚. Given that recent and historic tailings have identical unit weight and very similar strength properties, they were treated in this study as a single soil type. The natural foundation soil was reported to have c' between 7 to 15 kPa and φ' between 34˚ to 37.5˚.

4.8 Dam A – Brazil, 2009

Neto (2009), the sole reference for this case study, describes a Brazilian tailings dam referred to as Dam A. Neto (2009) uses Olson's methodology to assess the effect of the construction of a 3.5 m rise on the outer wall on the liquefaction potential of Dam A (Figure 4.20). The rise was built and, consistent with Neto's (2009) analysis, liquefaction was not triggered. The cross section of Dam A is shown in Figure 4.20. The date on which the rise was built is not mentioned in the reference, so this case history has been assigned the year of Neto's publication.

As a worst case scenario, the assumption made to investigate the slope stability of Dam A was that the construction of the 3.5 m rise would induce a fully undrained loading in the tailings below the water table. Under such condition, the construction of the 3.5 m rise would cause an increase in the total principal stresses $\Delta\sigma_1$ and $\Delta\sigma_3$ which would in turn cause an increase in pore water pressure Δu. The magnitude of Δu would depend on the magnitudes of $\Delta\sigma_1$, $\Delta\sigma_3$ and the Skempton pore water pressure parameters *A* and *B*. In order to calculate $\Delta\sigma_1$ and $\Delta\sigma_3$, the cross section of the 3.5 m rise was converted to a rectangular geometry with the same breadth (21.4 m) and same total area (50.6 m^2). The resulting rectangle had a height of 2.4 m and, considering that the γ_t of the dyke material is 17.7 kN/m^3, applies a uniform strip load of 42 kN/m^2 on the beach surface. The values of $\Delta\sigma_1$ and $\Delta\sigma_3$ caused by this strip at the depths corresponding to the location of the water table were calculated from a principal stress distribution chart that considers strip loads (Lambe and William 1969). As for the Skempton parameter *A*, its average value at failure (A_f) was found to be 0.54 from the results of undrained triaxial tests published by Neto (2009). Skempton's parameter *B* was taken as 1 as is usually the case in saturated soils. The values of Δu were then converted into equivalent pressure heads by dividing by the unit weight of water and the water table was raised a height equal to the pressure head. The resulting water table is shown in Figure 4.21 and the calculations are shown in detail in Appendix B.

No *CPT* results were available for this case study, so q_c values were inferred from three *SPT* soundings made on the tailings beach close to the outer wall. To accomplish this, the q_c-N_{60}-D_{50} correlation proposed by Stark and Olson (1995) was used here. N_{60} is the *SPT* blow count normalised to a 60% energy ratio and D_{50} is the median grain size. Table 4.5 to Table 4.7 show the N_{60}, D_{50}, q_c/N_{60} and q_c values for the three *SPT*s. N_{60} values were calculated from the reported *N* values and a 70% energy efficiency suggested by Neto (2009). D_{50} values were calculated from grain size distribution analyses made on the samples recovered from the *SPT*s. Based on the *SPT* profiles and the contractive-dilative boundary proposed by Olson and Stark (2003) (*SPT* equivalent of Eq. 3.16 in this work), Neto (2009) divided the impounded tailings into two distinct layers with the boundary at an elevation of 1089.4 m (Figure 4.20). Reportedly, the upper layer is liquefiable, whereas the lower layer is non-liquefiable. Such distinction was also used in some of the scenarios considered when analysing the stability of Dam A in this work (Appendix B). The water table was only encountered in one of the *SPT* soundings (SP-05) at 1 m below the ground surface. The two other soundings, despite having tested tailings above the water table and therefore not prone to liquefaction, are included here to help characterize the penetration resistance of the tailings.

FC was calculated from the samples recovered from the *SPT*s and varied from 54% to 81%. All samples were classified as cohesionless and had *PI* values that varied from 0% to 3%, i.e. non-plastic for practical purposes. *FC* and *PI* values are presented in Table 4.5 to Table 4.7.

The γ_t of the tailings (22.8 kN/m^3) and the outer wall material (17.7 kN/m^3) were determined from samples recovered from superficial boreholes on the beach and from experience with similar materials, respectively. The water table was located through the instrumentation installed on the tailings dam. *CU* triaxial loading tests were also performed on the samples recovered from the superficial boreholes on the beach. The samples were tested at relative densities (D_r) of 25%, 30% and 40%, and for each density the tests were made at isotropic consolidation stresses of 50 kPa, 100 kPa, 200 kPa and 400 kPa. Neto (2009) states that the in situ D_r of the tailings, as estimated from $(N_1)_{60} = 44 \cdot D_r^2$, falls within the range used for the triaxial tests and thus determines the *in situ* shear strength of the beach tailings from the triaxial tests results. The shear strength parameters of the outer wall were estimated from experience with similar materials. Figure 4.20 shows the total unit weights, location of the water table and shear strength parameters reported by Neto (2009).

4.9 Concluding Remarks

Ten seismic case histories have been described in this chapter. Half involve only static loads and the other half involve seismic loads. Also, half of the case histories exhibited flow failures, while the other half constitutes non-failure case histories. Two of the case histories, namely Mooifontein and GMTS tailings dams, had not been reported before in technical literature. The Robertson-based methodology will be applied to the five seismic case histories, whereas the Olson and Stark methodology will be applied to all ten case histories. The results are presented in Chapter 5.

4.10 Tables and figures

Table 4.1 Summary of case histories.

Tailings Dam	Year	Trigger: Static or Seismic?	Flow Failure?	Earthquake Magnitude (M_w)	a_{max} (m/s^2)	CPT readings in literature		
						q_c	f_s	u
Hokkaido	1968	Seismic	Yes	8.0	2.3	Yes	No	No
Mochikoshi 1	1978	Seismic	Yes	7.7	2.5	Yes	No	No
Mochikoshi 2	1978	Seismic	No	7.7	2.5	Yes	No	No
Dashihe Beach	1990	Seismic	Yes	7.5	1.2	Yes	Yes	No
Dashihe Outer Wall	1990	Seismic	No	7.5	1.2	Yes	No	No
Sullivan	1991	Static	Yes	--	--	Yes	Yes[a]	Yes[a]
Merriespruit	1994	Static	Yes	--	--	Yes	No	Yes[a]
GMTS	2001	Static	No	--	--	Yes	Yes[a]	Yes[a]
Mooifontein	2001	Static	No	--	--	Yes	Yes[a]	Yes[a]
Dam A	2009	Static	No	--	--	No	No	No

a. Readings not reported in this work.

Table 4.2 Average f_s values of *CPT* soundings made through the Dashihe dam beach (After Henian et al. 1990).

CPT Sounding	Depth of layer (m)	Average f_s (kPa)
I8	0.0 - 5.0	15
	5.0 - 10.6	36
	10.6 - 17.4	65
	17.4 - 21.0	102
	21.0 - 31.4	93
I9	0.0 - 2.3	6
	2.3 - 9.4	26
	9.4 - 15.0	56
	15.0 - 24.1	55
	24.1 - 31.5	50
II6	0.0 - 4.5	9
	4.5 - 8.1	22
	8.1 - 16.0	30
	16.0 - 20.4	46
	20.4 - 28.0	58
	28.0 - 33.5	68

Table 4.3 Soil types penetrated by the *CPT* soundings on the Dashihe dam outer wall (after Amante 1993).

CPT Sounding	Thickness of layer (m)	Soil type
I4	11.0	Medium sand
	12.5	Fine sand
	4.5	Silty sand
	2.0	Sandy loam
I5	24.0	Medium sand
	4.0	Fine sand
	3.5	Sandy loam
II2	16.0	Fine sand
	5.0	Silty sand
II4	24.0	Medium sand
	4.0	Fine sand
	3.5	Sandy loam

Table 4.4 Characteristic *FC* and *PI* values of the soils penetrated by the *CPT* soundings on the Dashihe dam outer wall (after Lee et al. 1992).

Soil type	FC (%)	PI (%)
Medium sand	6	0
Fine sand	9	0
Silty sand	31	0
Sandy loam	71	8.6

Table 4.5 Data of the SP-01 sounding made on the beach of Dam A (after Neto 2009).

Depth (m)	N_{60}	D_{50}[a] (mm)	q_c/N_{60}[b] (MPa/blow/ft)	q_c (MPa)	FC (%)	PI (%)
1	1.2			0.4		
2	2.3			0.7		
3	10.5			3.3		
4	5.8			1.8		
5	7.0			2.2		
6	14.0	0.064	0.31	4.3	59	N/A
7	23.3			7.2		
8	12.8			4.0		
9	2.3			0.7		
10	33.8			10.5		
10.45	26.8			8.3		

a. D_{50}, FC and PI were estimated from samples extracted at depths of 3.2 m, 6.2 m and 9.2 m.

b. q_c/N_{60} was estimated according to the correlation proposed by Stark and Olson (1995).

Table 4.6 Data of the SP-03 sounding made on the beach of Dam A (after Neto 2009).

Depth (m)	N_{60}	D_{50}[a] (mm)	q_c/N_{60}[b] (MPa/blow/ft)	q_c (MPa)	FC (%)	PI (%)
1	2.3			0.7		
2	3.5			1.1		
3	4.7			1.4		
4	3.5			1.1		
5	2.3			0.7		
6	3.5	0.053	0.3	1.1	81	0
7	9.3			2.8		
8	11.7			3.5		
9	10.5			3.2		
10	32.7			9.8		
10.45	26.8			8.1		

a. D_{50}, FC and PI were estimated from a sample extracted at depth of 10.2 m.

b. q_c/N_{60} was estimated according to the correlation proposed by Stark and Olson (1995).

Table 4.7 Data of the SP-05 sounding made on the beach of Dam A (after Neto 2009).

Depth (m)	N_{60}	D_{50}[a] (mm)	q_c/N_{60}[b] (MPa/blow/ft)	q_c (MPa)	FC (%)	PI (%)
1	2.3	0.065	0.31	0.7	60	0
2	3.5	0.066	0.31	1.1	54	3
3	4.7			1.4		
4	7.0	0.045	0.29	2.0	70	3
5	2.3			0.7		
6	2.3	0.047	0.29	0.7	73	2
7	24.5			7.1		
8	5.8	0.065	0.31	1.8	57	0
9	31.5			9.8		
10	29.2			9.0		
10.45	18.7			5.8		

a. D_{50}, FC and PI were estimated from a samples extracted at depths of 1.2 m, 2.2 m, 4.2 m, 6.2 m and 8.2 m.

b. q_c/N_{60} was estimated according to the correlation proposed by Stark and Olson (1995).

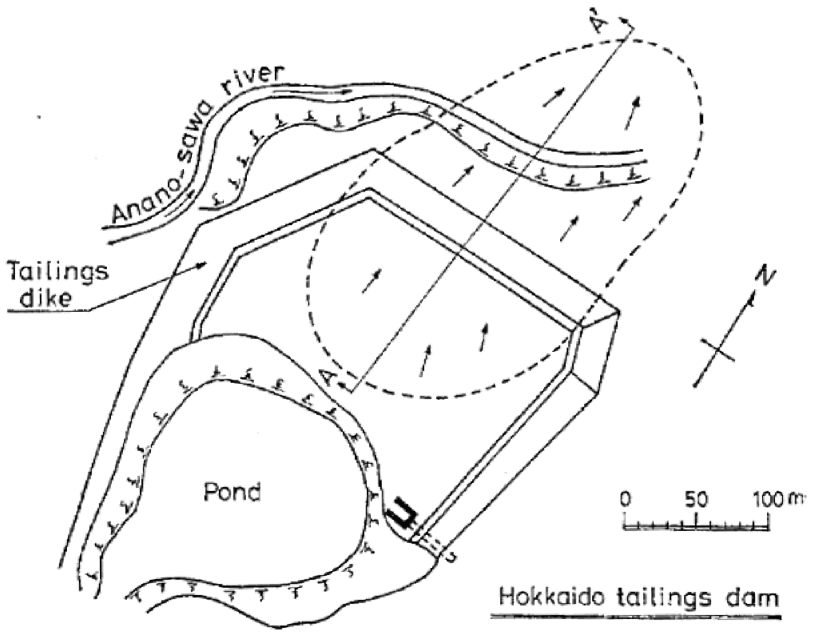

Figure 4.1 Plan view of Hokkaido tailings dam with flow failure outlined (from Ishihara et al. 1990).

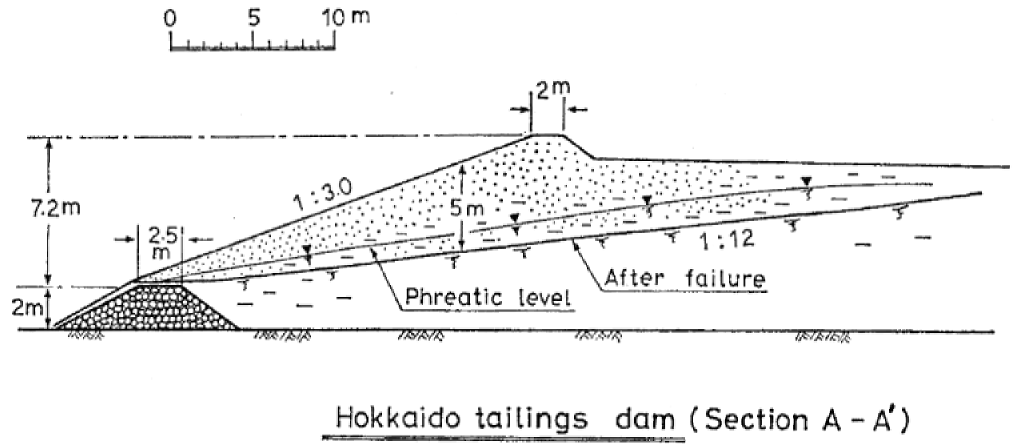

Figure 4.2 Cross section of Hokkaido tailings dam with pre and post-failure geometry (from Ishihara et al. 1990).

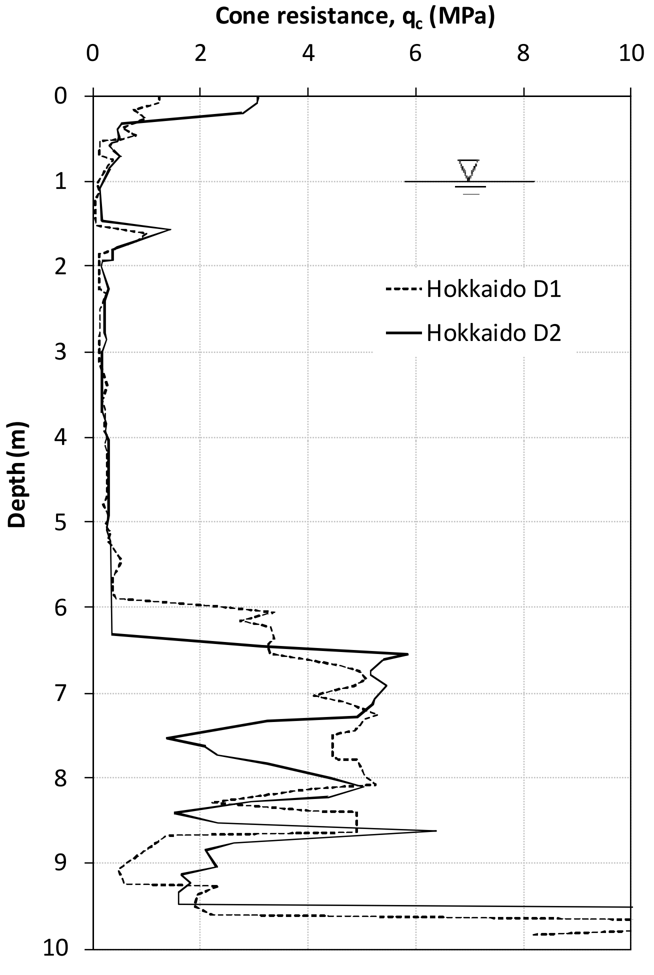

Figure 4.3 Dutch cone penetration resistance at Hokkaido tailings dam (after Ishihara et al. 1990).

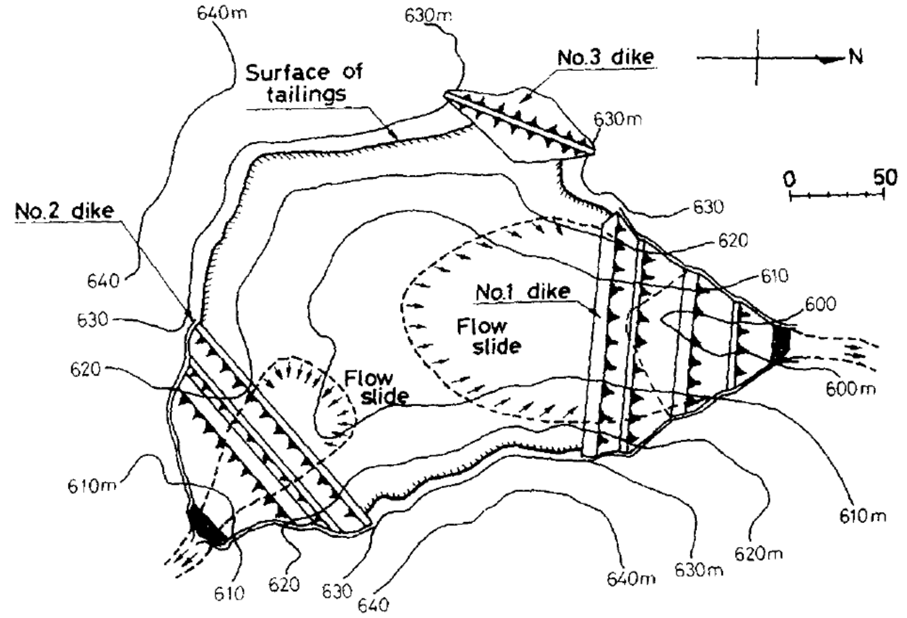

Figure 4.4 Plan view of the Mochikoshi tailings dam (from Okusa and Anma 1980).

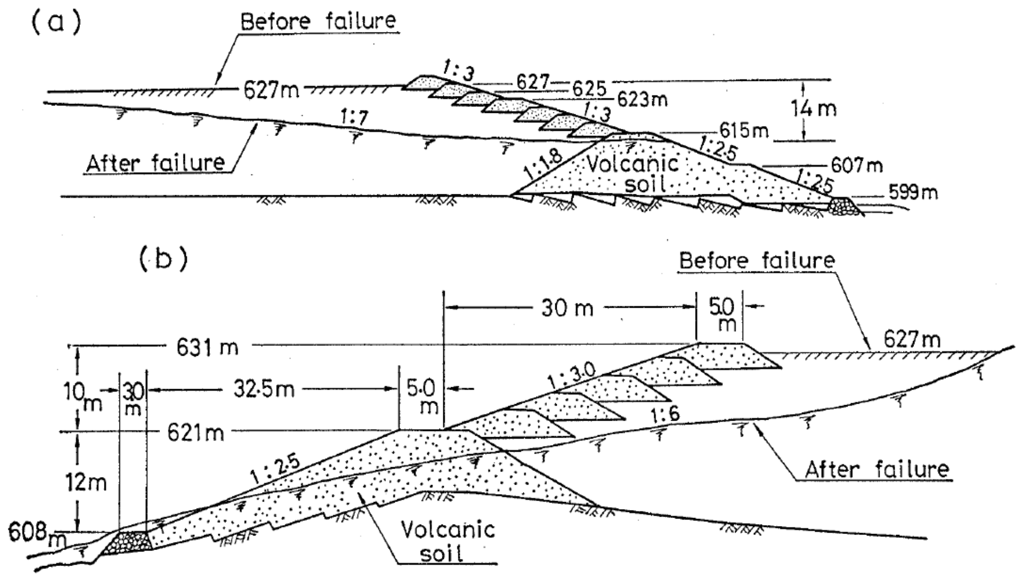

Figure 4.5 Pre and post-failure geometry of dikes 1 (upper) and 2 (lower) of the Mochikoshi tailings dam. (from Ishihara et al. 1990).

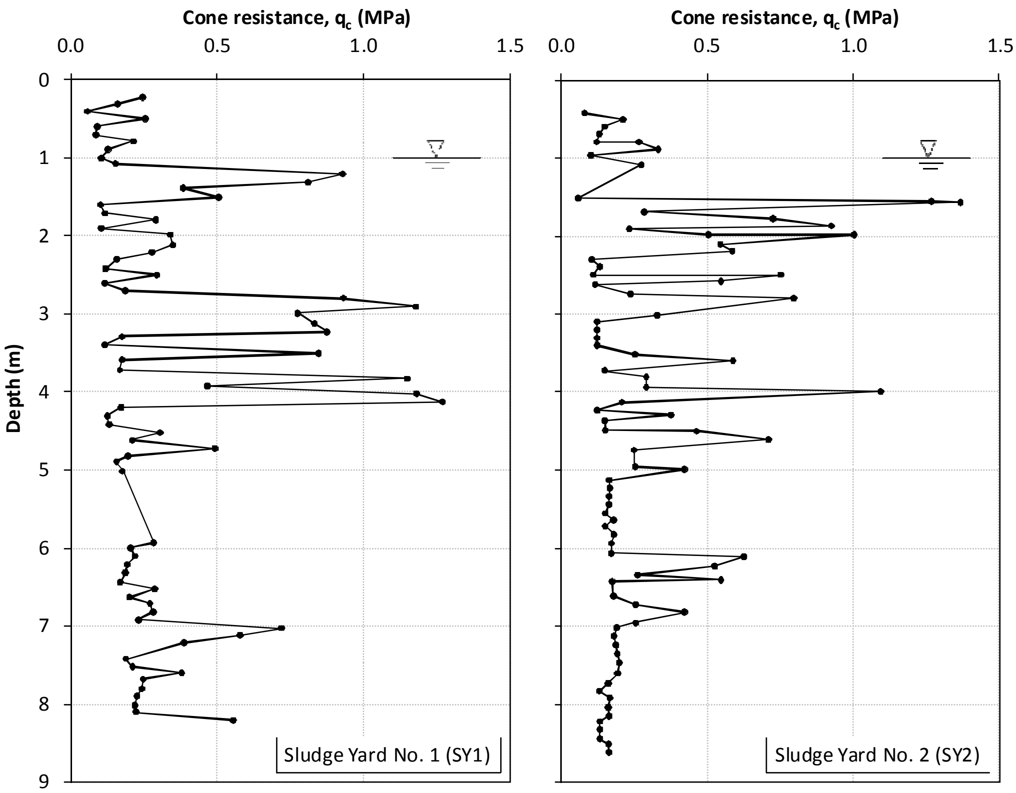

Figure 4.6 Double tube cone penetration test at Mochikoshi tailings dam. Sludge yard No. 1 (left) and sludge yard No. 2 (right). (After Ishihara et al. 1990).

Figure 4.7 Aerial view of the Dashihe tailings dam in its 2011 configuration (Image from Google Earth ™).

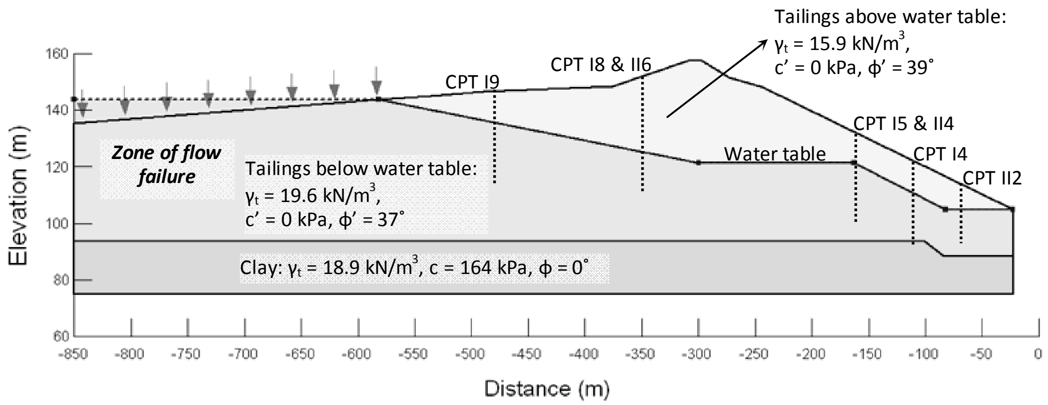

Figure 4.8 Pre-failure geometry of the Dashihe tailings dam and approximate location of the *CPT* soundings (After Amante 1993).

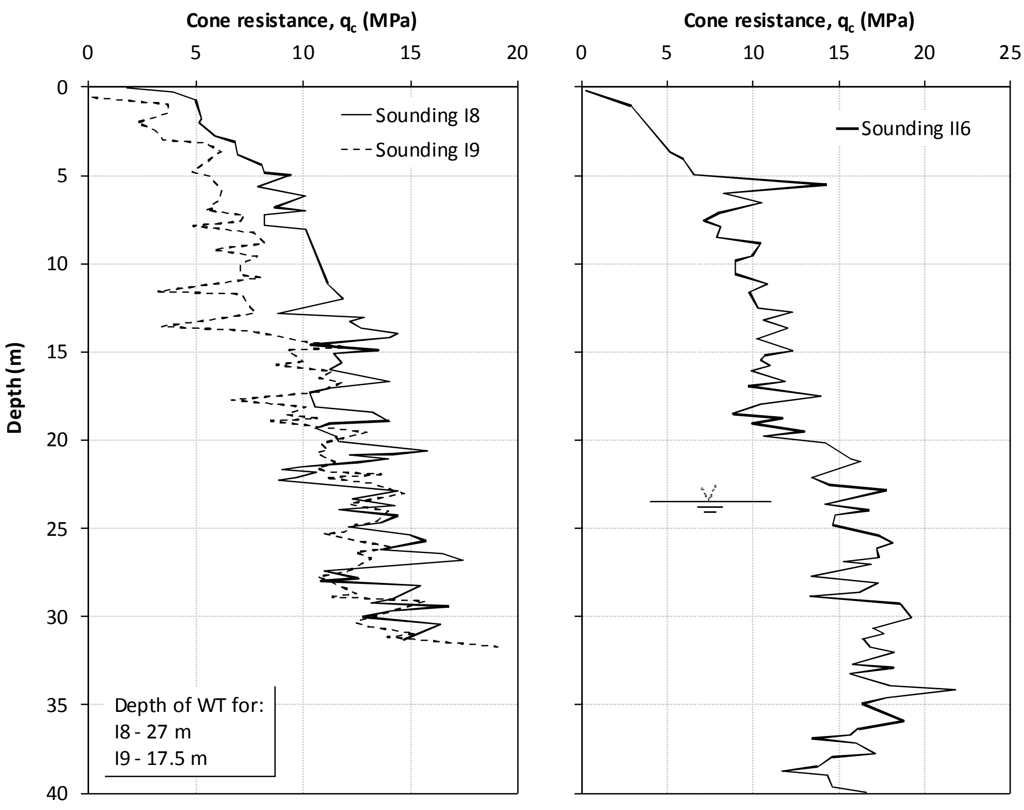

Figure 4.9 *CPT* soundings through the beach of Dashihe tailings dam (After Lee et al. 1992).

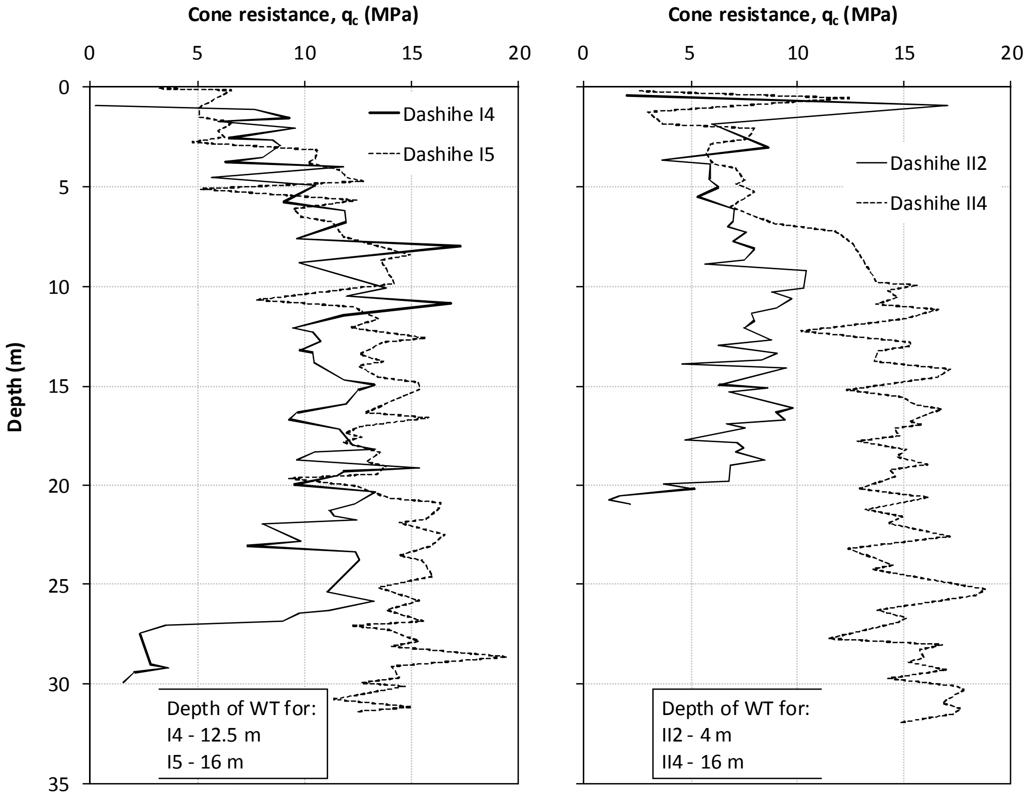

Figure 4.10 *CPT* soundings through the outer wall of Dashihe tailings dam (After Lee et al. 1992).

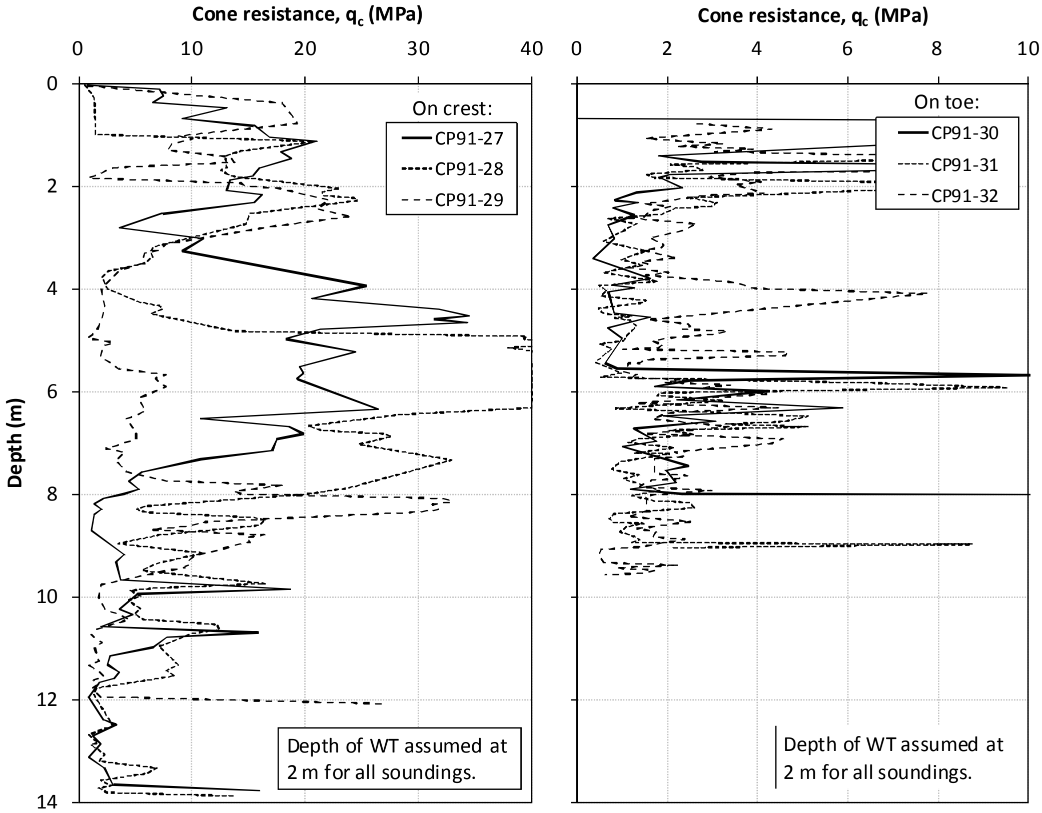

Figure 4.11 Cone penetration resistance (q_c) profiles obtained at the crest and toe of the Sullivan tailings dam (Replotted from Jefferies and Been 2006).

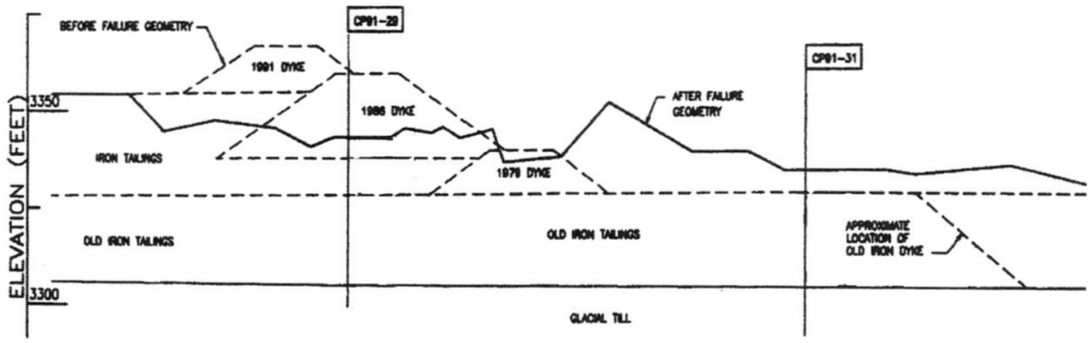

Figure 4.12 Pre and post-failure geometry of the Sullivan tailings dam and location of two *CPT* soundings (from Jefferies and Been 2006).

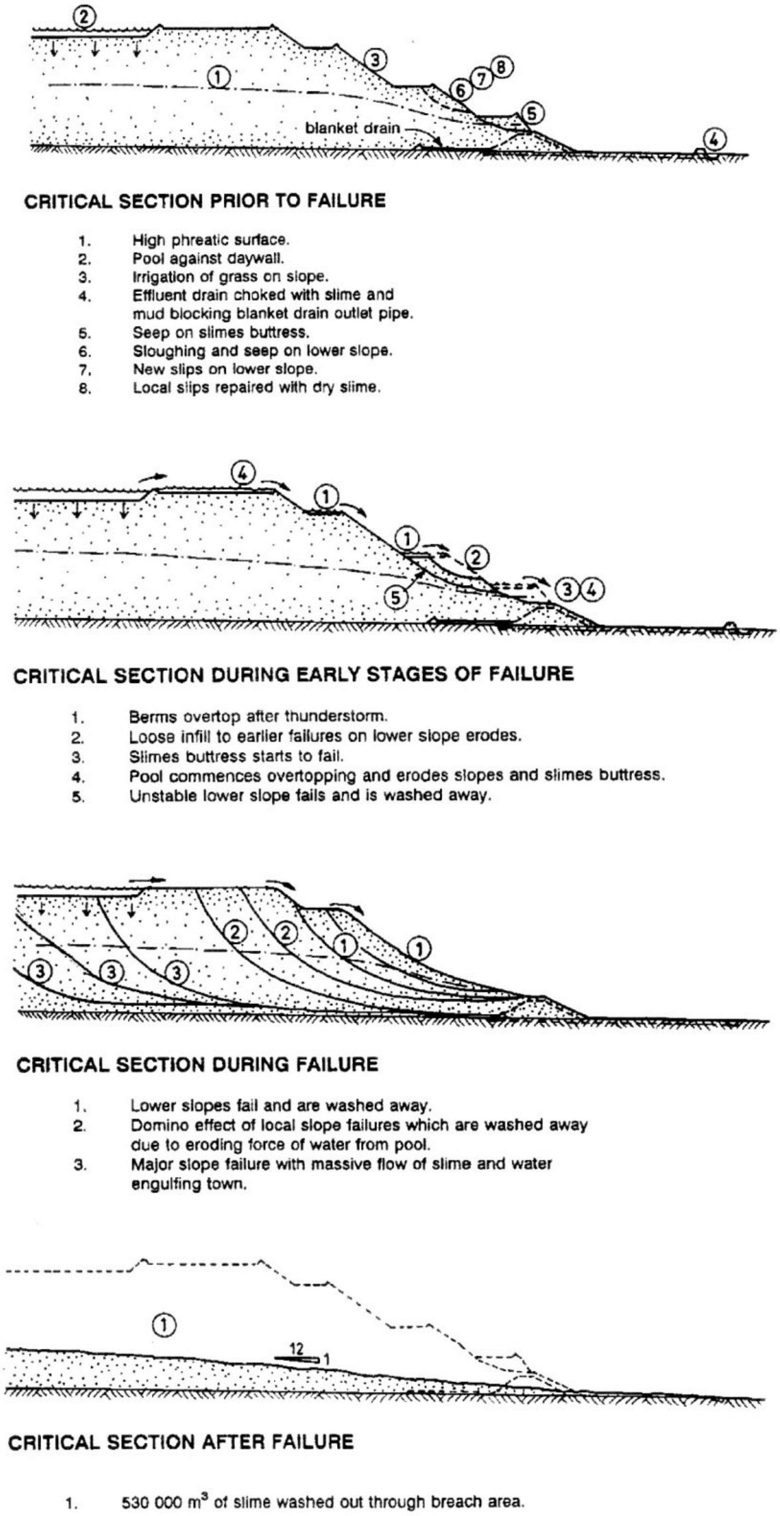

Figure 4.13 Most likely sequence of failure of the Merriespruit tailings dam (from Papageorgiou 2004).

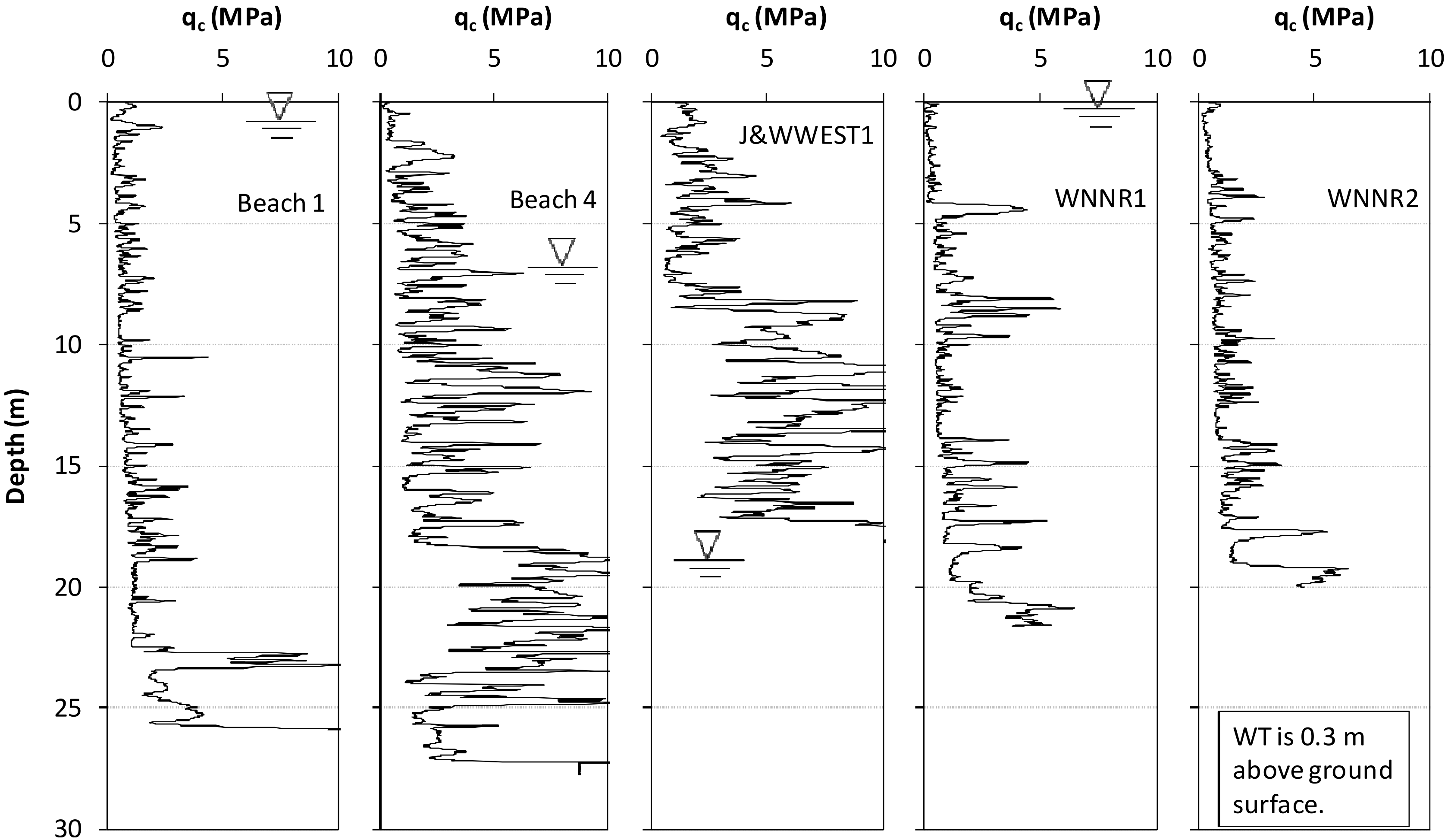

Figure 4.14 Cone penetration resistance (q_c) profiles of *CPT* soundings made on the beach of the Merriespruit tailings dam.

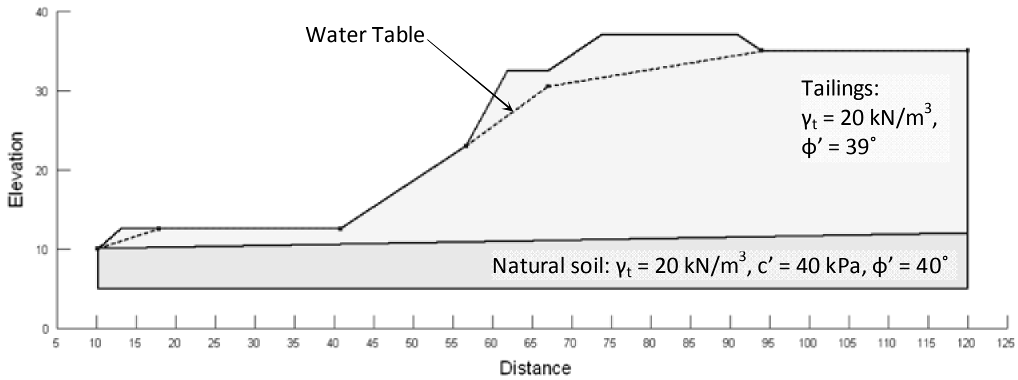

Figure 4.15 Fourth stage of retrogressive failure in Merriespruit Tailings Dam as modelled by Jones & Wagener Consulting Civil Engineers (from J&W files).

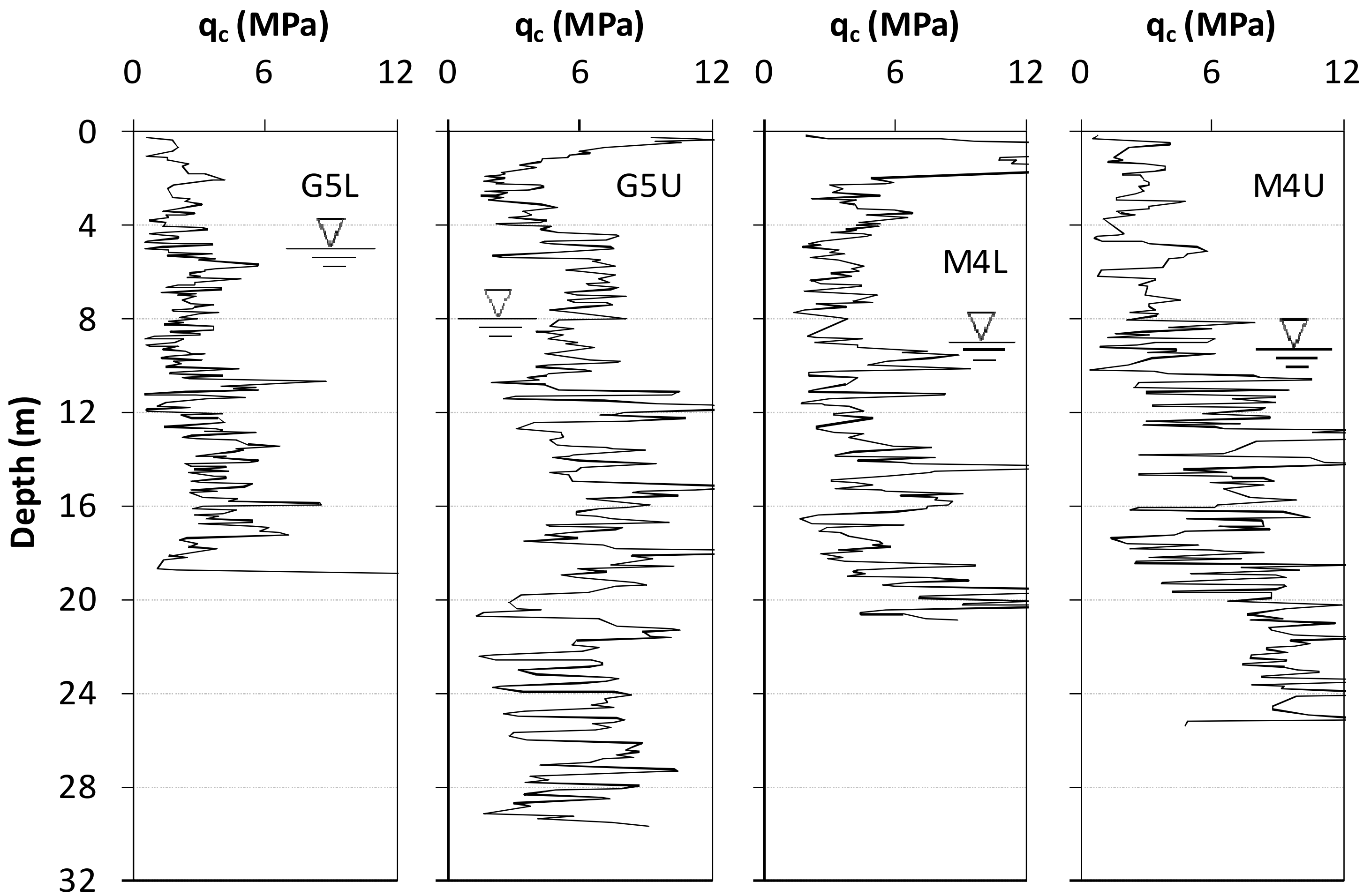

Figure 4.16 Cone penetration resistance (q_c) profiles of *CPT* soundings made on the beach of GMTS and Mooifontein tailings dams (after WM&B, 2001).

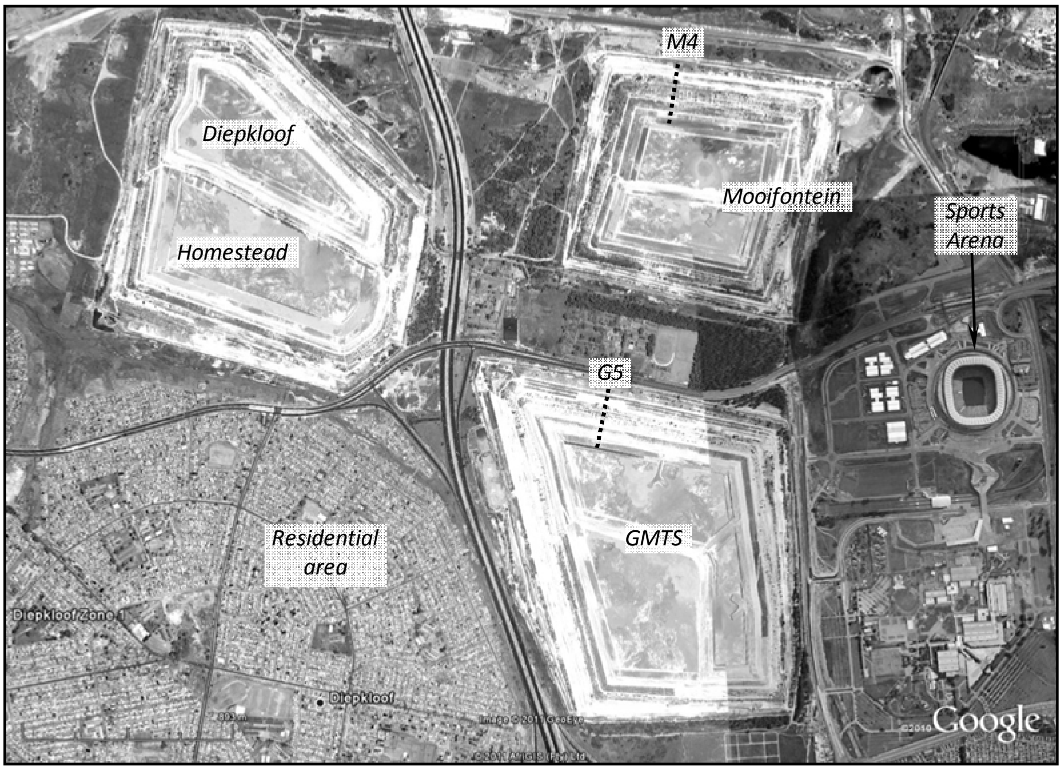

Figure 4.17 Aerial view of the Crown Tailings Complex in Johannesburg, South Africa (Image from Google Earth™).

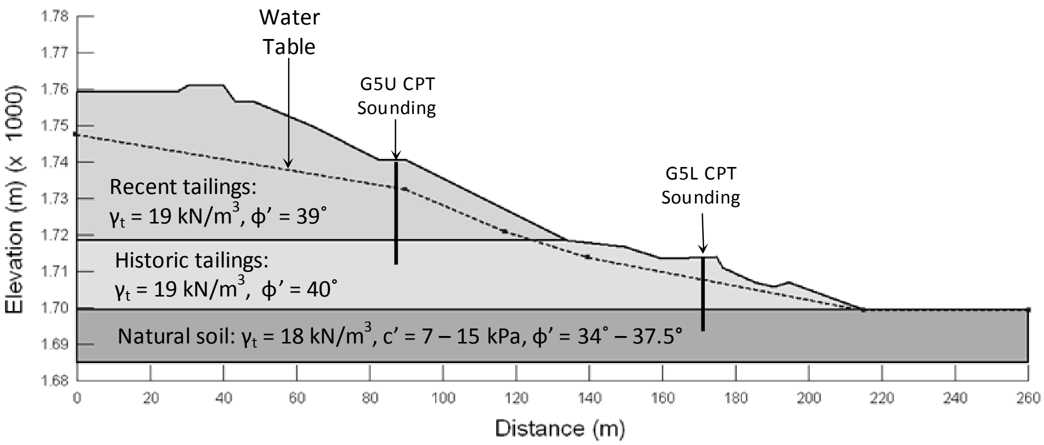

Figure 4.18 Cross section G5 of the GMTS tailings dam (after WM&B 2001).

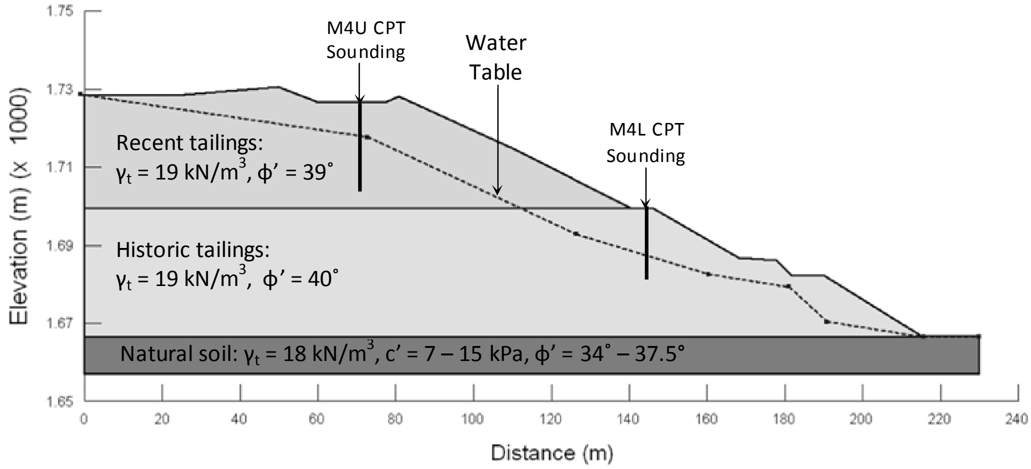

Figure 4.19 Cross section M4 of the Mooifontein tailings dam (after WM&B 2001).

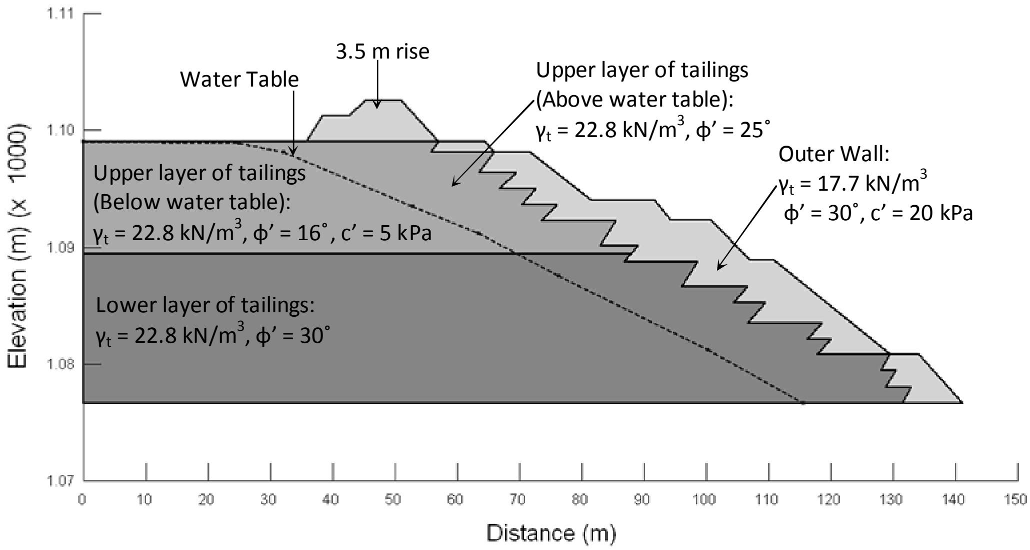

Figure 4.20 Cross section of Dam A (after Neto 2009).

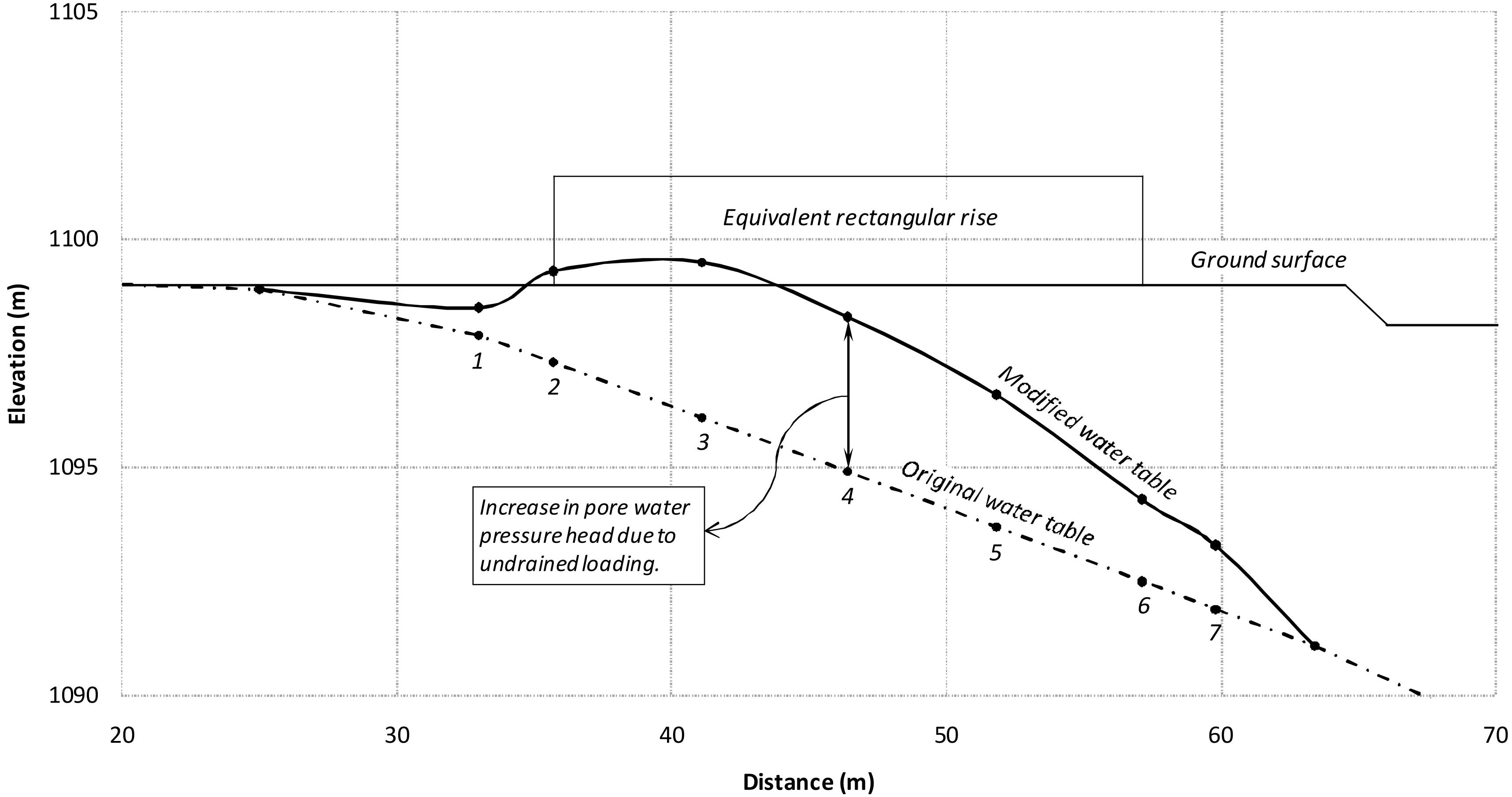

Figure 4.21 Modified water table used to account for undrained loading in Dam A.

5 Results

5.1 The Robertson-based methodology

The results of the application of the Robertson-based methodology to the five seismic case histories are presented in the following sections. Only the factors of safety profiles are presented in the figures herein. Additional figures illustrating the profiles of other parameters used by the methodology are shown in Appendix A.

5.1.1 Hokkaido Dam – Japan, 1968

Given that the tailings had been classified as silt-sized, the methodology was performed using I_c = 2.05 and I_c = 2.6 (Table 3.2). The results (Figure 5.1) show that, regardless of the I_c value used, liquefaction is clearly predicted to be triggered at depths between 2 to 6 m, and when considering only the calculations made with I_c = 2.05, liquefaction is predicted to be triggered on virtually the whole profile. This prediction is consistent with the flow failure that took place at the Hokkaido dam and therefore the results are taken as satisfactory.

5.1.2 Mochikoshi Dam – Japan, 1978

The methodology was applied using both penetration resistance (q_c) profiles shown in Figure 4.6 to Dykes 1 and 2. A constant I_c value of 2.65 was used throughout the soil profile of both dykes. This I_c value was calculated using the 'non-plastic fines' curve of Figure 3.4 and a *FC* of 85%.

The results for both dykes (Figure 5.2) show that triggering of liquefaction is predicted in several layers, especially at depths greater than 5 m. This prediction is certainly consistent with the performance of Dyke 1, which exhibited flow failure, but seems uncertain for Dyke 2 which endured the main shock and only failed following an aftershock (Section 4.3). However, this does not necessarily imply that liquefaction could have not been triggered in Dyke 2 by the main shock. That could have very well been the case, but a flow failure could have been impeded by the confinement provided by the outer wall. Furthermore, given that Dyke 2 had a subsequent flow failure due to an aftershock that was considerably smaller than the main shock, it is possible that the main shock could have left Dyke 2 in a state of incipient failure. Under these considerations, the triggering of liquefaction of Dyke 2 due to the main shock is not only possible but actually seems likely. The foregoing discussion leads the author to believe that the prediction made by the Robertson-based methodology of triggering of liquefaction in Dyke 2 due to the main shock is a satisfactory outcome.

It is interesting to notice that for both dykes, the results show considerable segments of the profile for which the factor of safety is zero. This is caused by τ_h/S_u estimations that are greater than 0.88 and thus lead to K_α (Eq. 3.6) and CRR_α equal to zero. The implication of this is that the methodology would have predicted the triggering of liquefaction (FS < 1) regardless of the magnitude or a_{max} of the earthquake, i.e. regardless of the value of *CSR*.

5.1.3 Dashihe Iron Tailings Dam – China, 1990

Dashihe Beach

Given the gentle slope of the beach (≈3%), horizontal static shear stresses were not considered. The I_c values were calculated using Eq. 3.7 together with the f_s and q_c profiles reported in Table 4.2 and Figure 4.9 respectively. The results of the classification (Figure 5.3) show that several data points fall in the region defined by $1.64 < I_c < 2.6$ and $F_r < 0.5\%$. As prescribed by Robertson and Wride (1998a), these data points were conservatively treated as clean sands, i.e. $K_c = 1$.

The results (Figure 5.4) show that, for all three *CPT* profiles considered, there are tailings below the water table with factors of safety very close to one. This outcome is consistent with the triggering of liquefaction predicted by Amante (1993) for the tailings under the pond and the beach area near the pond.

Dashihe Outer Wall

The I_c values for the outer wall of the Dashihe tailings dam were calculated from the *PI* and *FC* values reported in Table 4.4 together with the two curves of Figure 3.4. The 'non-plastic fines' curve was used to calculate I_c values of 1.4, 1.51, and 2.04 for the medium sand, fine sand, and silty sand respectively. Whereas the 'recommended general correlation' curve was used to estimate an I_c of 3.17 for the sandy loam.

The results (Figure 5.4) show that profiles I5 and II4, which are farthest away from the starter dyke (Figure 4.8), have one data point each indicating *FS* < 1 beneath the water table, but otherwise they consistently indicate no triggering of liquefaction. Profile I4, closer to the starter dyke than I5 and II4, indicates the presence of two layers where liquefaction is predicted to be triggered. Profile II2, the closest of the four profiles to the starter dyke, indicates more consistently than profile II2 the triggering of liquefaction. The general trend of the results can be considered to be in agreement with the results reported by Amante (1993), that is, the possibility of triggering of liquefaction is higher towards the starter dyke of the dam. However, in Amante's analysis, liquefaction is only predicted to be triggered in a very limited portion of the outer wall adjacent to the crest of the starter dyke. Therefore, although the Robertson-based methodology captures the general trend in the development of liquefaction of the outer wall, the results do not agree with the performance predicted by the more thorough analysis of Amante (1993).

5.2 The Olson and Stark methodology

5.2.1 Results of the liquefaction susceptibility analysis

Figure 5.5 to Figure 5.7 show the application of step 1 of the methodology to all case histories, i.e., they compare the q_{c1} profiles of the different *CPT* soundings with the contractive-dilative boundary defined by Eq. 3.20. With the exception of Dashihe beach, Dashihe outer wall, and Sullivan, the q_{c1} profiles of all cases clearly indicate a predominantly contractive state.

It is interesting to notice that the results for Dam A do not confirm the suggestion made by Neto (2009) regarding the division of the tailings, at an elevation of 1089.4 m, into an upper liquefiable deposit and a lower non-liquefiable deposit. However, since Neto (2009) worked with the original *SPT* values, which can be considered more reliable than the converted *CPT* values that were used here, such division into liquefiable and non-liquefiable tailings was also considered in this study (Appendix B.9).

In the case of Dashihe Beach, the q_{c1} profile from sounding I8 indicates contractiveness of the tailings only for σ'_{vo} values greater than 150 kPa, which is approximately equivalent to a depth of 7.5 m, whereas the q_{c1} profiles from soundings I9 and II6 indicate contractiveness at much shallower depths. Therefore, as a conservative assumption, the entire profile of the beach was taken as contractive.

For the Dashihe outer wall, the q_{c1} profiles indicate that contractiveness starts at σ'_{vo} values of 200 kPa, 270 kPa, 140 kPa and 270 kPa for soundings I4, I5, II2 and II4 respectively. The depths associated with these levels of stress are 12 m, 16.5 m, 13.5 m and 17 m respectively. Comparison of these depths with the data reported in Figure 4.10 reveals that, except for sounding II2, there is a close correspondence between the depth of the water table and the depth at which contractive soils are detected. Therefore, all tailings below the water table of the Dashihe outer wall were taken here as contractive.

The toe and crest results for Sullivan do not allow for a straight-forward interpretation. The different CPT profiles indicate contractiveness at rather dissimilar depths. The issue is further complicated by the fact that the soundings were performed through the post-failure geometry of the dam, making it virtually impossible to determine the pre-failure depth at which tailings can be expected to be contractive. As a simplifying assumption, it was considered here that the dyke tailings were in a dilative state, whereas the deposited tailings were in a contractive state.

The previous observations regarding the location of contractive and dilative tailings were incorporated into the slope stability scenarios used in the implementation of the triggering and post-triggering analyses. Given the uncertainties involved, and following the approach used by Olson (2001), several scenarios were analysed for each case history. Appendix B illustrates the scenarios and describes the assumptions made for each one of them.

5.2.2 Results of the triggering analysis

The results of the triggering analysis, obtained using the mean value of Eq. 3.26, are shown in (Figure 5.8). Liquefaction was predicted to be triggered for seven case histories: Hokkaido, Mochikoshi Dykes 1 and 2, Sullivan, Merriespruit, GMTS, and Mooifontein. In the case of Hokkaido, Mochikoshi Dyke 1, Sullivan and Merriespruit, full flow failures did actually develop in these case histories, so the prediction of triggering of liquefaction is accurate. Furthermore, as discussed previously, it is likely that liquefaction could have been triggered by the main shock in Mochikoshi Dyke 2, therefore, the prediction of triggering of liquefaction for this case history is deemed a satisfactory outcome. As for GMTS and Mooifontein, the prediction of triggering of liquefaction is inconsistent with the observed performance. The geometry of these dams analysed in this study corresponds to the end of the year 2000. To the date of writing (May 2011), both dams have continued to operate without interruptions and no evidence of liquefaction has been observed. It is interesting to notice that for one of the scenarios modelled for the GMTS dam, liquefaction is not predicted to be triggered, however, this scenario used a circular slip surface suggested by WM&B (2001) in which optimization was not used to alter the circular geometry of the slip surface to find a weaker path. For all other GMTS scenarios in which the slip surface was optimised, liquefaction was predicted to be triggered. The factors of safety for GMTS and Mooifontein did not change significantly with variations in the strength properties of the foundation soil. See Appendix B for results of specific scenarios and Table 5.1 for the average values of $FS_{Triggering}$.

Liquefaction was not predicted to be triggered in three case histories: Dashihe Beach, Dashihe Outer Wall and Dam A. These predictions are accurate in the case of the Dashihe Outer Wall, for which only a very limited portion of the outer wall was predicted to liquefy (Amante 1993), and for Dam A, for which no liquefaction was reported after building the 3.5 m rise of the outer wall. In the case of the Dashihe Beach, the triggering analysis did not detect the triggering of liquefaction reported by Amante

(1993). Furthermore, the $FS_{Triggering}$ values obtained for this case history are rather large, ranging from 1.7 to 2.5.

Overall, the Olson and Stark methodology has correctly predicted the triggering of liquefaction for seven of the ten case histories considered. It is also interesting to note that when considering only the five static case histories, the Robertson-based and the Olson and Stark methodology both correctly predicted the triggering of liquefaction in four case histories.

5.2.3 Results of the post-triggering analysis

The results of the post-triggering analysis, obtained using the mean value of Eq. 3.29, are shown in (Figure 5.8). This analysis was performed for all scenarios with $FS_{Triggering} \leq 1$. For all seven case histories for which the analysis was performed, a flow failure was predicted to occur. This implied an incorrect prediction for Mochikoshi Dyke 2, GMTS and Mooifontein. Additionally, as mentioned before, the development of the flow failure in the Dashihe Beach was not predicted by the methodology. Overall, the Olson and Stark methodology correctly predicted the occurrence of a flow failure in six of the ten case histories analysed. Table 5.1 shows the average values of FS_{Flow}.

5.2.4 Further analyses of the incorrectly predicted case histories

The Olson and Stark methodology provides upper and lower bounds to estimate *YSR* (Eq. 3.26) and *LSR* (Eq. 3.29) from q_{c1} as a means of accounting for the scatter in these correlations. These bounds were used here to further analyse the four case histories whose performance was incorrectly predicted when using the mean values of Eqs. 3.29 and 3.32. Upper bounds were used to re-analyse case histories for which flow failure was predicted but did not really happen: Mochikoshi Dyke 2, GMTS and Mooifontein. Lower bounds were used to re-analyse the case history for which flow failure was not predicted but it did happen: Dashihe Beach. Additionally, given the considerable level of uncertainty involved in estimating a_{max}, the a_{max} values for Mochikoshi Dyke 2 and Dashihe Beach were modified to 70% and 130% of their original value, respectively. The object of these analyses was to determine whether the Olson and Stark methodology could arrive at satisfactory performance predictions of the case histories when using favourable *YSR*, *LSR* and a_{max} values that were within reasonable confidence margins. The results (Figure 5.9) show that, although factors of safety have increased as expected, flow failures continue to be predicted for Mochikoshi Dyke 2, GMTS and Mooifontein. It is interesting to note that all of these three case histories include one scenario for which triggering of liquefaction was not predicted. However, in these scenarios a circular slip surface was used without allowing optimization to modify the circular geometry to find a weaker sliding path. All other scenarios clearly predict the occurrence of a flow failure. This result highlights the importance of considering non-circular slip surfaces as recommended by the Olson and Stark methodology. As for the Dashihe Beach, the factors of safety have been reduced as expected but triggering of liquefaction is still not predicted in any of the scenarios considered. The average values of $FS_{Triggering}$ and FS_{Flow} are reported in Table 5.2.

An additional type of triggering analysis was made on three case histories: Merriespruit, GMTS and Mooifontein. The analysis consisted in comparing the S_u profiles of the deposited tailings (as computed with Eq. 3.5) with the driving shear stresses acting along the critical slip surface of the models when using φ' = 39˚ for the tailings. In the case of the Mooifontein Dam, two models, A and B, were used. In model A the foundation soil was assigned c' = 7 kPa and φ' = 34˚. In model B the foundation soil was assigned c' = 15 kPa and φ' = 37.5˚. In both cases the critical slip surface was found to intercept the foundation soil. However, given the similarity in the results (Figure 5.10) of both models, GMTS was only modelled with c' = 7 kPa and φ' = 34˚ for the natural foundation soil.

The S_u profiles were plotted against the initial vertical effective stress (σ'_{vo}) and the driving shear stresses were plotted against the normal effective stress acting on the portion of the slip surface where the driving shear stress was measured. When computing the normal effective stress, the pore water pressure values yielded by the model were increased by 50% to account for the effect of undrained loading in a potentially contractive soil. The results (Figure 5.10 to Figure 5.12) show that for both GMTS and Mooifontein, the triggering shear stresses are mostly lower than the S_u profile. As for Merriespruit, the graphs indicate that the triggering shear stresses are generally higher than the S_u profile. All three graphs are consistent with the actual performance of the tailings dams. This approach towards the assessment of the triggering of liquefaction in a tailings dam could be further explored with more case histories to establish its suitablity.

5.3 Concluding Remarks

The main results of the implementation of the Robertson-based and the Olson and Stark methodologies have been presented. The Robertson-based methodology was applied to the five seismic case histories and yielded satisfactory predictions of liquefaction triggering in four instances. The Olson and Stark methodology was implemented in all ten case histories (Figure 5.8). The methodology correctly predicted the triggering of liquefaction and development of flow failure for seven and six case histories respectively. The four case histories for which the flow failure behaviour was not correctly predicted were analysed a second time using estimates of *YSR*, *LSR* and a_{max} that were within reasonable confidence margins and that would favour a better performance of the methodology. The results (Figure 5.9) show that incorrect performance prediction persisted.

It is interesting to note that when considering only the five seismic case histories, both methodologies correctly predicted the triggering or not of liquefaction in four cases. The results have also highlighted the importance of considering non-circular slip surfaces when using the Olson and Stark methodology. Several instances were pointed out in which a tailings dam was predicted to remain stable when considering a circular slip surface, but predicted to exhibit flow failure when considering optimized non-circular slip surfaces.

An alternative approach towards the assessment of the triggering of liquefaction was described. The approach was tried on three case histories and yielded results that are consistent with their field performance. Further exploration of this approach to other case histories is necessary to assess its reliability.

5.4 Tables and figures

Table 5.1 Average *FS* values obtained with the Olson and Stark methodology.

Case history	**Average $FS_{Triggering}$**	**Average FS_{Flow}**
Hokkaido Dam	0.5	0.2
Mochikoshi Dyke 1	0.5	0.2
Mochikoshi Dyke 2	0.5	0.3
Dashihe Beach	2.1	--
Dashihe Outer Wall	1.2	--
Sullivan Dam	0.9	0.2
Merriespruit Dam	0.4	0.1
GMTS Dam	0.9	0.2
Mooifontein Dam	0.7	0.2
Dam A	6.8	--

Table 5.2 Average *FS* values obtained with the Olson and Stark methodology in the second analysis of the case histories whose performance was incorrectly predicted.

Case history	**Average $FS_{Triggering}$**	**Average FS_{Flow}**
Mochikoshi Dyke 2	0.8	0.3
Dashihe Beach	1.4	--
GMTS Dam	1.0	0.3
Mooifontein Dam	0.8	0.3

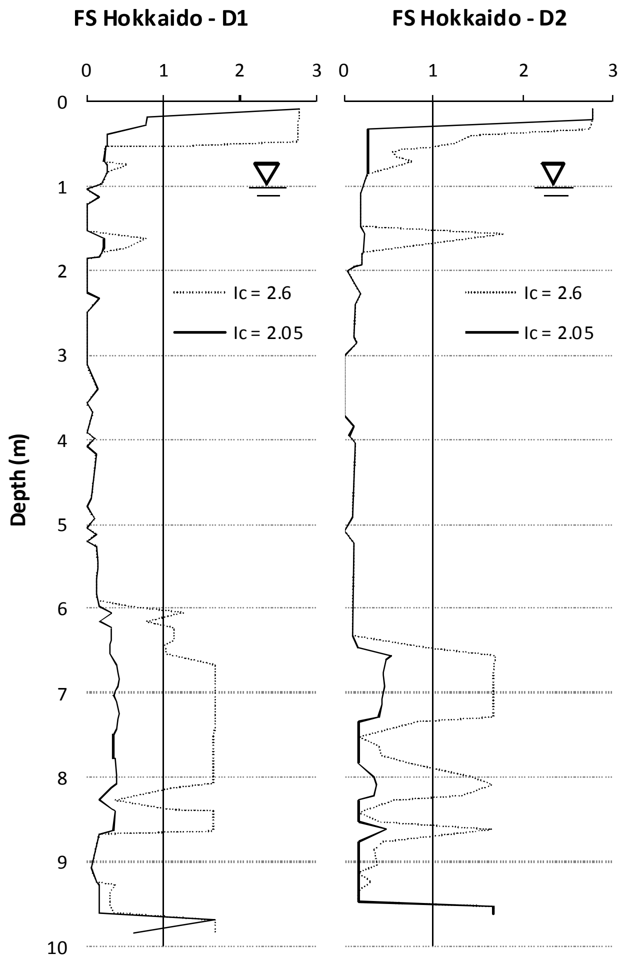

Figure 5.1 Factors of safety (*FS*) against triggering of liquefaction of the Hokkaido case history using the Robertson-based methodology. Note: The code after the hyphen in each title denotes the *CPT* sounding used to perform the calculations.

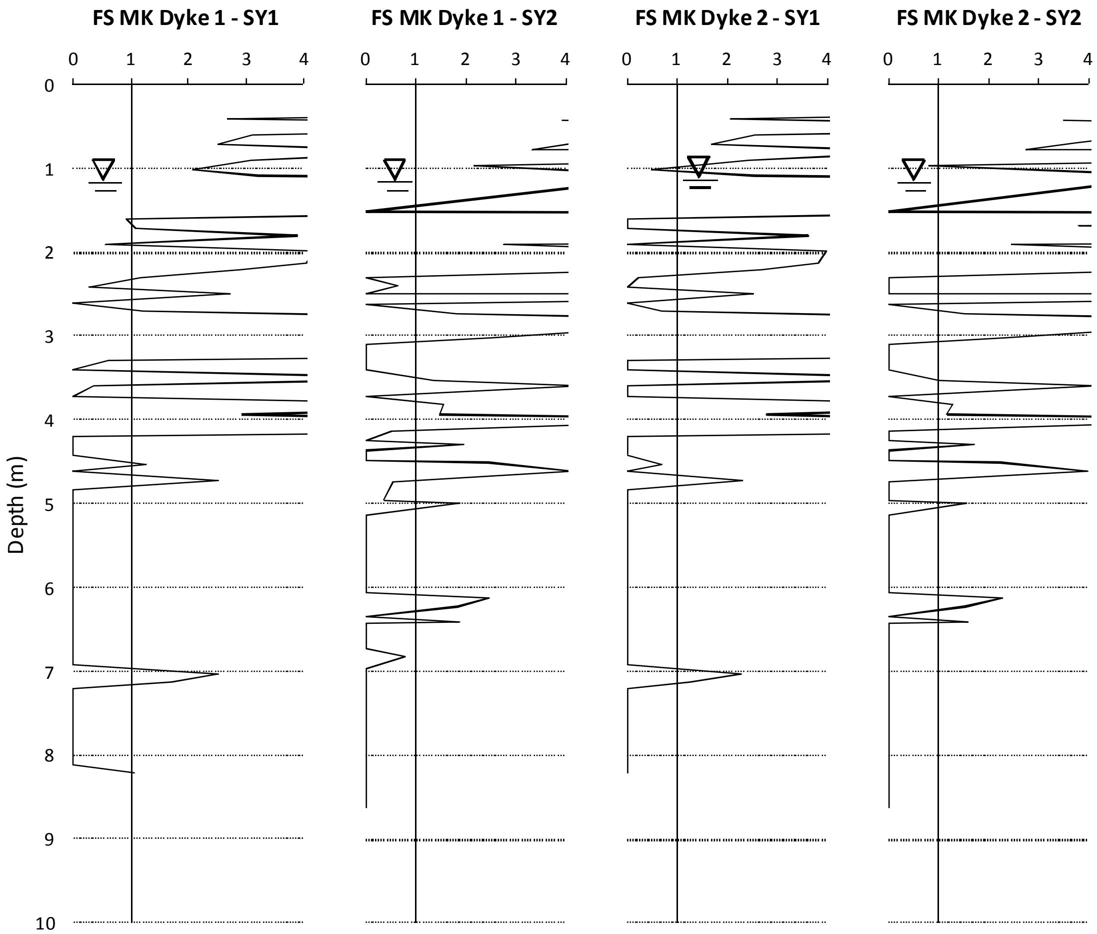

Figure 5.2 Factors of safety (*FS*) against triggering of liquefaction of the Mochikoshi case history using the Robertson-based methodology. Note: The code after the hyphen in each title denotes the *CPT* sounding used to perform the calculations.

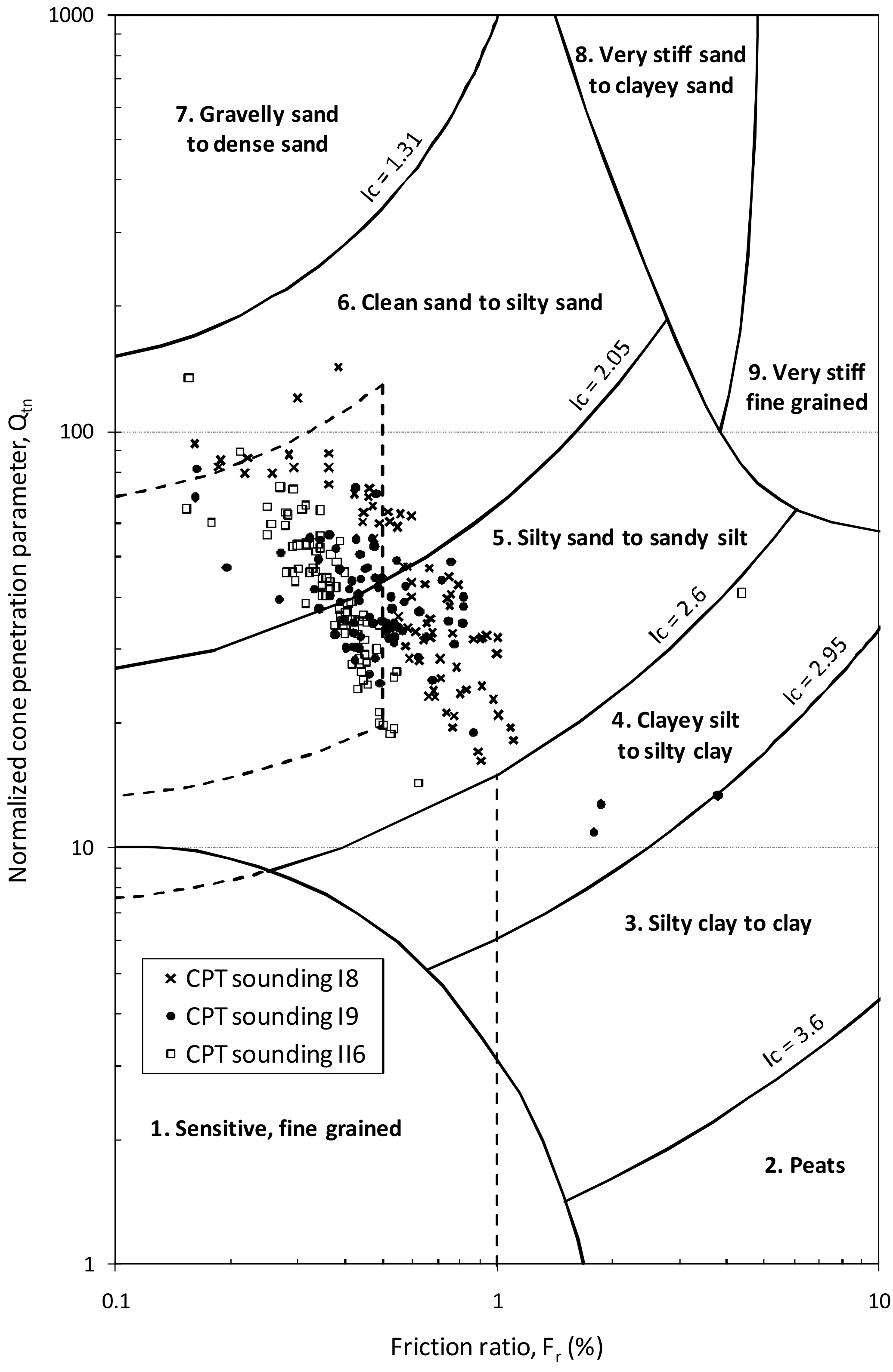

Figure 5.3 Q_{tn} vs. F_r chart showing the data points corresponding to the *CPT* soundings made on the Dashihe tailings dam beach.

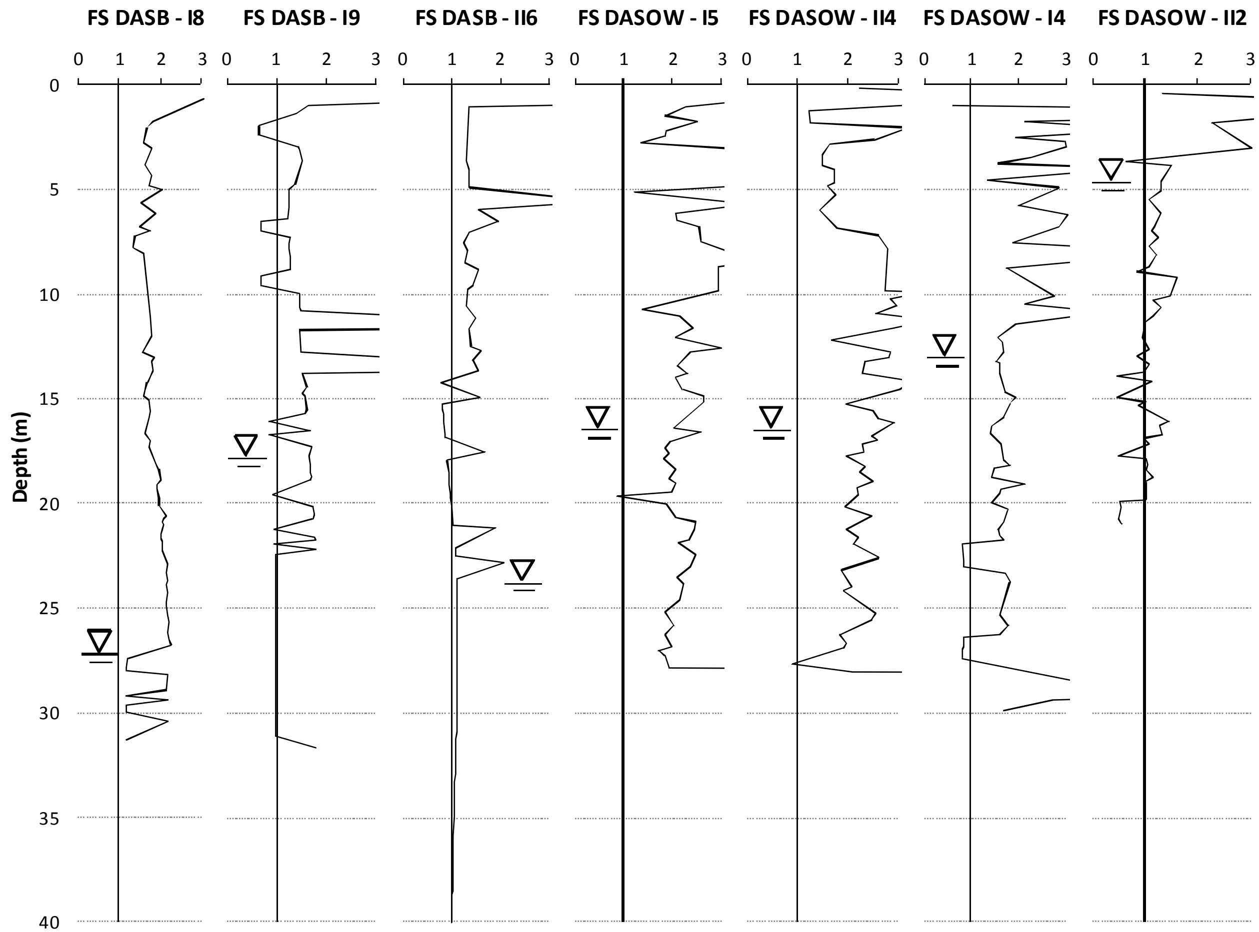

Figure 5.4 Factors of safety (*FS*) against triggering of liquefaction for Dashihe Beach (DASB) and Dashihe Outer Wall (DASOW) case histories using the Robertson-based methodology. Note: The code after the hyphen in each title denotes the *CPT* sounding used to perform the calculations.

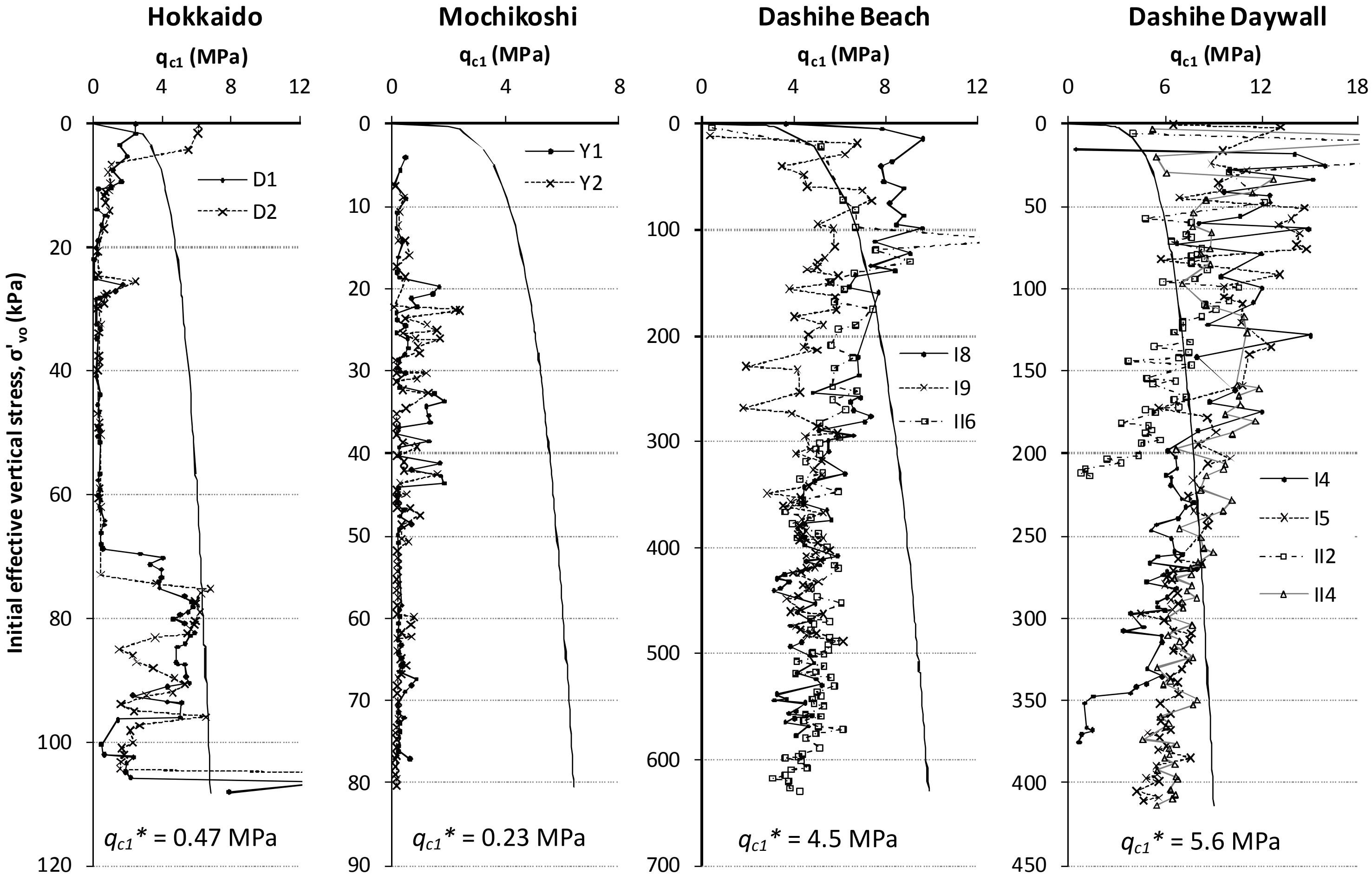

Figure 5.5 Application step 1 of the Olson and Stark methodology to case histories: Hokkaido, Mochikoshi, Dashihe Beach and Dashihe Outer Wall. q_{c1}* denotes the characteristic q_{c1} value used to implement the triggering and post-triggering analyses.

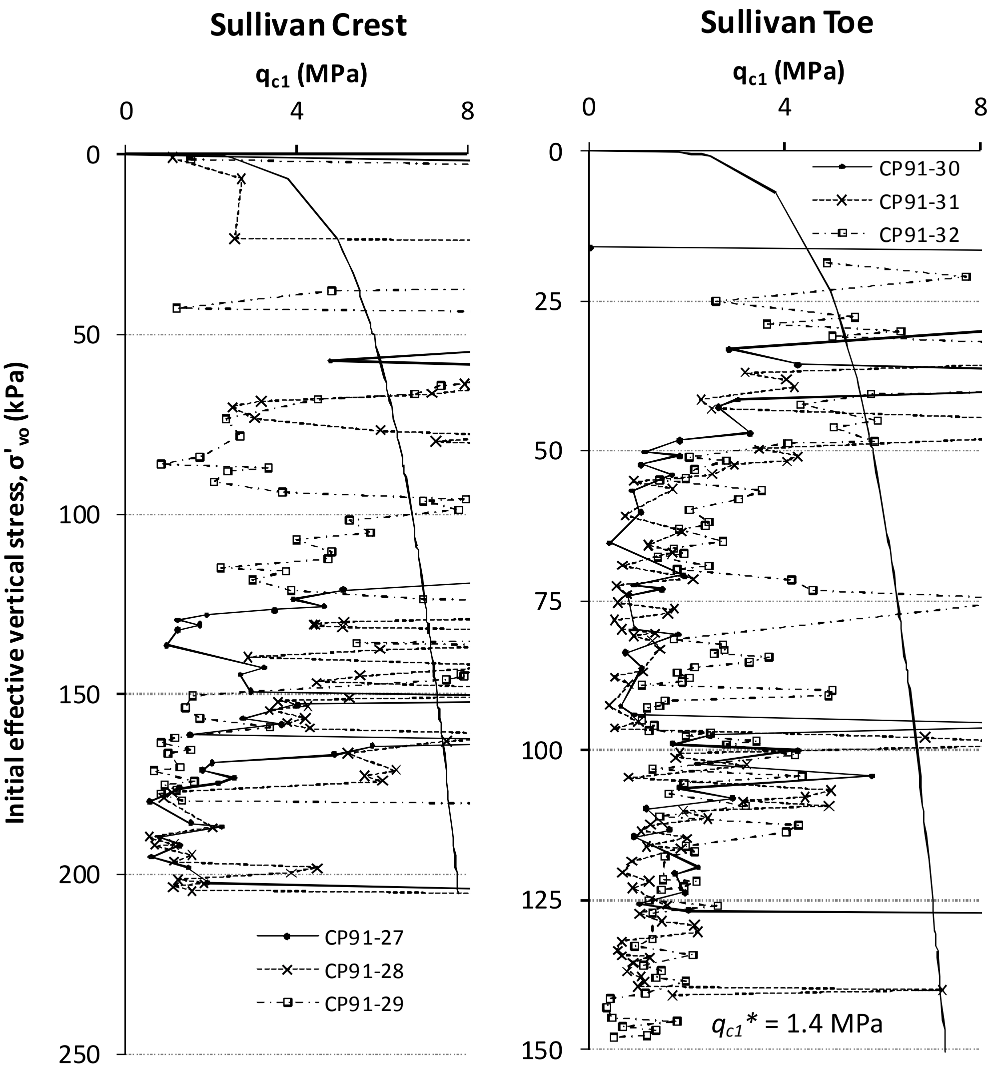

Figure 5.6 Application step 1 of the Olson and Stark methodology to the Sullivan case history. q_{c1}* denotes the characteristic q_{c1} value used to implement the triggering and post-triggering analyses.

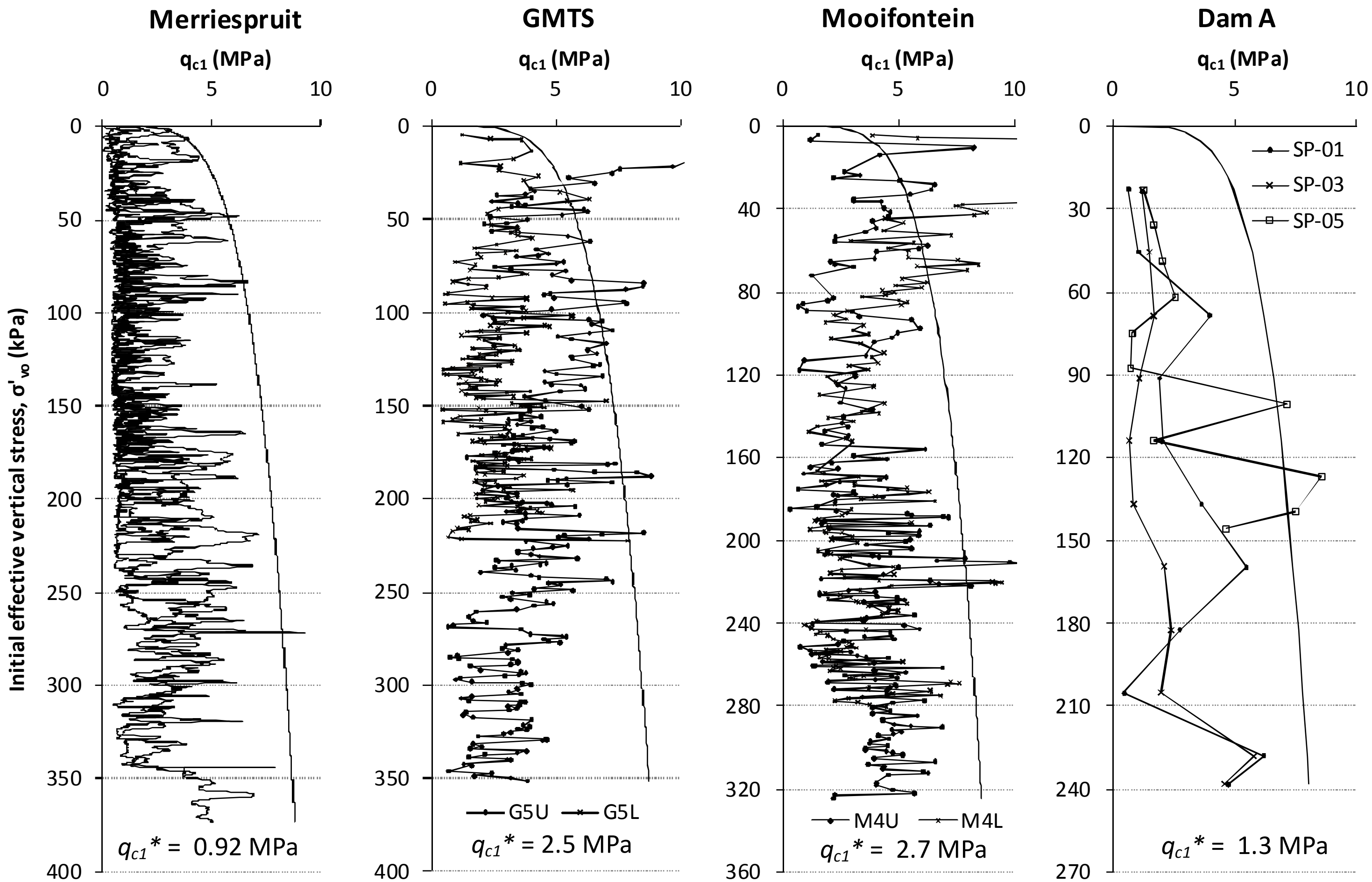

Figure 5.7 Application step 1 of the Olson and Stark methodology to case histories: Merriespruit, GMTS, Mooifontein and Dam A. q_{c1}* denotes the characteristic q_{c1} value used to implement the triggering and post-triggering analyses.

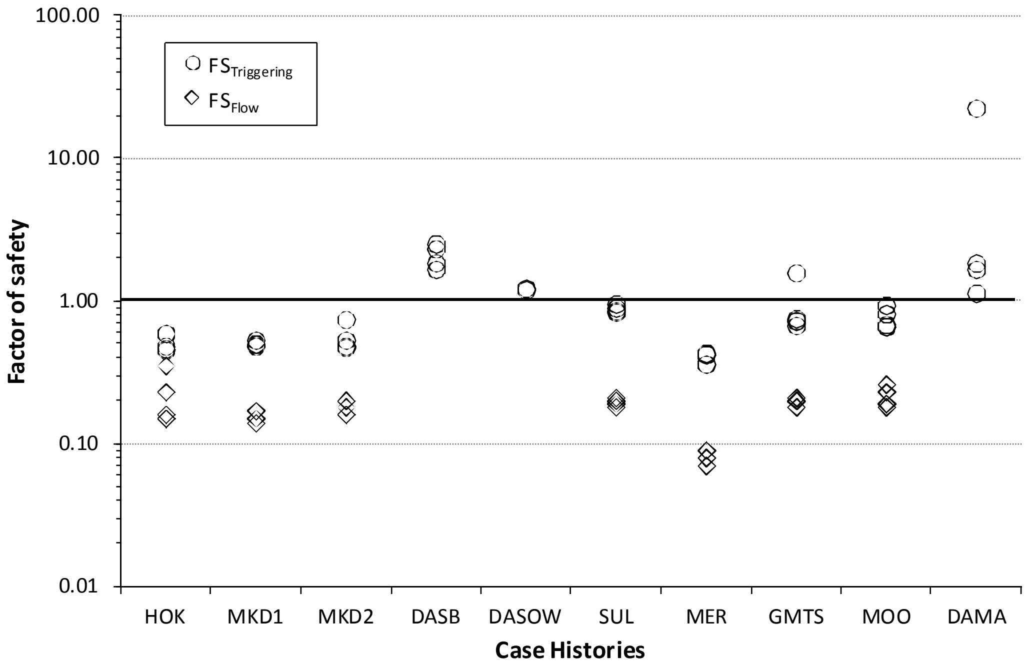

Figure 5.8 Factors of safety from the triggering and post-triggering analyses of the Olson and Stark methodology using the mean versions of **Eq. 3.26** and **Eq. 3.29**. Note: HOK = Hokkaido, MKD1 = Mochikoshi Dyke 1, MKD2 = Mochikoshi Dyke 2, DASB = Dashihe Beach, DASOW = Dashihe Outer Wall, SUL = Sullivan Dam, MER = Merriespruit Dam, MOO = Mooifontein Dam and DAMA = Dam A.

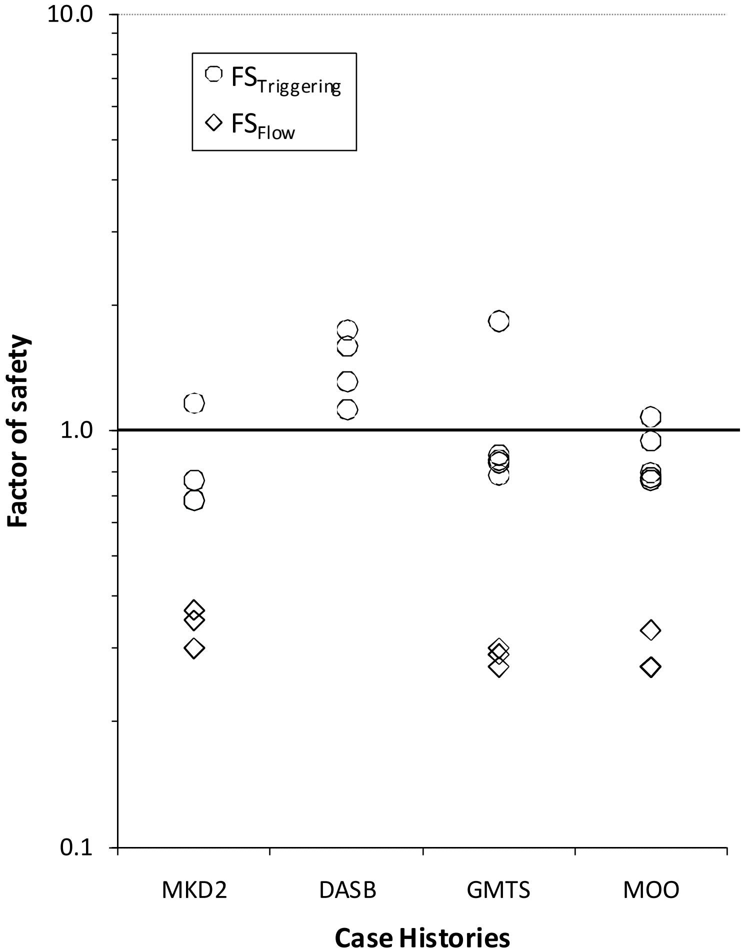

Figure 5.9 Re-analysis of the four case histories whose performance was not correctly predicted by the Olson and Stark methodology. Note: MKD2 = Mochikoshi Dyke 2, DASB = Dashihe Beach and MOO = Mooifontein Dam.

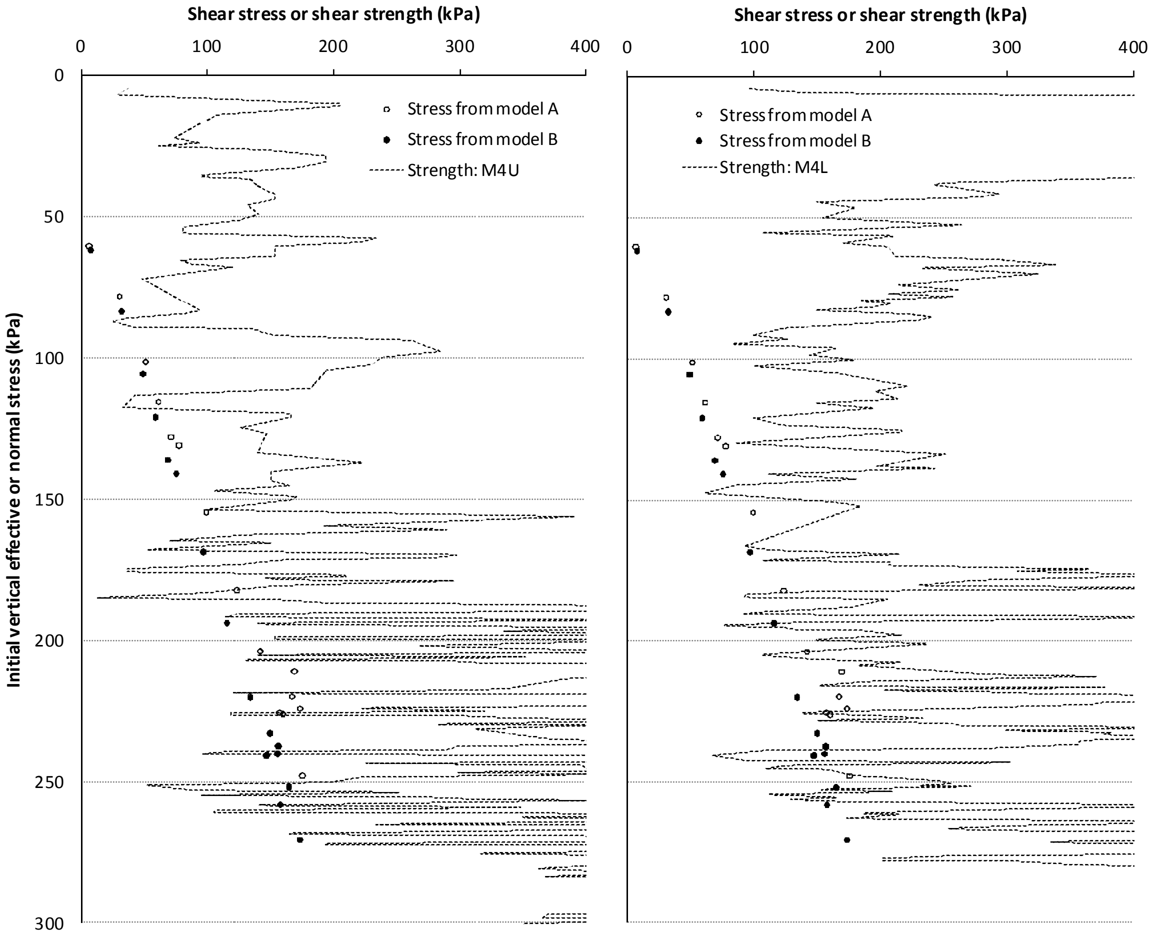

Figure 5.10 Comparison between triggering shear stresses and undrained shear strength profiles for Mooifontein.

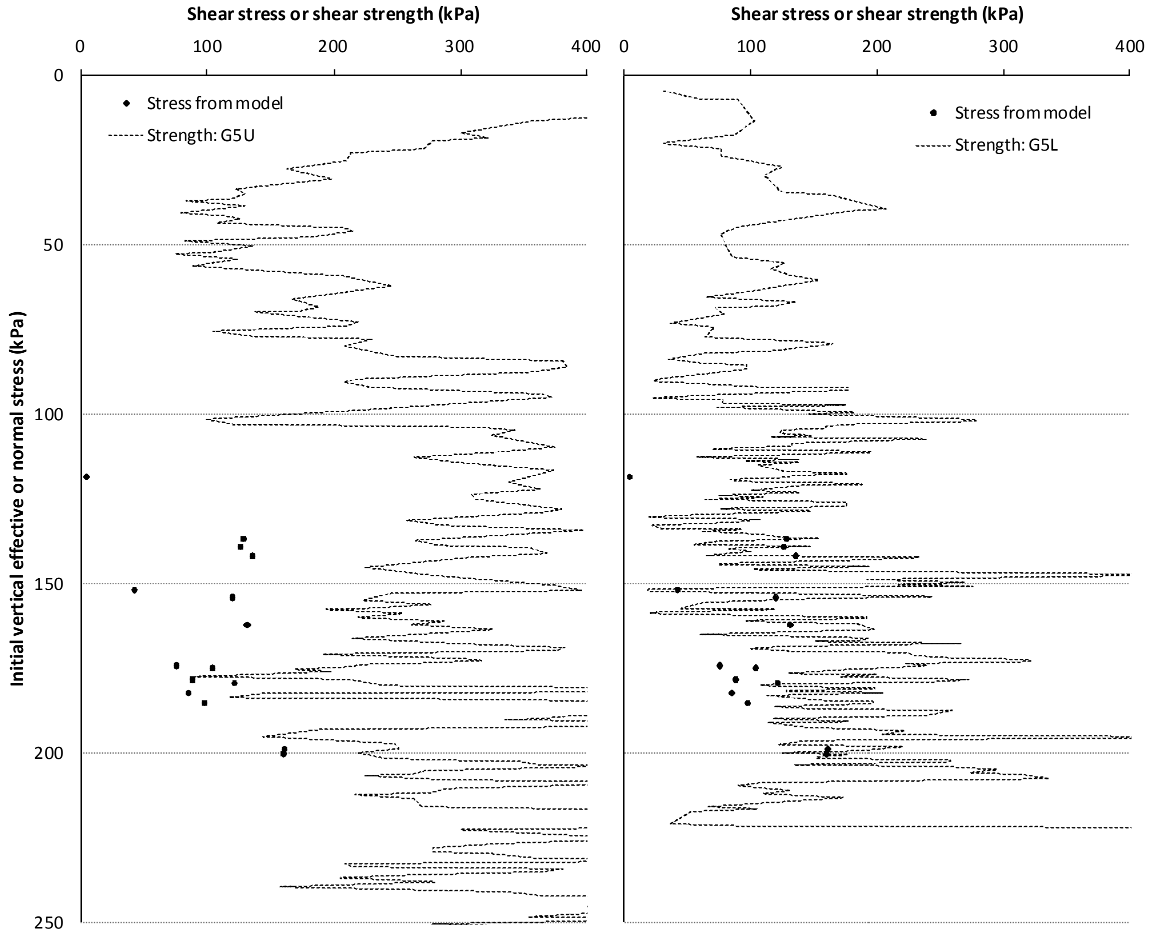

Figure 5.11 Comparison between triggering shear stresses and undrained shear strength profiles for GMTS.

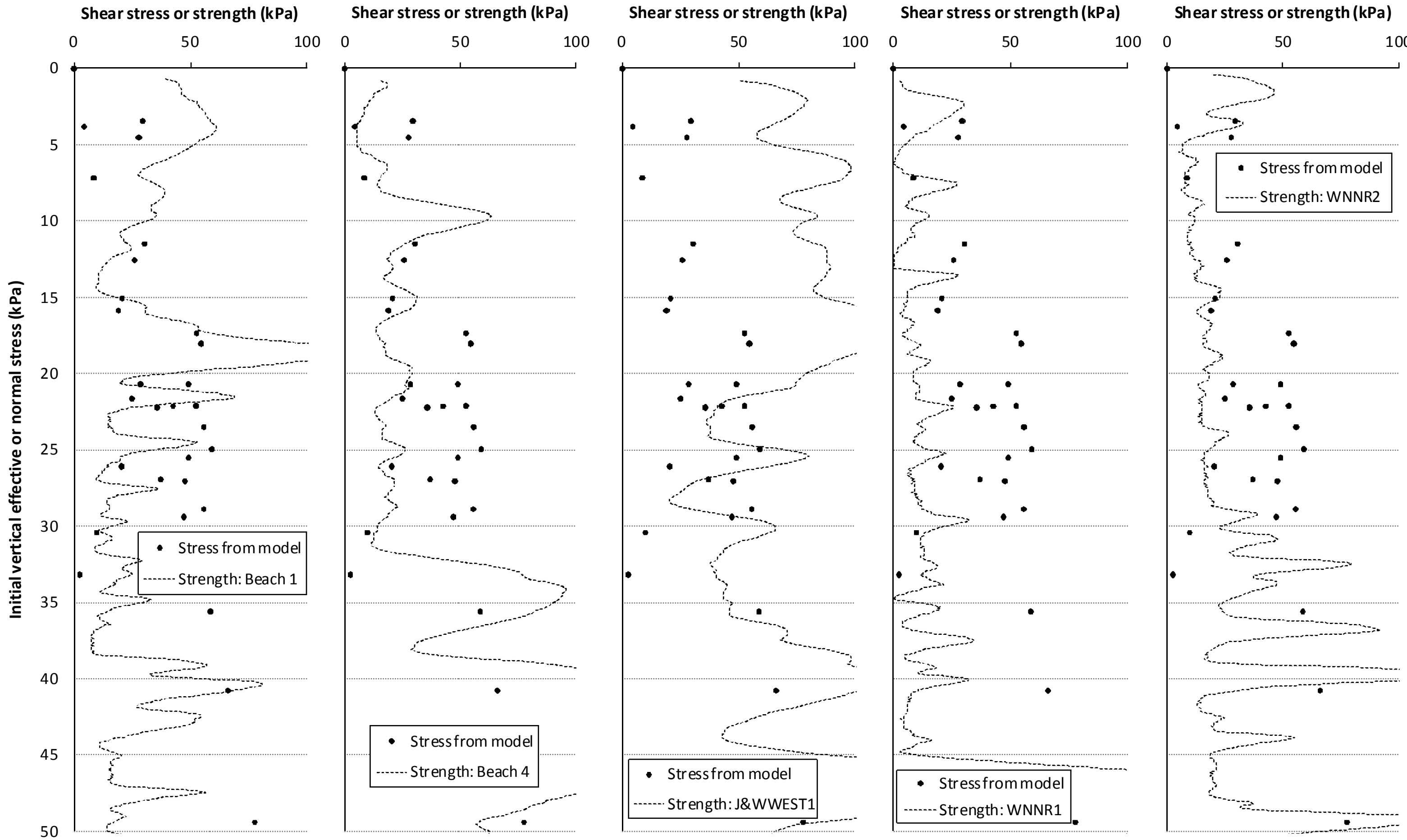

Figure 5.12 Comparison between triggering shear stresses and undrained shear strength profiles for Merriespruit.

6 Summary and Conclusions

Liquefaction leading to flow failure is one of the major threats to the stability of tailings dams. Given the brittle nature of flow failures and the often close proximity of tailings dams to human settlements, the development of liquefaction assessment tools is of great relevance to the mining industry. Due to the difficulties and high costs of obtaining undisturbed samples of tailings, several liquefaction assessment tools have been developed that rely on field tests such as the *SPT* and *CPT*. Given the greater repeatability of the test, *CPT*-based liquefaction assessment methods are becoming increasingly popular.

Two *CPT*-based liquefaction potential assessment methodologies have been reviewed and assessed for their applicability to tailings dams. The first was referred to here as the Robertson-based methodology and derives mainly from the procedures outlined by Robertson (2009a) to assess liquefaction potential of level ground under seismic loading. An extension to the methodology has been proposed here to make it applicable to sloping ground conditions. The methodology uses the cone penetration resistance and sleeve friction readings of the *CPT*. The second methodology was proposed by Olson and Stark (2002 and 2003). This methodology is applicable to sloping ground conditions under static and seismic loading and uses only the cone penetration resistance reading of the *CPT*. The Robertson-based methodology is aimed at predicting the triggering of liquefaction and is not intended to assess post-triggering behaviour, i.e., occurrence of flow failure or not. The Olson and Stark methodology does consider post-triggering behaviour and thus is intended to predict the occurrence of flow failure.

Both methodologies have a considerable degree of empiricism built into them and are therefore recommended by their authors for use in small projects or as a screening tool for large projects. Their greatest value lies in their ease and low cost of applicability. In order to attain these benefits, the methodologies rely on approximations and empirical correlations whose theoretical soundness might be questionable. Several of these approximations and correlations have been discussed here (Chapter 3). Amongst the objections applicable to both methodologies are: uncertainties and suitability of the stress normalization approach; lack of consideration of horizontal stresses; and uncertainties in the estimation of a_{max} and r_d. Objections that only apply to the procedures endorsed by Robertson (2009a) include the apparently empirical nature of Eqs. 3.10 and 3.13; the first of which is used to calculate the stress exponent n and the second used to calculate the correction factor K_c. Additionally, the extensions proposed here to the Robertson-based methodology are also questionable in that the formulae for K_α (Eq. 3.4), proposed by Boulanger and Idriss (2007), and for S_u (Eq. 3.5), recommended by Robertson (2009a), are intended for use with claylike soils as opposed to low plasticity silt-sized tailings. Objections applicable to the Olson and Stark methodology include: uncertainty of the origin of the contractive-dilative boundary defined by Eq. 3.20 and moreover the validity of a single boundary applicable to different types of soils; the weak correlations of the data sets YSR-q_{c1} (R^2 = 0.15) and LSR-q_{c1} (R^2 = 0.21); and the differences between the linear regressions of data sets YSR-q_{c1} and LSR-q_{c1}, and Eq. 3.26 and Eq. 3.29, respectively.

Ten case histories were used to assess the performance of the methodologies. Half of the case histories involved seismic loads, and also half involved flow failures. The Robertson-based methodology was applied to the five case histories involving seismic loads and correctly estimated the triggering of liquefaction of four of the case histories. The Dashihe outer wall was the only case history whose performance was not correctly predicted. I.e. the Robertson-based methodology predicted the triggering of liquefaction when it did not really occur. Nonetheless, the methodology revealed a trend of greater liquefaction triggering close to the starter dyke which is consistent with the results of the analysis performed by Amante (1993).

The Olson and Stark methodology was applied to all ten case histories to predict triggering of liquefaction and occurrence of flow failure. To account for the uncertainties involved, several slope stability models were considered for each case history. Triggering of liquefaction and occurrence of flow failure was correctly predicted for seven and six case histories respectively. The four case histories for which flow failure occurrence was not correctly predicted by the Olson and Stark methodology were analysed a second time adopting values of YSR, LSR and a_{max} that would favour a correct prediction, but that were still within reasonable confidence intervals. The values *YSR* and *LSR* adopted in the second analysis came from the upper or lower bounds suggested in the Olson and Stark methodology. Two of the four case histories that were analysed a second time involved seismic loads. The a_{max} value used in the second analysis of these cases was taken as 70% of the original value when flow failure had erroneously been predicted to occur, or as 130% of the original value when flow failure had erroneously been predicted to not occur. The results of the second analysis showed that incorrect performance prediction of the case histories persisted.

The only incorrect performance prediction that was not on the conservative side was the stability of the Dashihe beach which was predicted by the Olson and Stark methodology. Nonetheless, it should be noticed that given the small slope (3%) involved in this case history, a large flow failure is unlikely.

References

Amante, C. V. (1993). “Seismic response and post-liquefaction analysis of the 1990 Dashihe tailings dam.” MSc Thesis, Univ. of British Columbia, 81 pp.

Anderson, D. L., Byrne, P. M., DeVall, R. H., Naesgaard, E. and Wijewickreme, D. (2007). “Geotechnical design guidelines for buildings on liquefiable sites in accordance with NBC 2005 for greater Vancouver region.” Canadian Task Force Report.

Been, K., and Jefferies, M. G. (1985). “A state parameter for sands.” Géotechnique, 35, 2, 99-112.

Blight, G. (2010). “Geotechnical engineering for mine waste storage facilities.” Taylor and Francis. 634 pp.

Boulanger, R. W., and Idriss, I. M. (2007). “Evaluation of cyclic softening in silts and clays.” J. of Geotech. and Geoenviron. Eng., 133(6), 641-652.

Casagrande, A. (1936). “Characteristics of cohesionless soils affecting the stability of earth fills.” J. of Boston Society of Civil Eng., 23, 257-276.

Cetin, K. O., and Seed, R. B., (2004). “Nonlinear shear mass participation factor (r_d) for cyclic stress ratio evaluation.” Soil Dyn. Earthquake Eng. 24(2) 103-113.

Cunning, J. C., Robertson, P. K., and Sego, D. C. (1995). “Shear wave velocity to evaluate in situ state of cohesionless soils.” Can. Geotech. J., 32, 848-858.

Davies, M. P. (1999). “Piezocone technology for the geoenvironmental characterization of mine tailings.” PhD Thesis, Univ. of British Columbia, 431 pp.

Davies, M., Martin, T., and Lighthall, P. (2000). “Tailings dam stability: Essential ingredients for success.” *In* “Slope Stability in Surface Mining.” Society for Mining, Metallurgy, and Exploration, Inc. (SME).

Fear, C.E., and Robertson, P.K. (1995). “Estimating the undrained strength of sand: a theoretical framework.” Can. Geotech. J., 32, 859-870.

Finn, W. D. L., Yogendrakumar, M., Yoshida, N., and Yoshida, H. (1986). “TARA-3: A program to compute the response of 2-D embankments and soil structure interaction systems to seismic loadings.” Dept. of Civil Eng., Univ. of British Columbia, Vancouver, Canada.

Fourie, A. B., Blight, G. E. and Papageorgiou G. (2001). “Static liquefaction as a possible explanation for the Merriespruit tailings dam failure.” Can. Geotech. J., 38, 707-719.

Fourie, A. B. and Papageorgiou, G. (2001). “Defining an approximate steady state line for Merriespruit gold tailings.” Can. Geotech. J., 38, 695-706.

Gao, J. S., Robertson, P. K. and Morgenstern, N. R. (1991). “Site data analysis on Dashihe tailings dam.” Report 3-2-1 for the Sino-Canadian joint investigation on earthquake safety of Chinese tailings dams.

Geo-Slope International Ltd. (2010). “Stability modelling with Slope/W 2007 version.” Fourth edition.

Hanks, T. C., and Kanamori, H. (1979). “A moment magnitude scale.” Journal of Geophysical Research, 84, 2348-2350.

Henian, L., Yuqing, W., Zhiping, W., Zhejun, L., Wansheng, L., Jiansheng, G., Hongbo, X., Zhilin, L., and Ying, W. (1990). “Report 3-2 for the Sino-Canadian joint investigation on earthquake safety of Chinese tailings dams”.

Ishihara, K. (1993). “Liquefaction and flow failure during earthquakes.” Géotechnique 43(3), 351-415.

Ishihara, K., and Nagao, A. (1983). “Analysis of landslides during the 1978 Izu-Oshima-Kinkai earthquake.” Soils and Foundations, 23(1), 19-37.

Ishihara, K., Yasuda, S., and Yoshida, Y. (1990). “Liquefaction-induced flow failure of embankments and residual strength of silty sands.” Soils and Foundations, 30(3), 69-80.

Jaky, J. (1944). “The coefficient of earth pressure at rest.” Journal of the Society of Hungarian Architects and Engineers, 355-358.

Jefferies, M., and Been, K. (2006). “Soil liquefaction – A critical state approach.” Taylor and Fracis. 479 pp.

Kanamori, H. (2004). “The diversity of the physics of earthquakes.” J. of Geophysical Research, 82(20), 2981-2987.

Kanamori, H. (1977). “The energy release in great earthquakes.” Proc. Jpn. Acad., Ser. B, 80, 297-316.

Kayen, R. E., Mitchell, J. K., Seed, R. B., Lodge, A., Nishio, S., and Coutinho, R. (1992). “Evaluation of SPT-, CPT-, and shear wave-based methods for liquefaction potential assessments using Loma Prieta data." Proceedings of the 4th Japan-U.S. workshop on earthquake resistant design of lifeline facilities and countermeasures for soil liquefaction, Honolulu, Hawaii, Vol. 1, 177-192.

Lambe, T. W., Whitman, R. V. (1969). "Soil Mechanics." John Wiley & Sons. 553 pp.

Lee, W. S., Robertson, P.K. and Morgenstern, N.R. (1992). "Laboratory test data analysis on Dashihe tailings sands." Report 3-5 for the Sino-Canadian joint investigation on earthquake safety of Chinese tailings dams.

Neto, J. P. F. (2009). "Study of static liquefaction in tailings and application of a stability methodology." *In Portuguese*. MSc Thesis, Universidade Federal de Ouro Preto, Brazil. 179 pp.

Okusa, S. and Anma, S. (1980). "Slope failures and tailings dam damage in the 1978 Izu-Ohshima-Kinkai earthquake." Engineering Geology, 16, 195-224.

Olson, S. M. (2001). "Liquefaction analysis of level and sloping ground using field case histories and penetration resistance." PhD Thesis, Univ. of Illinois-Urbana-Champaign, Urbana, Ill. 549 p.

Olson, S. M. (2006). "Liquefaction analysis of Duncan Dam using strength ratios." Can. Geotech. J., 43, 484-499.

Olson, S. M., and Stark, T.D. (2002). "Liquefied strength ratio from liquefaction flow failure case histories." Can. Geotech. J., 39, 629-647.

Olson, S. M., and Stark, T.D. (2003). "Yield strength ratio and liquefaction analysis of slopes and embankments." J. of Geotech. and Geoenviron. Engineering, 129(8), 727-737.

Papageorgiou, P. (2004). "Liquefaction assessment and flume modelling of the Merriespruit gold and Bafokeng platinum tailings." PhD Thesis, Univ. of the Witwatersrand, Johannesburg, South Africa.

Poulos, S. J., Castro, G., and France, J. W. (1985). "Liquefaction evaluation procedure." J. of Geotech. Eng. 111(6), 772-792.

Robertson, P. K. (2009a). "Performance based earthquake design using the CPT." *In* Proceedings of the international conference on performance-based design in earthquake geotechnical engineering (IS-Tokyo 2009). *Edited by* T. Kokusho, Y. Tsukamoto & M. Yoshimine

Robertson, P. K. (2009b). “Interpretation of cone penetration tests – a unified approach.” Can. Geotech. J., 46, 1337-1355.

Robertson, P. K. (2009c). Discussion of “Evaluation of cyclic softening in silts and clays.” J. of Geotech. and Geoenviron. Eng., 135(2), 306-307.

Robertson, P. K. (1990). “Soil classification using the cone penetration test.” Can. Geotech. J., 27, 151-158.

Robertson, P. K., and Wride (Fear), C. E. (1998a). “Evaluating cyclic liquefaction potential using the cone penetration test.” Can. Geotech. J., 35, 442-459.

Robertson, P. K., and Wride (Fear), C. E. (1998b). “Cyclic liquefaction and its evaluation based on the SPT and CPT.” *In* Proceedings of the 1996 NCEER workshop on evaluation of liquefaction resistance of soils. *Edited by* T.L. Youd and I.M. Idriss. NCEER-97-0022.

Seed, H. B., (1983). “Earthquake resistant design of earth dams.” Proc. of the Symposium on Seismic Design of Embankments and Caverns, Pennsylvania, ASCE, New York, 41-64.

Seed, H. B., and Idriss, I. M. (1971). “Simplified procedure for evaluating soil liquefaction potential.” J. Soil Mech. Found. Div., ASCE, 97(9), 1249-1273.

Seed, H. B., Tokimatsu, K., Harder, L. F., and Chung, R. M. (1985). “Influence of SPT procedures in soil liquefaction resistance evaluations.” J. of Geotechnical Eng., ASCE, 111(12), 1425-1445.

Stark, T. D. and Olson, S. M. (1995). “Liquefaction resistance using CPT and field case histories.” J. of Geotechnical Engineering, 121(12), 856-869.

Strydom, J. H. and Williams, A. A. B. (1999). “A review of important and interesting technical findings regarding the tailings dam failure at Merriespruit.” Journal of the South African Institution of Civil Engineering, 41(4), 1-9.

Wagener, F., Craig, H., Strydom, K. and Blight, G. (1997). “The tailings dam flow failure at Merriespruit, South Africa: Causes and consequences.” *In:* Tailings and mine waste ’97, Balkema, Rotterdam, 657-666.

Wagener, F. von M., McPhail, G., Craig, H. J., Williams, A. A. B., Blight, G. and Strydom, J. H. (1998). “The Merriespruit tailings dam failure – A review.” *In:* Tailings and mine waste ’98, Balkema, Rotterdam, 925-952.

WM&B – Wates, Meiring and Barnard (2001). “Crown tailings complex risk assessment report on state of residue deposits” Report No: 4215/2594/3/S.

Youd, T. L., Idriss, I. M., Andrus, R. D., Arango, I., Castro, G., Christian, J. T., Dobry, R., Finn, W. D. L., Harder Jr., L. F., Hynes, M. E., Ishihara, K., Koester, J. P., Liao, S. S. C., Marcuson, W. F., Martin, G. R., Mitchell, J. K., Yoshiharu, M., Power, M. S., Robertson, P. K., Seed, R. B., and Stokoe, K. H. (2001). "Liquefaction resistance of soils: Summary report from the 1996 NCEER and 1998 NCEER/NSF workshops on evaluation of liquefaction resistance of soils." J. of Geotech. and Geoenv. Eng. 127(10), 817-833.

Yoshimi, Y. and Akagi, T. (1968). "News Report: Tokachioki earthquake of 1968." Soils and Foundations, 8(3), 87-95.

Yoshimine, M., Robertson, P. K., and Wride, C. E. (1999). "Undrained shear strength of clean sands to trigger flow liquefaction." Can. Geotech. J., 36, 891-906.

Zhang, G., Robertson, P. K., and Brachman, R. W. I. (2002). "Estimating liquefaction-induced ground settlements from CPT for level ground." Can. Geotech. J., 39, 1168-1180.

A. Appendix A – Detailed results from the implementation of the Robertson-based methodology

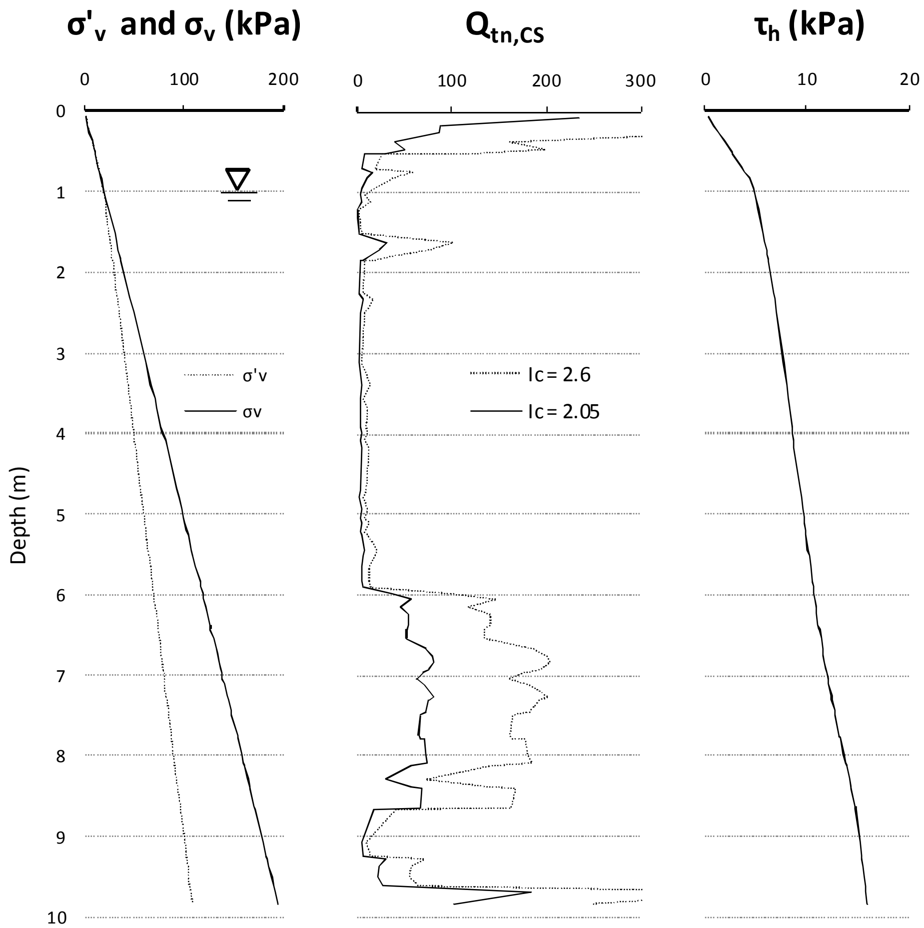

Figure A.1 Profiles corresponding to Hokkaido using *CPT* sounding D1: Effective (σ'_v) and total (σ_v) vertical stress, clean sand equivalent of the normalised cone penetration parameter ($Q_{tn,CS}$) and horizontal shear stress (τ_h).

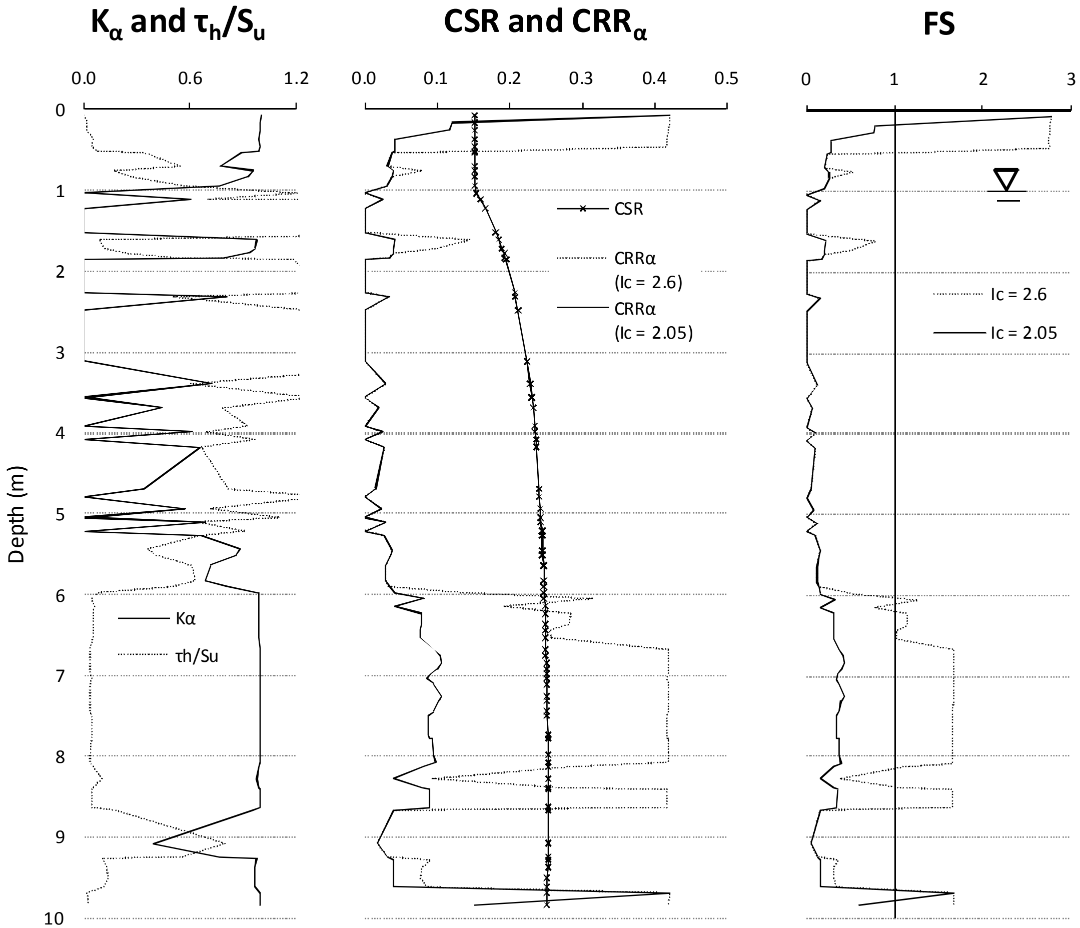

Figure A.2 Profiles corresponding to Hokkaido using *CPT* sounding D1: Static shear stress correction factor (K_{α}), horizontal shear stress to undrained shear strength ratio (τ_h/S_u), cyclic stress ratio (*CSR*), cyclic resistance ratio (CRR_{α}) and factor of safety (*FS*).

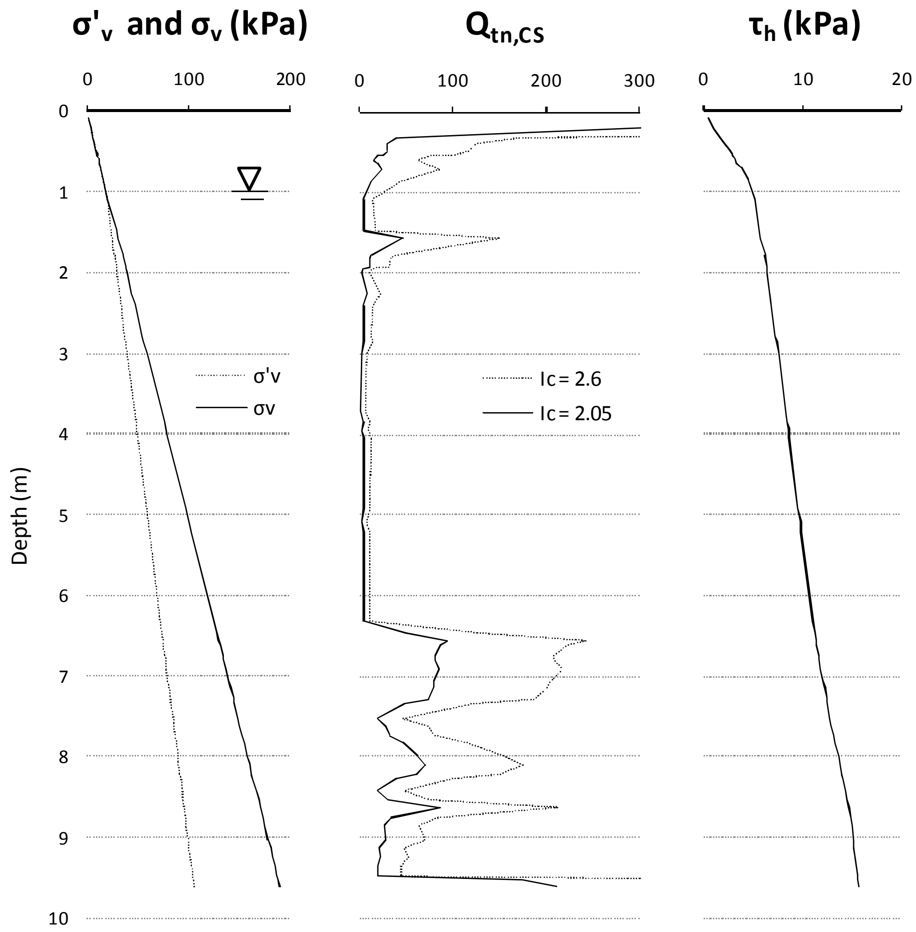

Figure A.3 Profiles corresponding to Hokkaido using *CPT* sounding D2: Effective (σ'_v) and total (σ_v) vertical stress, clean sand equivalent of the normalised cone penetration parameter ($Q_{tn,CS}$) and horizontal shear stress (τ_h).

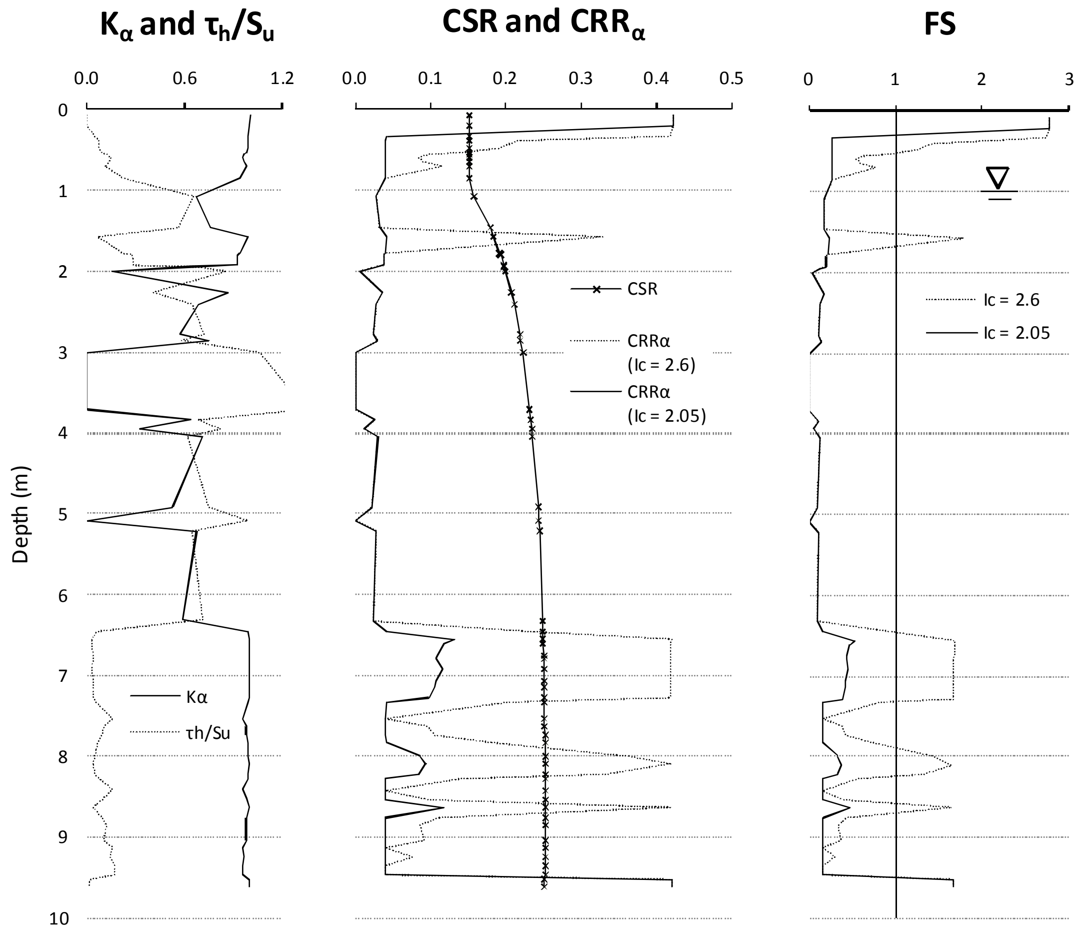

Figure A.4 Profiles corresponding to Hokkaido using *CPT* sounding D2: Static shear stress correction factor (K_{α}), horizontal shear stress to undrained shear strength ratio (τ_h/S_u), cyclic stress ratio (*CSR*), cyclic resistance ratio (CRR_{α}) and factor of safety (*FS*).

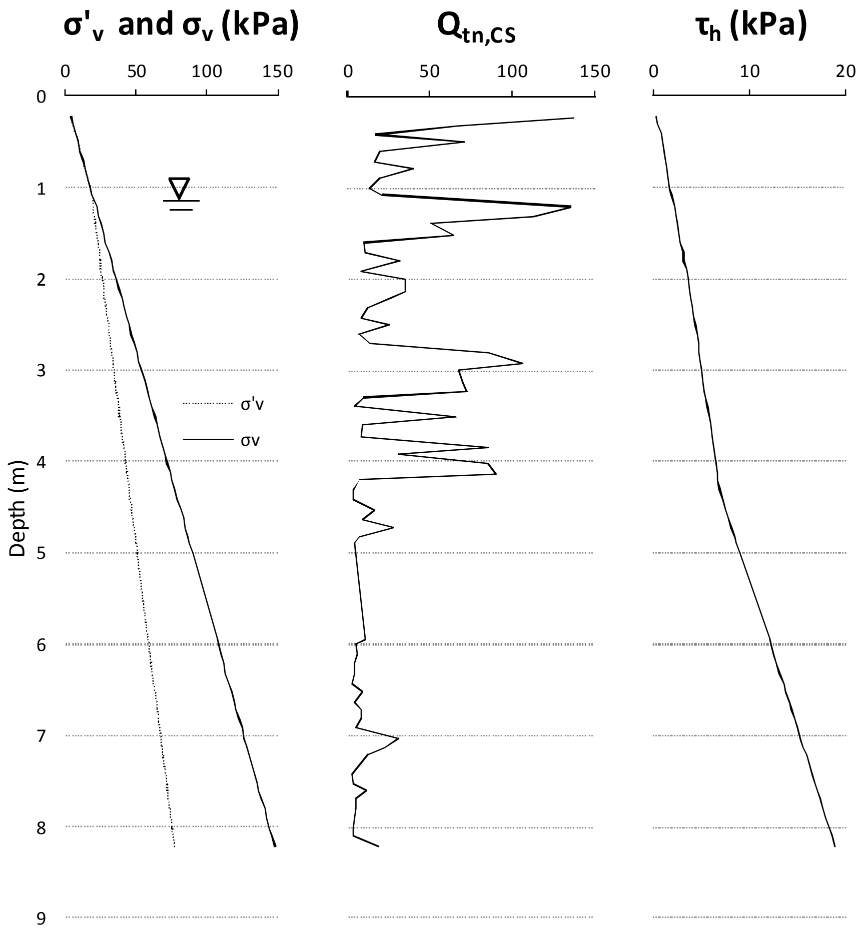

Figure A.5 Profiles corresponding to Mochikoshi Dyke 1 using *CPT* sounding SY1: Effective (σ'_v) and total (σ_v) vertical stress, clean sand equivalent of the normalised cone penetration parameter ($Q_{tn,CS}$) and horizontal shear stress (τ_h).

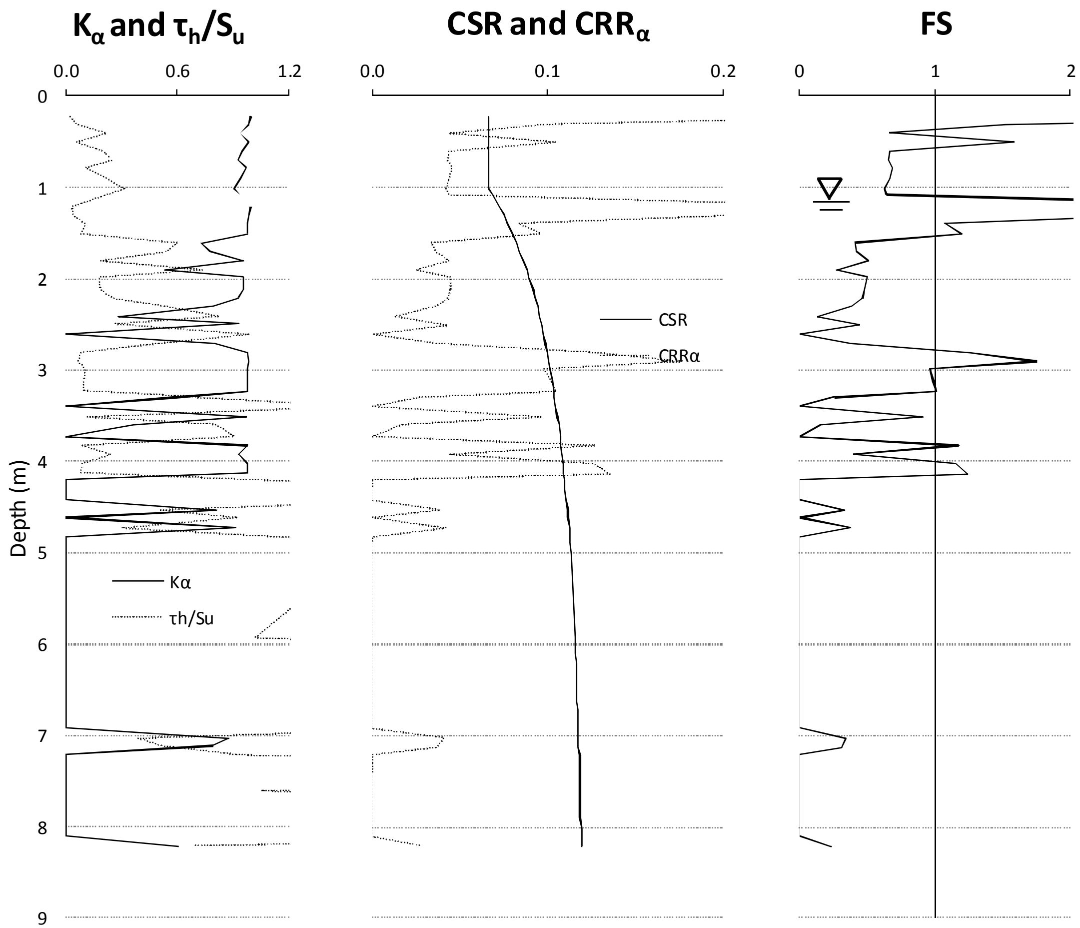

Figure A.6 Profiles corresponding to Mochikoshi Dyke 1 using *CPT* sounding SY1: Static shear stress correction factor (K_α), horizontal shear stress to undrained shear strength ratio (τ_h/S_u), cyclic stress ratio (CSR), cyclic resistance ratio (CRR_α) and factor of safety (FS).

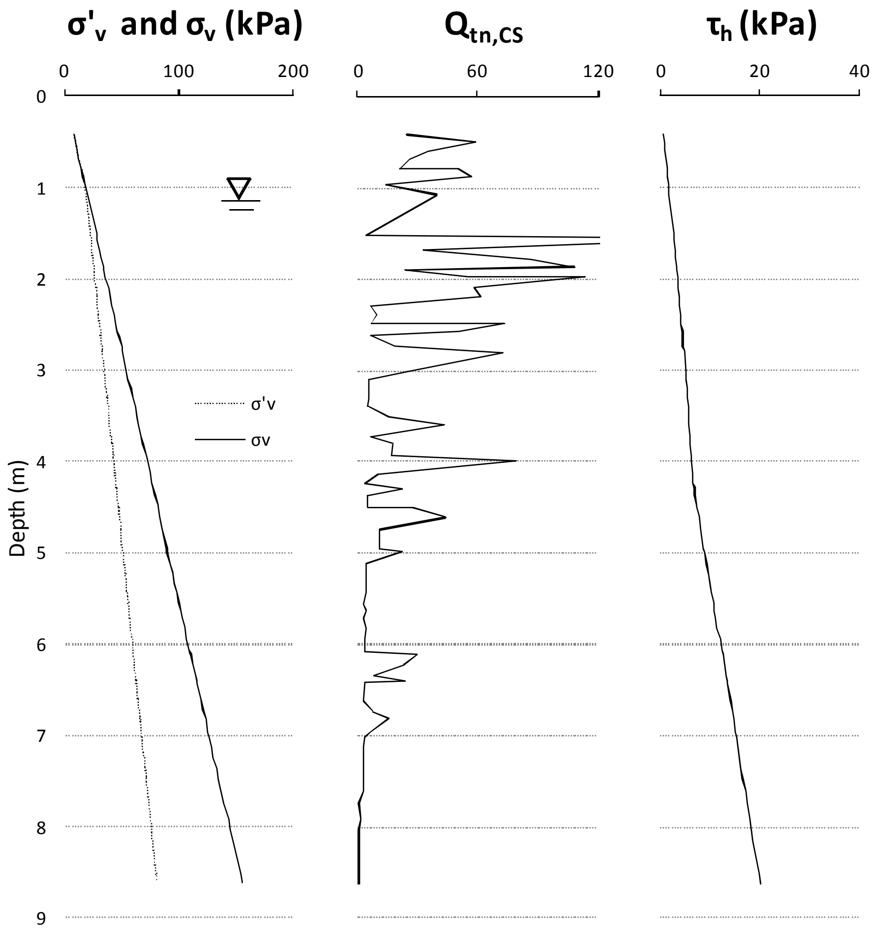

Figure A.7 Profiles corresponding to Mochikoshi Dyke 1 using *CPT* sounding SY2: Effective (σ'_v) and total (σ_v) vertical stress, clean sand equivalent of the normalised cone penetration parameter ($Q_{tn,CS}$) and horizontal shear stress (τ_h).

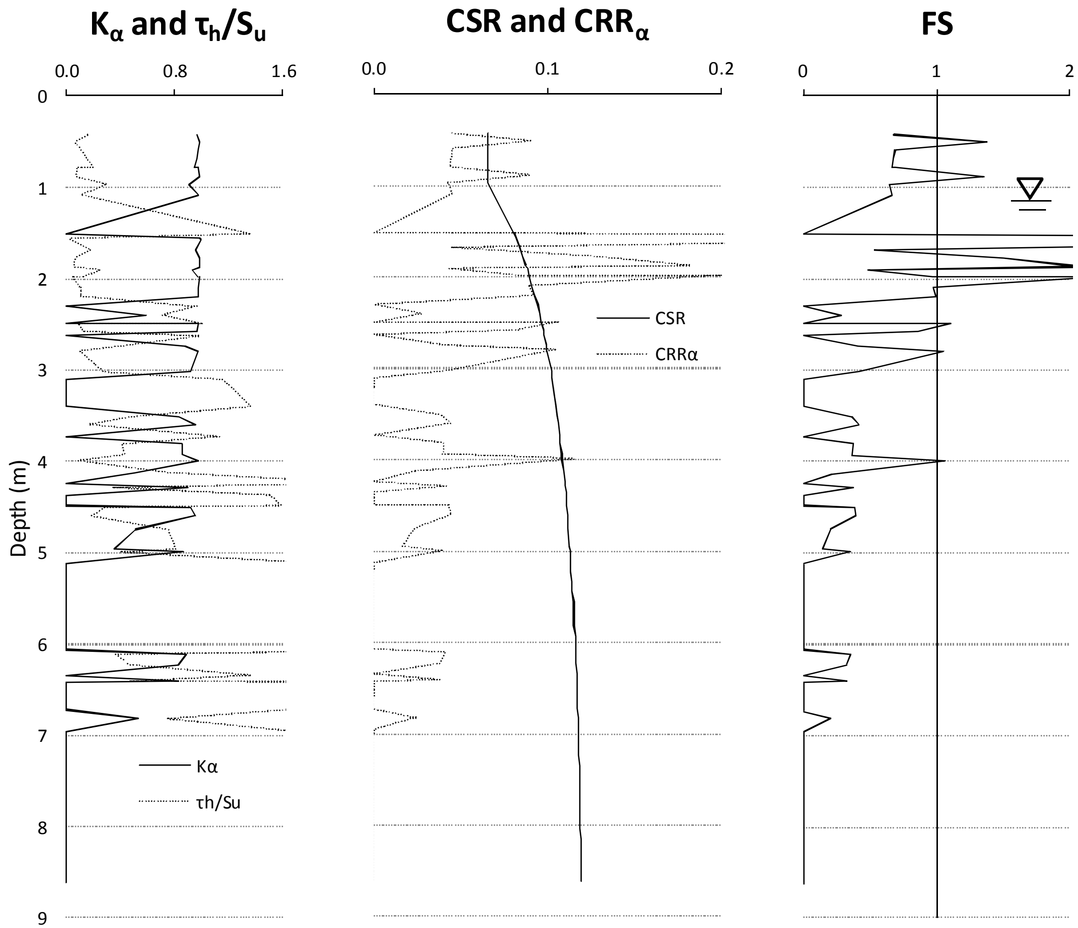

Figure A.8 Profiles corresponding to Mochikoshi Dyke 1 using *CPT* sounding SY2: Static shear stress correction factor (K_α), horizontal shear stress to undrained shear strength ratio (τ_h/S_u), cyclic stress ratio (*CSR*), cyclic resistance ratio (CRR_α) and factor of safety (*FS*).

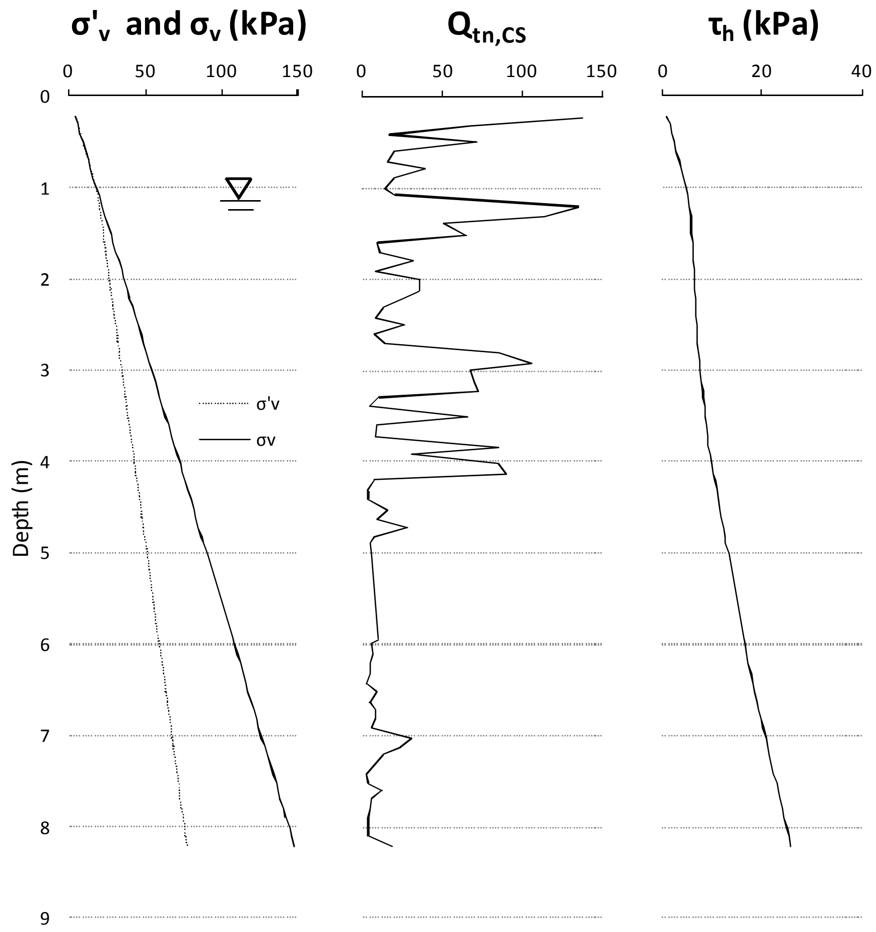

Figure A.9 Profiles corresponding to Mochikoshi Dyke 2 using *CPT* sounding SY1: Effective (σ'_v) and total (σ_v) vertical stress, clean sand equivalent of the normalised cone penetration parameter ($Q_{tn,CS}$) and horizontal shear stress (τ_h).

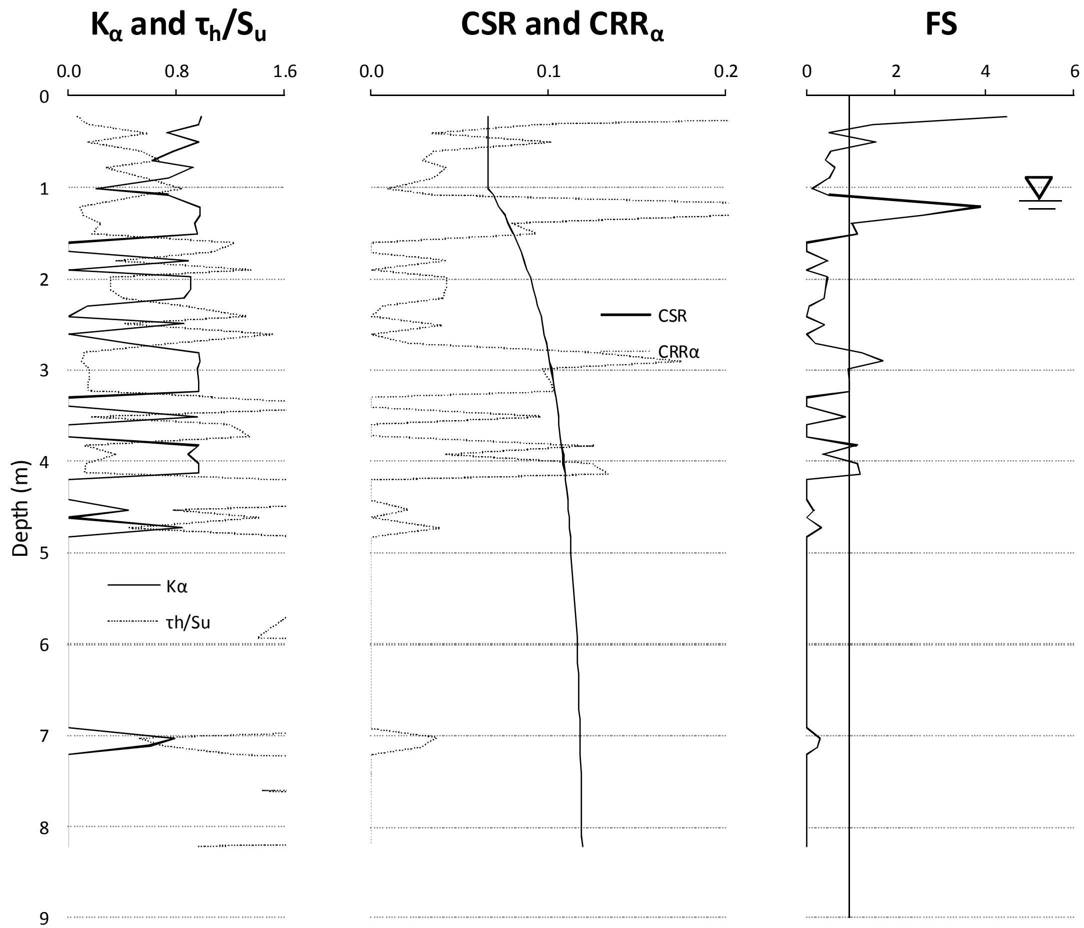

Figure A.10 Profiles corresponding to Mochikoshi Dyke 2 using *CPT* sounding SY1: Static shear stress correction factor (K_α), horizontal shear stress to undrained shear strength ratio (τ_h/S_u), cyclic stress ratio (CSR), cyclic resistance ratio (CRR_α) and factor of safety (FS).

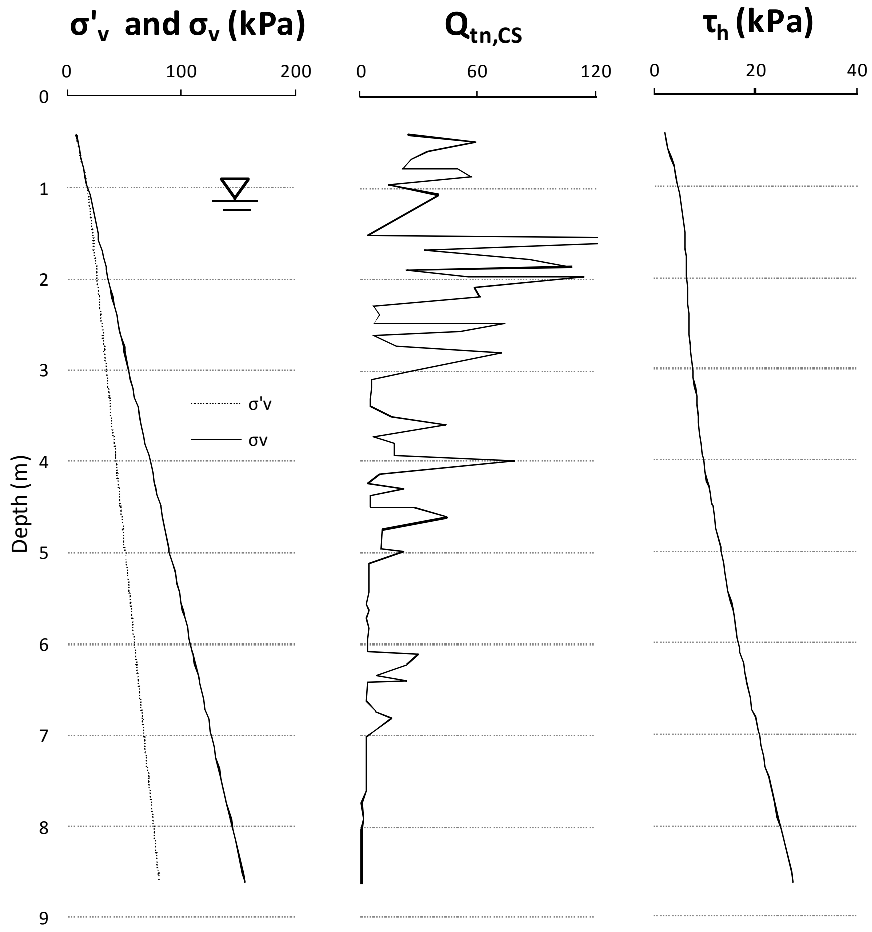

Figure A.11 Profiles corresponding to Mochikoshi Dyke 2 using *CPT* sounding SY2: Effective (σ'_v) and total (σ_v) vertical stress, clean sand equivalent of the normalised cone penetration parameter ($Q_{tn,CS}$) and horizontal shear stress (τ_h).

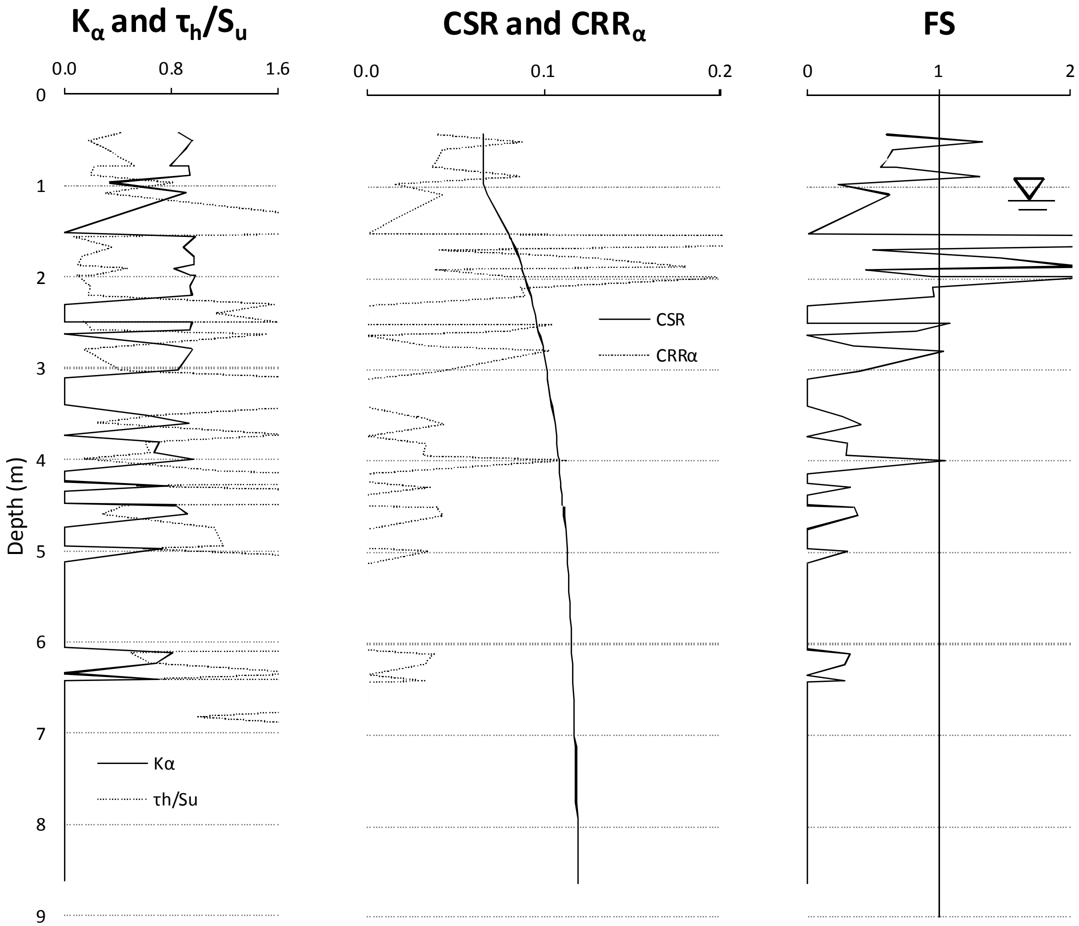

Figure A.12 Profiles corresponding to Mochikoshi Dyke 2 using *CPT* sounding SY2: Static shear stress correction factor (K_{α}), horizontal shear stress to undrained shear strength ratio (τ_h/S_u), cyclic stress ratio (CSR), cyclic resistance ratio (CRR_{α}) and factor of safety (FS).

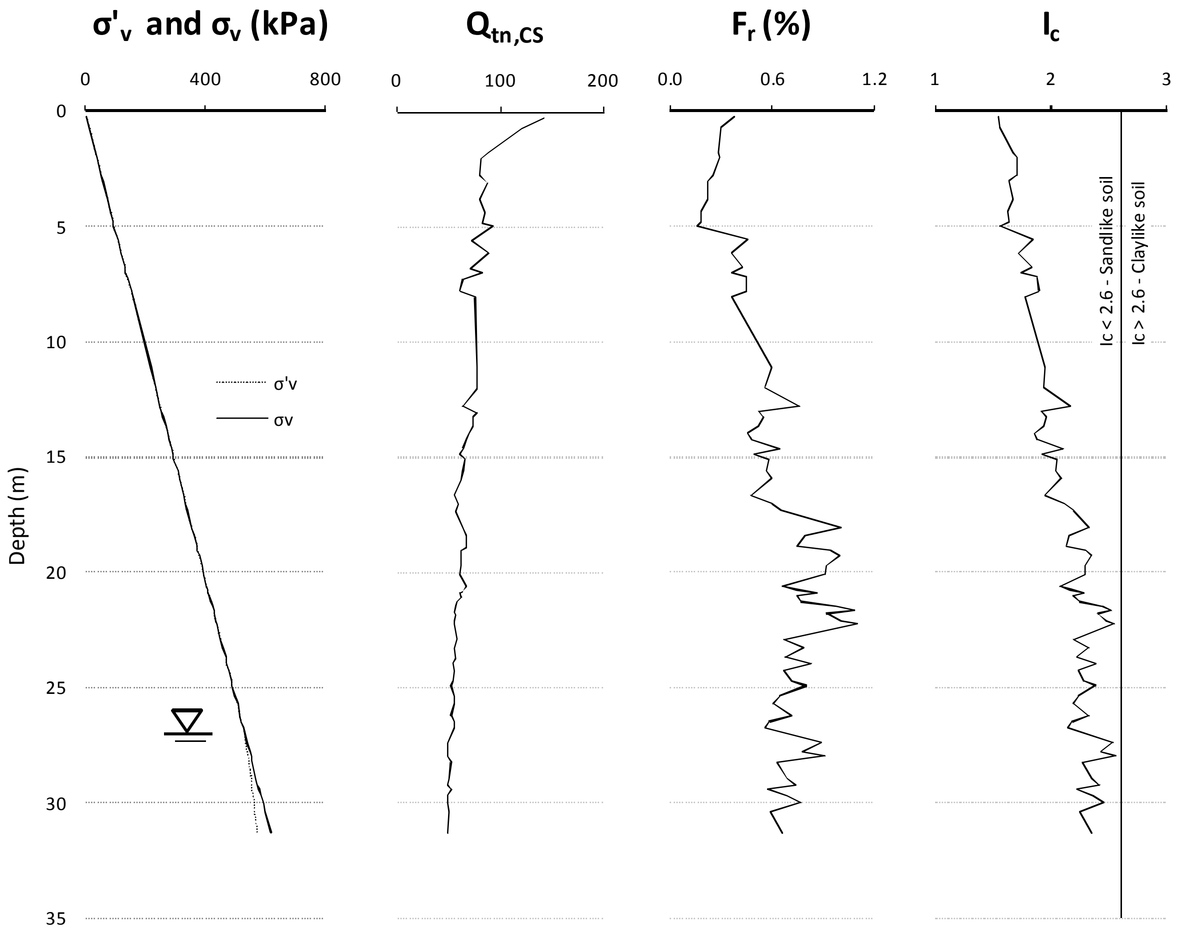

Figure A.13 Profiles corresponding to Dashihe Beach using *CPT* sounding I8: Effective (σ'_v) and total (σ_v) vertical stress, clean sand equivalent of the normalised cone penetration parameter ($Q_{tn,CS}$), friction ratio (F_r) and soil behaviour type index (I_c).

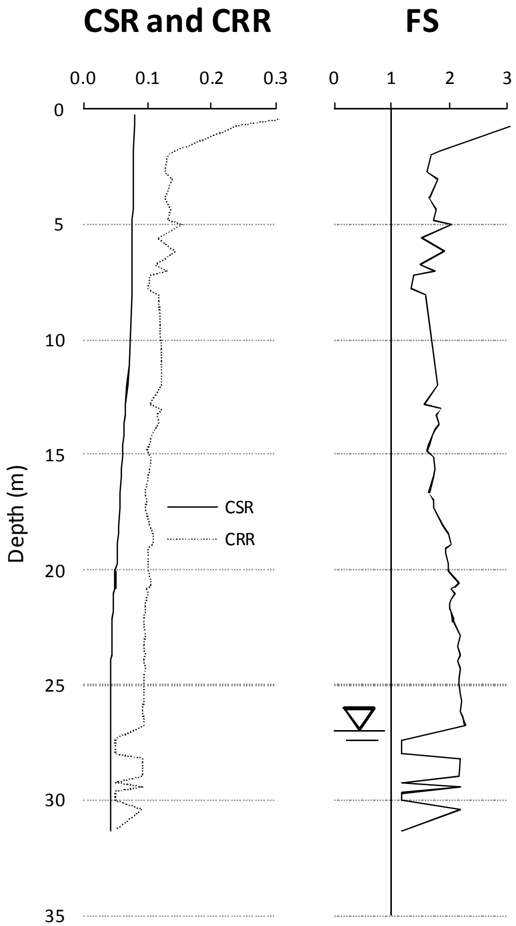

Figure A.14 Profiles corresponding to Dashihe Beach using *CPT* sounding I8: Cyclic stress ratio (*CSR*), cyclic resistance ratio (*CRR*) and factor of safety (*FS*).

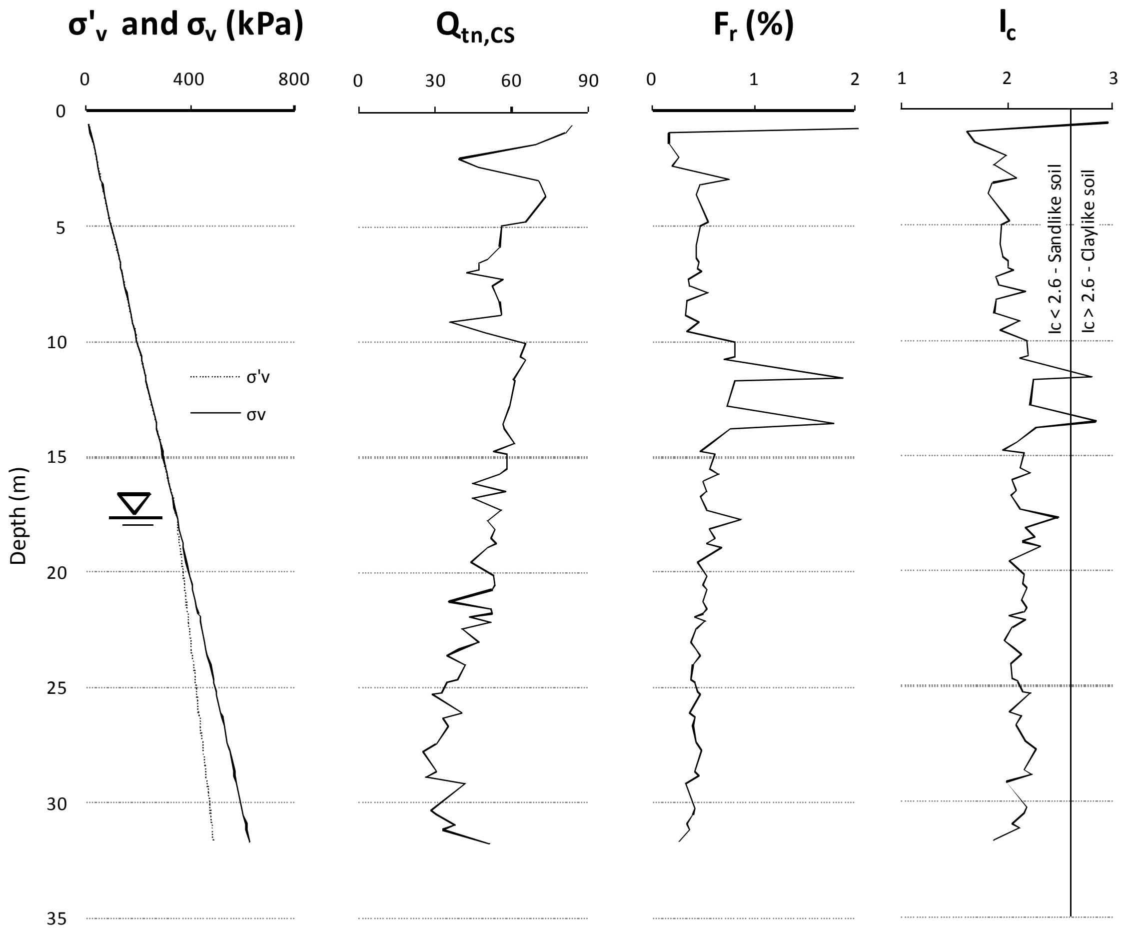

Figure A.15 Profiles corresponding to Dashihe Beach using *CPT* sounding I9: Effective (σ'_v) and total (σ_v) vertical stress, clean sand equivalent of the normalised cone penetration parameter ($Q_{tn,CS}$), friction ratio (F_r) and soil behaviour type index (I_c).

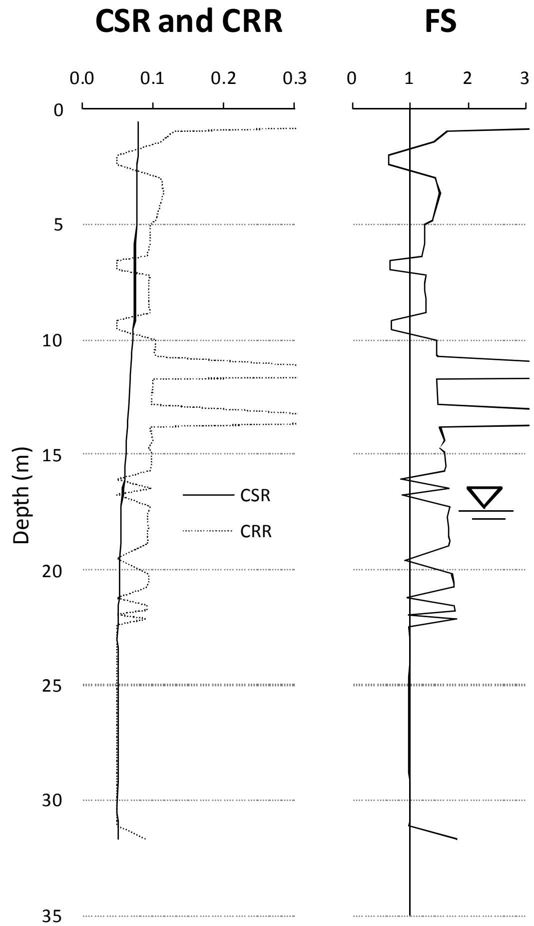

Figure A.16 Profiles corresponding to Dashihe Beach using *CPT* sounding I9: Cyclic stress ratio (*CSR*), cyclic resistance ratio (*CRR*) and factor of safety (*FS*).

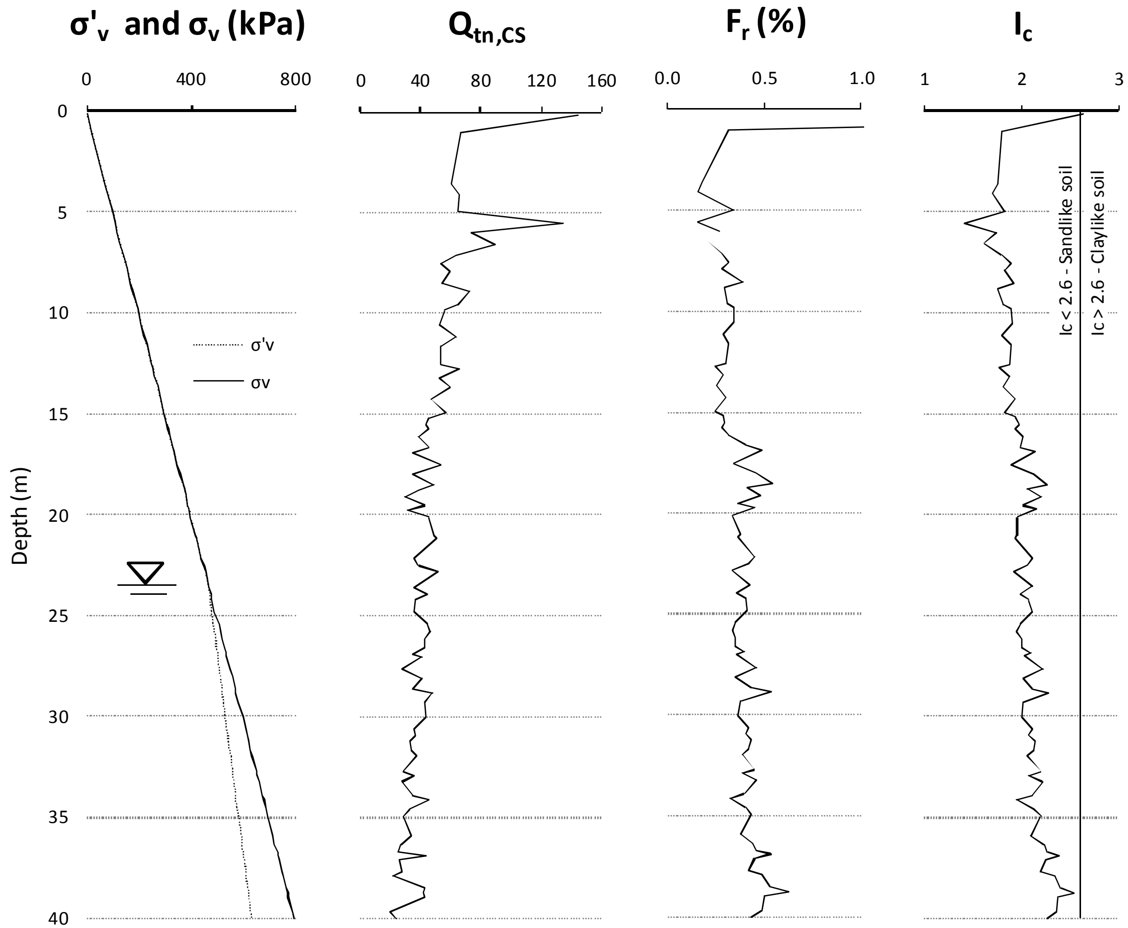

Figure A.17 Profiles corresponding to Dashihe Beach using *CPT* sounding II6: Effective (σ'_v) and total (σ_v) vertical stress, clean sand equivalent of the normalised cone penetration parameter ($Q_{tn,CS}$), friction ratio (F_r) and soil behaviour type index (I_c).

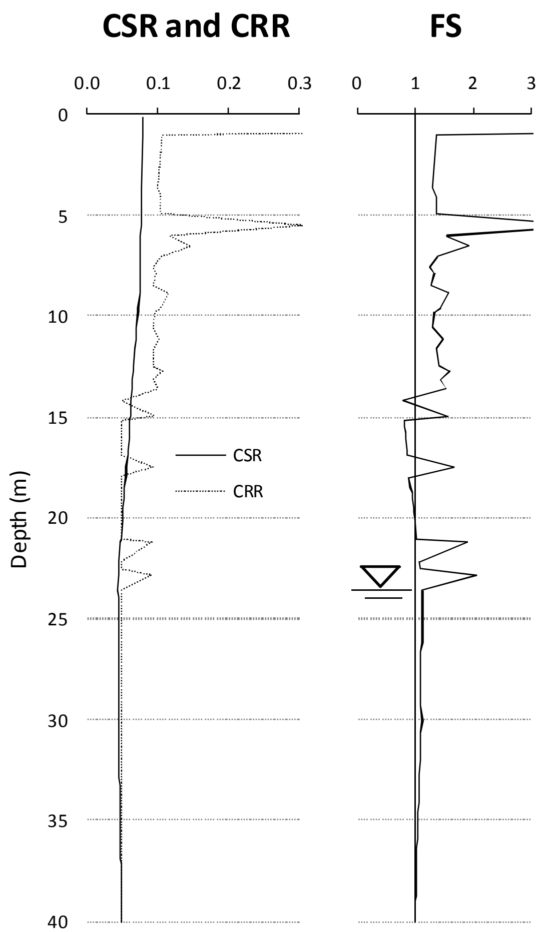

Figure A.18 Profiles corresponding to Dashihe Beach using *CPT* sounding I9: Cyclic stress ratio (*CSR*), cyclic resistance ratio (*CRR*) and factor of safety (*FS*).

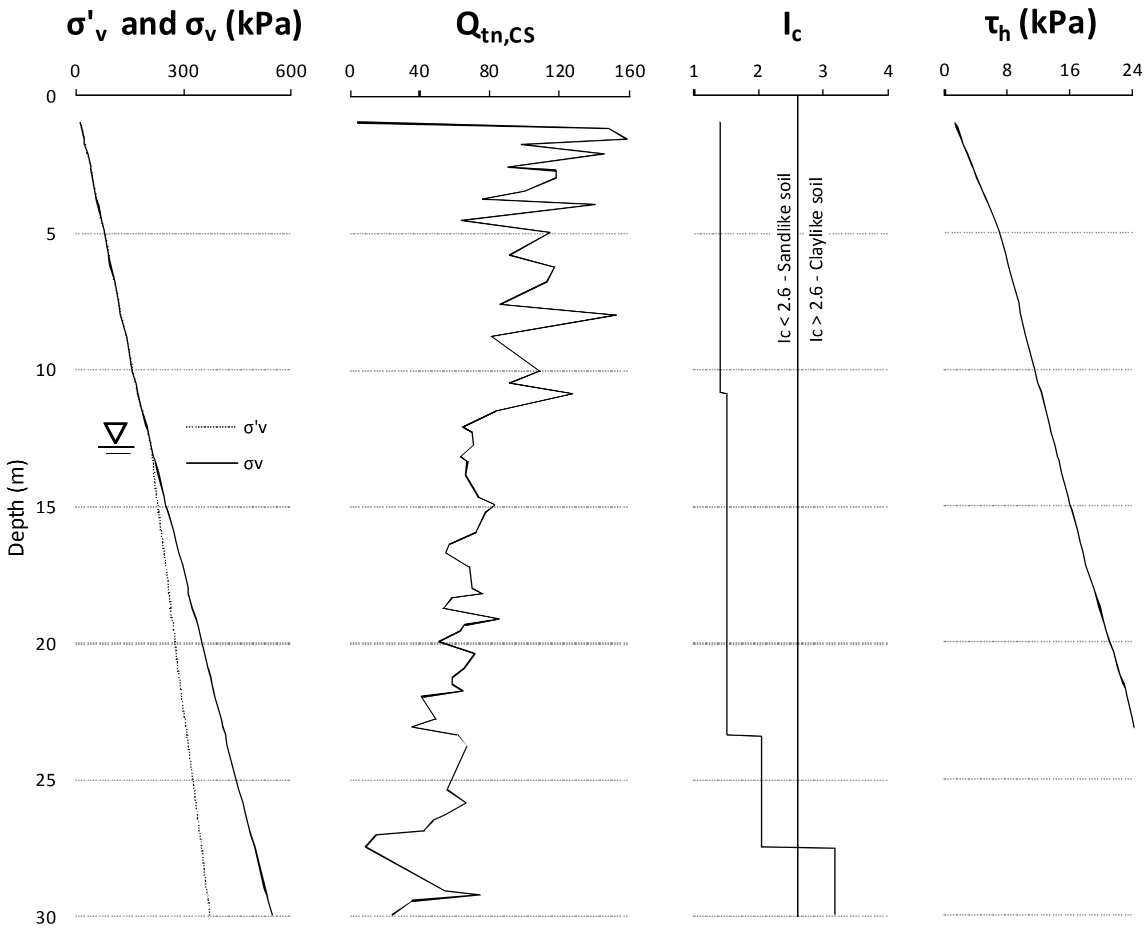

Figure A.19 Profiles corresponding to Dashihe Outer Wall using *CPT* sounding I4: Effective (σ'_v) and total (σ_v) vertical stress, clean sand equivalent of the normalised cone penetration parameter ($Q_{tn,CS}$), soil behaviour type index (I_c) and horizontal shear stress (τ_h).

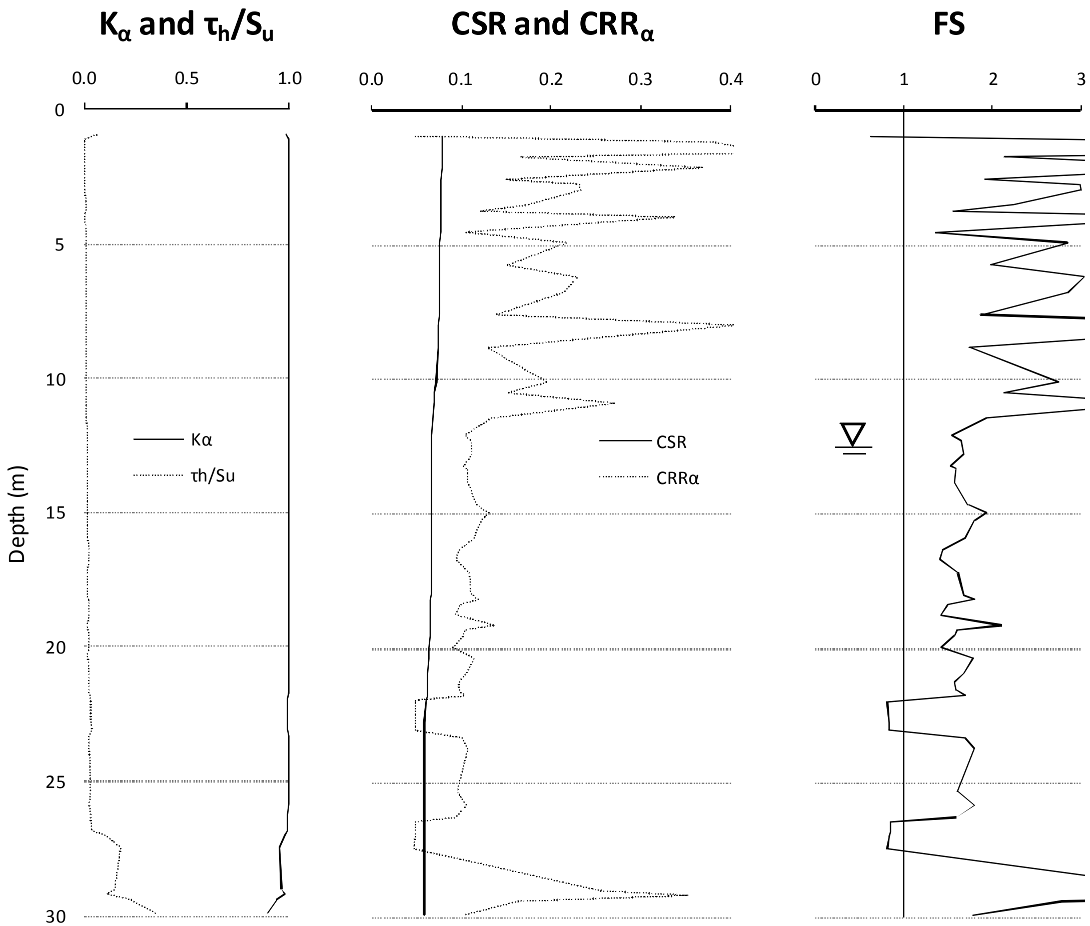

Figure A.20 Profiles corresponding to Dashihe Outer Wall using *CPT* sounding I4: Static shear stress correction factor (K_α), horizontal shear stress to undrained shear strength ratio (τ_h/S_u), cyclic stress ratio (*CSR*), cyclic resistance ratio (CRR_α) and factor of safety (*FS*).

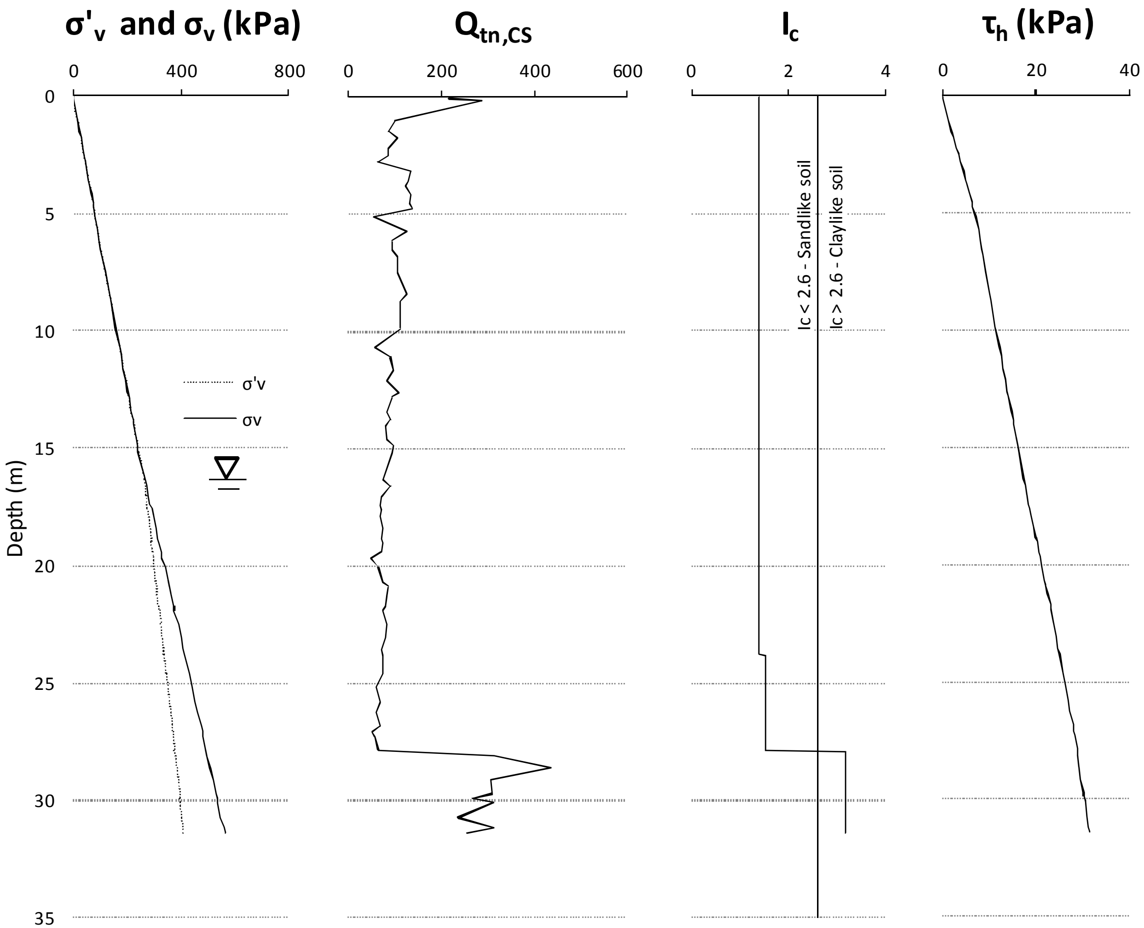

Figure A.21 Profiles corresponding to Dashihe Outer Wall using *CPT* sounding I5: Effective (σ'_v) and total (σ_v) vertical stress, clean sand equivalent of the normalised cone penetration parameter ($Q_{tn,CS}$), soil behaviour type index (I_c) and horizontal shear stress (τ_h).

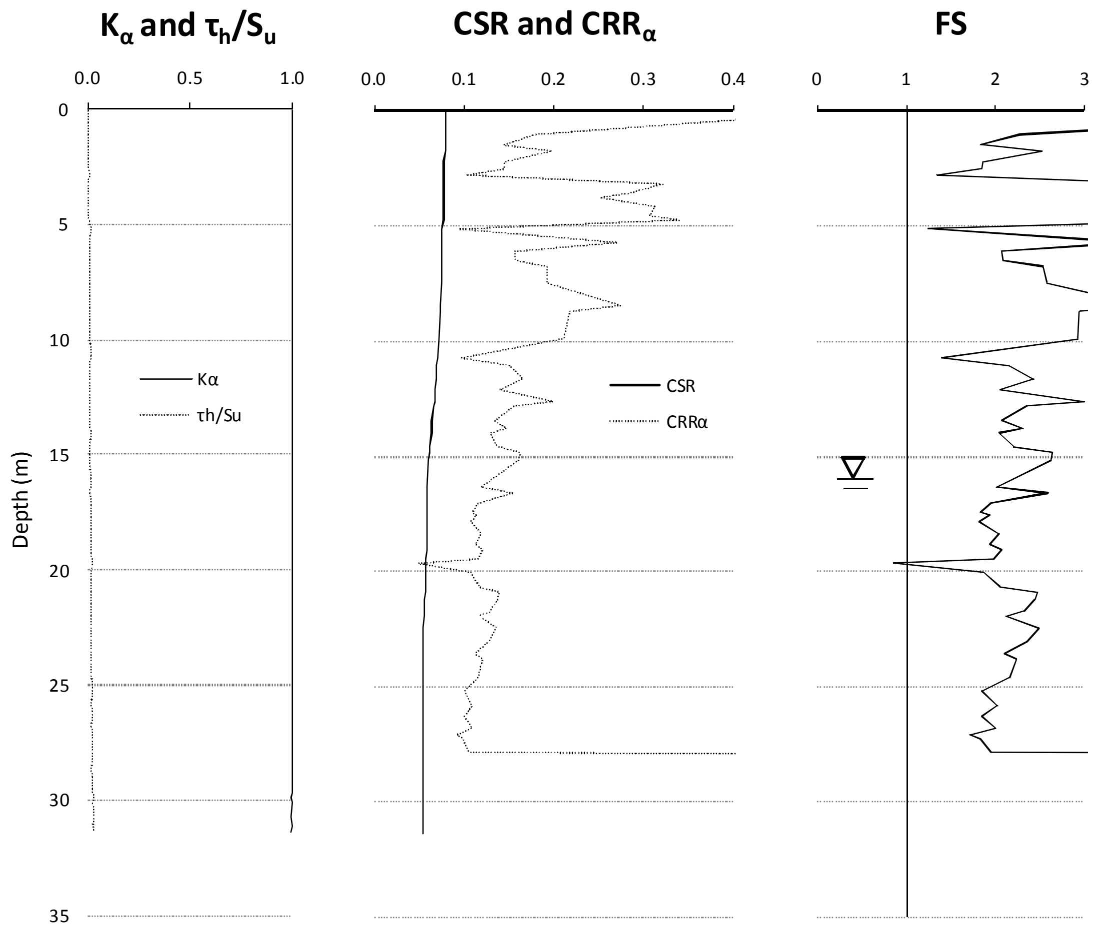

Figure A.22 Profiles corresponding to Dashihe Outer Wall using *CPT* sounding I5: Static shear stress correction factor (K_α), horizontal shear stress to undrained shear strength ratio (τ_h/S_u), cyclic stress ratio (*CSR*), cyclic resistance ratio (CRR_α) and factor of safety (*FS*).

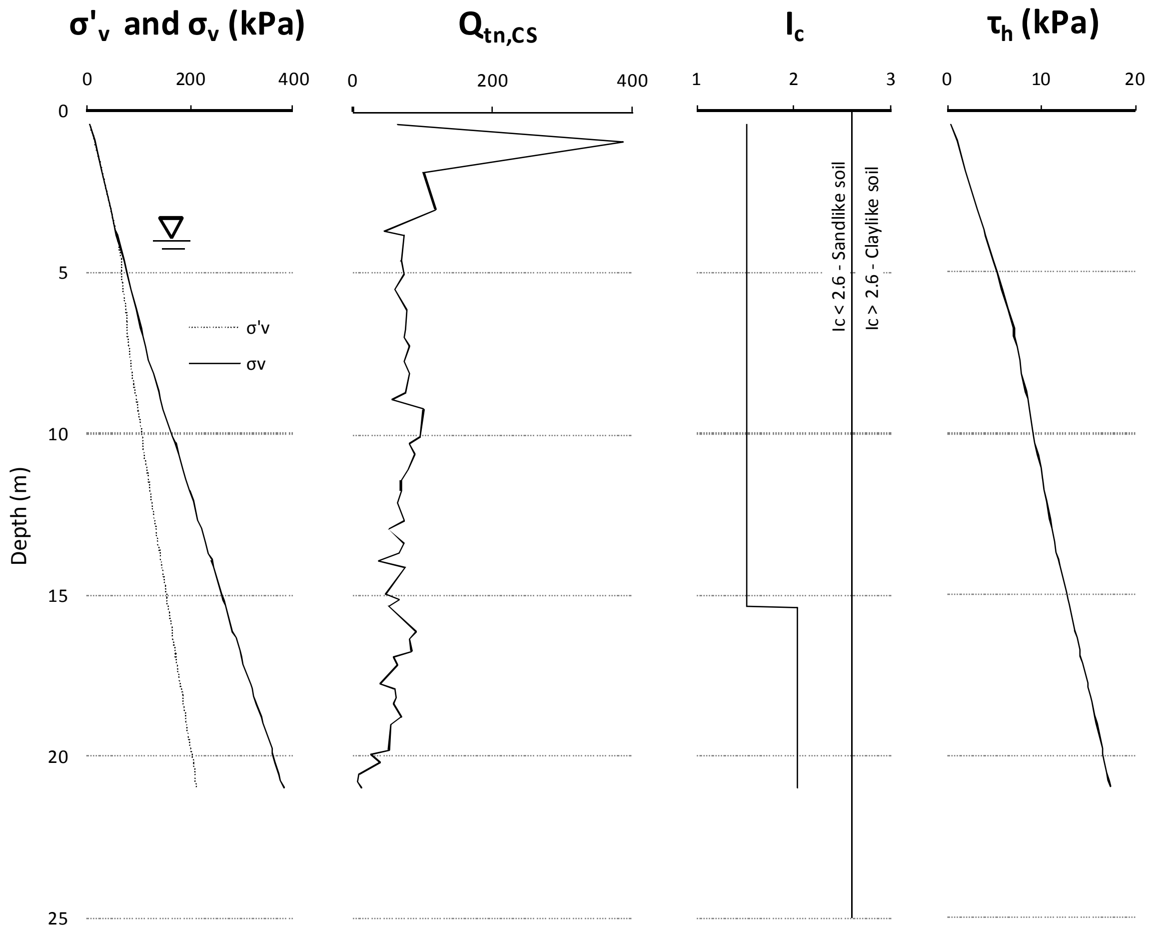

Figure A.23 Profiles corresponding to Dashihe Outer Wall using *CPT* sounding II2: Effective (σ'_v) and total (σ_v) vertical stress, clean sand equivalent of the normalised cone penetration parameter ($Q_{tn,CS}$), soil behaviour type index (I_c) and horizontal shear stress (τ_h).

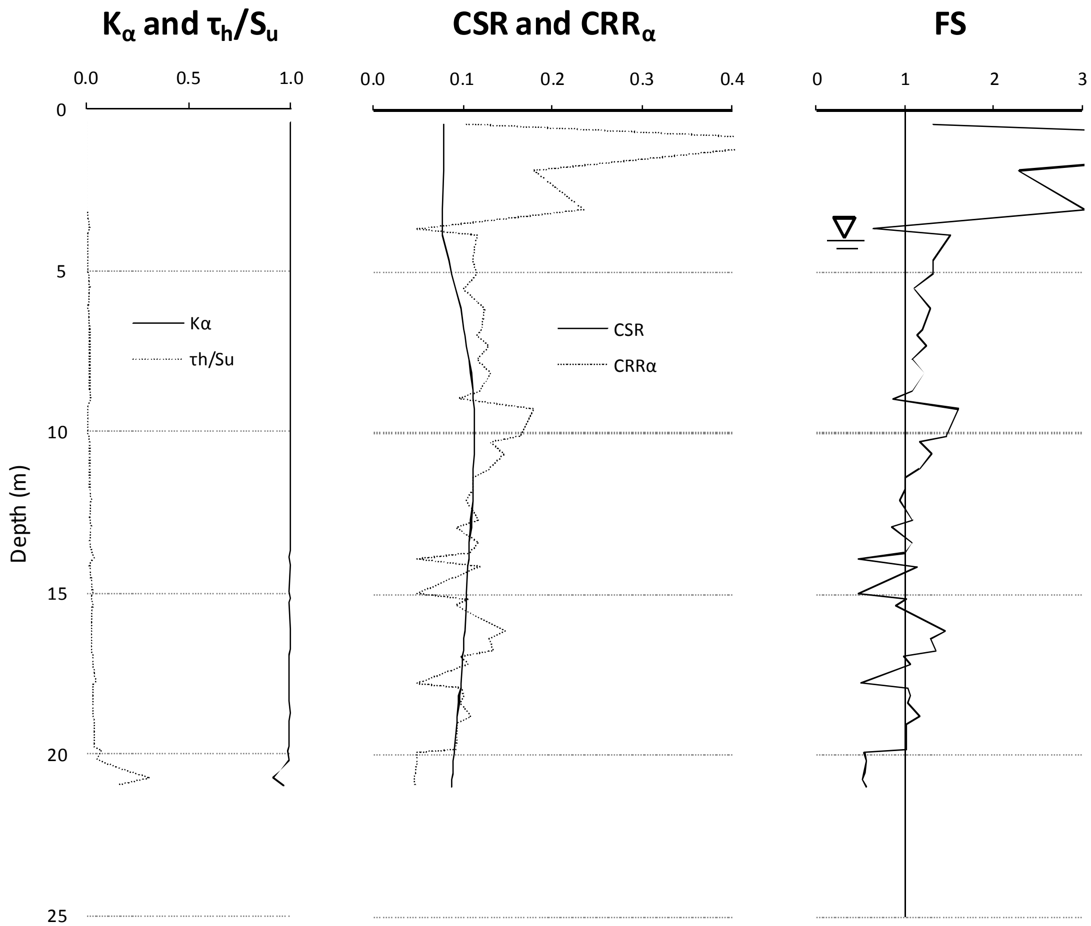

Figure A.24 Profiles corresponding to Dashihe Outer Wall using *CPT* sounding II2: Static shear stress correction factor (K_{α}), horizontal shear stress to undrained shear strength ratio (τ_h/S_u), cyclic stress ratio (*CSR*), cyclic resistance ratio (CRR_{α}) and factor of safety (*FS*).

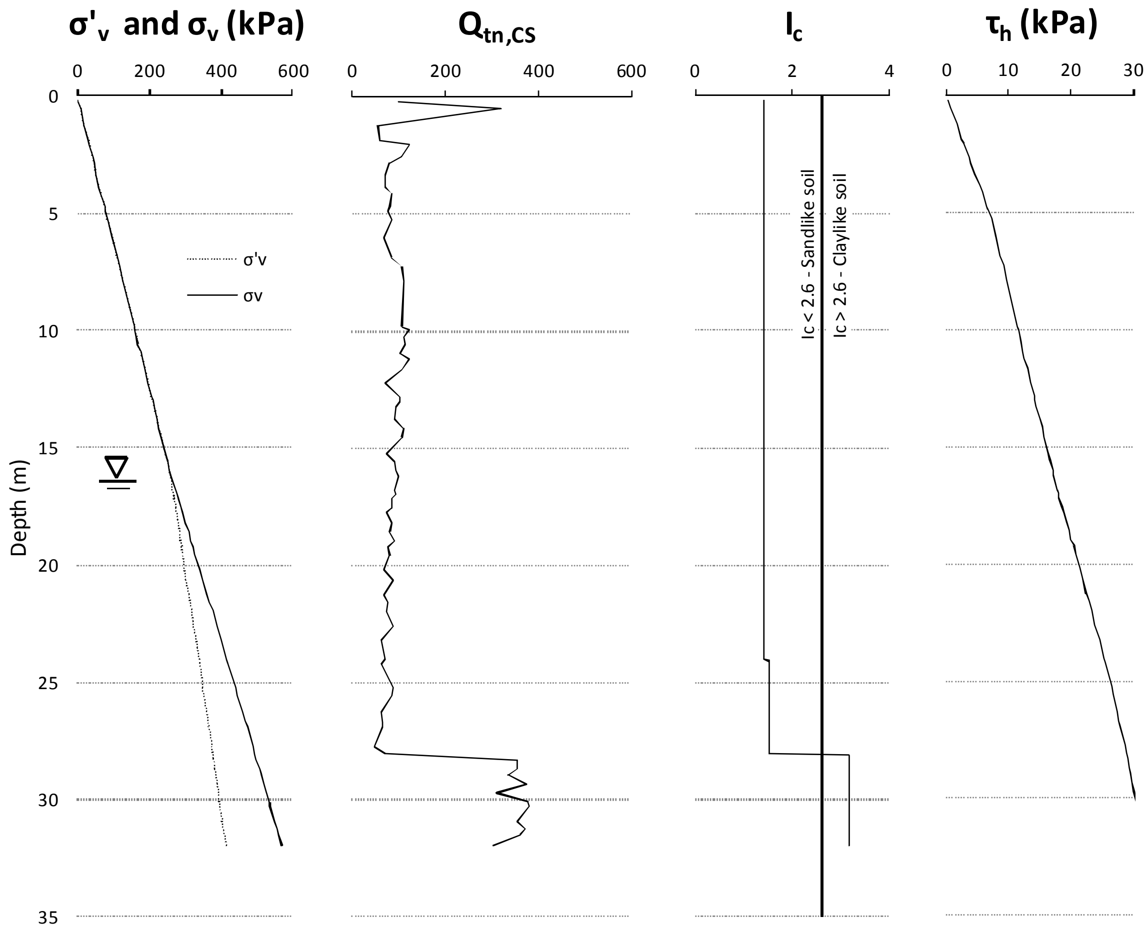

Figure A.25 Profiles corresponding to Dashihe Outer Wall using *CPT* sounding II4: Effective (σ'_v) and total (σ_v) vertical stress, clean sand equivalent of the normalised cone penetration parameter ($Q_{tn,CS}$), soil behaviour type index (I_c) and horizontal shear stress (τ_h).

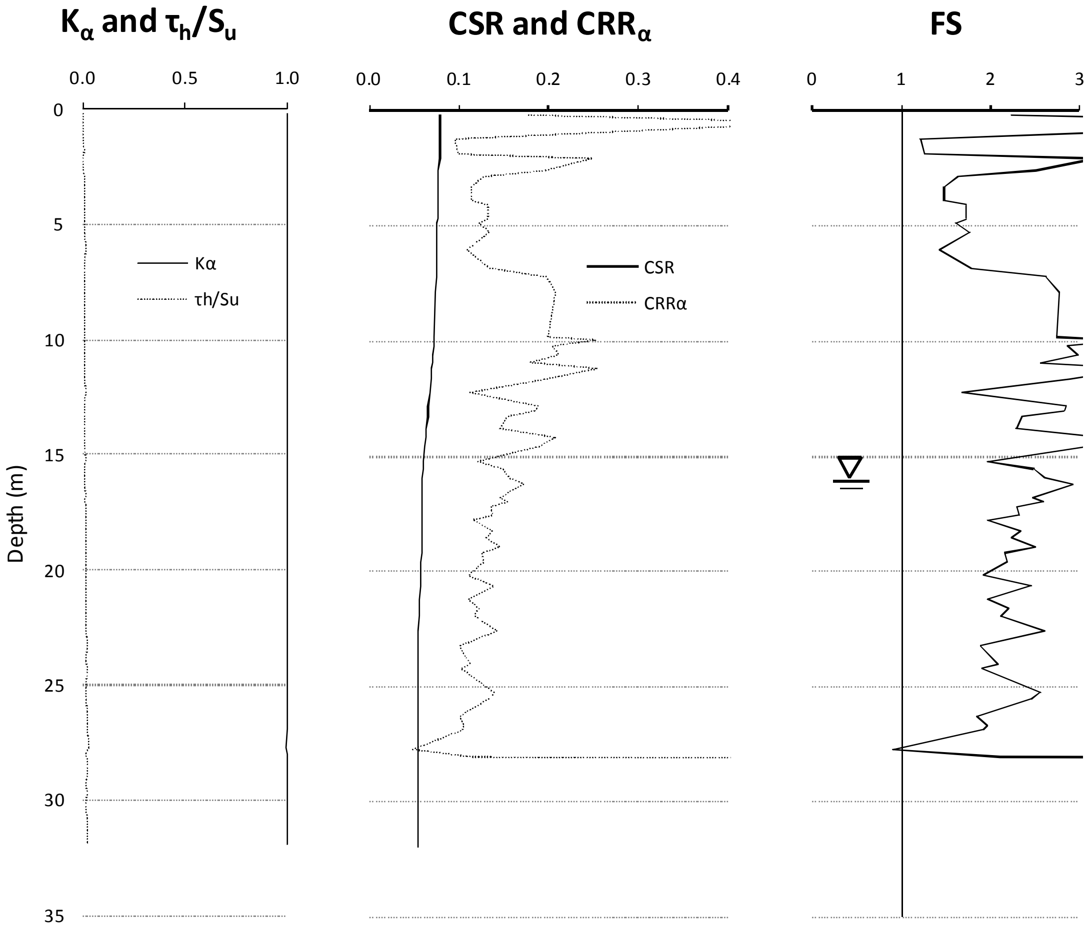

Figure A.26 Profiles corresponding to Dashihe Outer Wall using *CPT* sounding II4: Static shear stress correction factor (K_α), horizontal shear stress to undrained shear strength ratio (τ_h/S_u), cyclic stress ratio (*CSR*), cyclic resistance ratio (CRR_α) and factor of safety (*FS*).

B. Appendix B – Description of the slope stability scenarios considered when implementing the Olson and Stark methodology

B.1 Introduction

Slope stability analyses are required to implement the Olson and Stark methodology. Due to the uncertainties involved in the case histories considered, several scenarios were modelled for each case to consider different values of parameters such as:

1. Friction angle (φ')
2. Effective cohesion (c')
3. Geometry of the failure surface
4. Location of the water table
5. Capillary head
6. Yield strength ratio (*YSR*)
7. Liquefied strength ratio (*LSR*)
8. Peak horizontal acceleration (a_{max})

This appendix describes the different scenarios considered when analysing the slope stability of the case histories. The scenarios are mostly described with the aid of figures and tabulated data. The figures describe the geometry, soil types involved and slip failure surface used. The tables give the strength parameters, unit weight, characteristic q_{c1} value, resulting factors of safety and, in the case of the seismic case histories, they also give earthquake moment magnitude (M_w) and peak acceleration (a_{max}). All models were created using module Slope/W of the software package GeoStudio 2007 (Geo-Slope International Ltd.).

For some analyses, the software was allowed to search for a circular critical slip surface and subsequently optimise it to find sliding surfaces that may be weaker but do not have a circular geometry. The 'grid and radius' method was used to find the critical circular slip surface. The optimisation consisted of small modifications to the slip surface that were conducive to a smaller factor of safety. These procedures are explained in detail in Geo-Slope International Ltd. (2010). There were also some scenarios for which non-critical slip surfaces were used. This was done either because such a slip surface had been suggested by another author or because it was considered convenient to force a slip surface to intersect a region of the tailings that had not been intersected by the critical slip surface. The latter motivation is suggested by Olson (2001).

B.2 Hokkaido Dam – Japan, 1968

Seven scenarios were considered when modelling the slope stability of the Hokkaido Dam (Figure B.1 to Figure B.7 and Table B.1). Critical slip surfaces were not used in three of the scenarios: For scenarios 3 and 4, the slip surfaces suggested by Olson (2001) were used, whereas for scenario 7 a planar critical slip surface was considered.

B.3 Mochikoshi Dam – Japan, 1978

Dyke 1

Four scenarios were considered when modelling the slope stability of Dyke 1 of the Mochikoshi Dam (Figure B.8 to Figure B.11 and Table B.1). Scenarios 1 and 2 used an optimised critical slip surface and differed only on the location of the water table. Given that the same factor of safety was obtained regardless of the location of the water table, scenarios 3 and 4 only considered water table at ground level in the beach. For scenarios 3 and 4, the slip surfaces suggested by Olson (2001) were used.

Dyke 2

Five scenarios were considered when modelling the slope stability of Dyke 2 of the Mochikoshi Dam (Figure B.12 to Figure B.16 and Table B.3). Scenarios 1 and 2 used an optimised critical slip surface and differed only on the location of the water table. Given that the same factor of safety was obtained regardless of the location of the water table, scenarios 3, 4 and 5 only considered water table at ground level in the beach. For scenarios 3, 4 and 5 the slip surfaces suggested by Olson (2001) were used.

As explained in Section 5.2.4, the flow failure behaviour of this case history was not correctly predicted by the Olson and Stark methodology and therefore each scenario was analysed a second time with different *YSR*, *LSR* and a_{max} values. For the second analysis the *YSR* and *LSR* values were calculated using the upper bound values, and a_{max} was taken as 70% of the original value. The scenarios corresponding to the first and second rounds of analyses are identified with the letters *a* and *b*, respectively, in Table B.3.

B.4 Dashihe Iron Tailings Dam – China, 1990

The slope stability models of the Dashihe tailings dam used in this research were based on, but not identical to, the model used by Amante (1993). Specifically, only three types of soil were considered in this research: tailings above and below the water table, and a foundation material that was modelled as clay with a total strength c = 164 kPa. In the model used by Amante (1993), the tailings above and below the water table are further subdivided into different types of soils. However, since there are only small variations of unit weight and shear strength between these two major groups, it was considered reasonable to disregard the subdivisions for the purpose of slope stability analyses and to only use two groups of tailings with average properties. Furthermore, Amante (1993) reports that the foundation material is not composed entirely of clay, but that the clay does represent a weak layer in the foundation. Therefore in this study, the conservative simplification of assigning c = 164 kPa was made. Figure B.17 and Figure B.19 show that even under this assumption, the slip surfaces do not intersect the foundation material.

Beach

Four scenarios were considered when modelling the slope stability of the beach at the Dashihe Dam (Figure B.17 to Figure B.20 and Table B.4). For scenarios 1 and 2 a capillary rise of 5 m was adopted, whereas no capillary rise was adopted for scenarios 3 and 4. Scenarios 1 and 3 used an optimised critical slip surface and scenarios 2 and 4 used the slip surface suggested by Amante (1993).

As explained in Section 5.2.4, the flow failure behaviour of this case history was not correctly predicted by the Olson and Stark methodology and therefore each scenario was analysed a second time with different *YSR*, *LSR* and a_{max} values. For the second analysis the *YSR* and *LSR* values were calculated using the lower bound values, and a_{max} was taken as 130% of the original value. The scenarios corresponding to the first and second rounds of analyses are identified with the letters *a* and *b*, respectively, in Table B.4.

Outer Wall

Four scenarios were considered when modelling the slope stability of the outer wall at the Dashihe Dam (Figure B.21 to Figure B.24 and Table B.5). For scenarios 1 and 2 a capillary rise of 5 m was adopted, whereas no capillary rise was adopted for scenarios 3 and 4. Scenarios 1 and 3 used an optimised critical slip surface and scenarios 2 and 4 used the slip surface suggested by Amante (1993). The results in Table B.5 show that when considering the slip surface suggested by Amante (1993), the shear strength of the liquefiable tailings cannot be reduced enough to obtain a factor of safety equal to 1.

B.5 Sullivan Tailings Dam – Canada, 1991

Four scenarios were considered when modelling the slope stability of the outer wall at the Dashihe Dam (Figure B.25 to Figure B.28 and Table B.6). Optimised critical slip surfaces were used in scenarios 1 and 2, and non-critical slip surfaces were used in scenarios 3 and 4. There was uncertainty regarding the strength of the dyke material, therefore a strong dyke was assumed in scenarios 1 and 3, and a weak dyke was assumed in scenarios 2 and 4.

B.6 Merriespruit Tailings Dam – South Africa, 1994

The static shear stress that triggered liquefaction of the tailings was a function of the eroded geometry created by the overtopping water (Figure 4.13). An analysis of the retrogressive failure is included in the files of Jones and Wagener Consulting Civil Engineers (J&W), a firm hired to conduct an investigation to determine the causes of the Merriespruit failure. The geometries used in this retrogressive analysis were based on field evidence and detailed eyewitness accounts. The retrogressive failure was modelled by J&W in four stages. Given that the first three stages mainly involved failure of the consolidated tailings in the outer wall, it is reasonable to assume that it was only in the fourth stage that the impounded tailings were subjected to the static shear stress that triggered liquefaction. The geometry of this fourth stage was used in this research to analyse the slope stability of the tailings dam.

Four scenarios were considered when modelling the slope stability of the Merriespruit Dam (Figure B.29 to Figure B.32 and Table B.7). A non-critical slip surface was used in scenario 2, in which a slip surface used in the analyses conducted by J&W was adopted. All other scenarios used a critical slip surface. Scenario 4 considers that the foundation soil is impenetrable.

B.7 GMTS Tailings Dam – South Africa, 2001

Five scenarios were considered when modelling the slope stability of the GMTS Dam (Figure B.33 to Figure B.37 and Table B.8). Optimised critical slip surfaces were used in scenarios 3 and 4, and non-critical slip surfaces were used in scenarios 1, 2 and 5. The slip surface used in scenario 1 is suggested in WM&B (2001). Scenario 2 used the same slip surface as a starting point but the software was allowed to optimise it. The results show that in scenario 1, the strength of the liquefiable tailings cannot be reduced enough to bring the factor of safety down to one. In scenario 5 the slip surface was forced to intersect a portion of the tailings that had not been intersected in the first four scenarios, and a weaker foundation soil was assumed.

Scenarios 3, 4 and 5 assume that the tailings above the water table are not saturated and thus not susceptible to liquefaction. To account for the uncertainty of the strength parameters of these non-liquefiable tailings, scenarios 3 and 4 use different strength parameters, however the resulting factors of safety remain unchanged.

As explained in Section 5.2.4, the flow failure behaviour of this case history was not correctly predicted by the Olson and Stark methodology and therefore each scenario was analysed a second time with different *YSR* and *LSR* values. For the second analysis the *YSR* and *LSR* values were calculated using the upper bound values. The scenarios corresponding to the first and second rounds of analyses are identified with the letters *a* and *b*, respectively, in Table B.8.

B.8 Mooifontein Tailings Dam – South Africa, 2001

Seven scenarios were considered when modelling the slope stability of the Mooifontein Dam (Figure B.38 to Figure B.44 and Table B.9). Scenarios 1 and 4 use the lower bound limit of shear strength of the foundation soil, where as the other scenarios use the upper bound limit. The results show that the factors of safety show little dependence on the strength properties of the foundation soil, i.e., the slip surface mostly intercepts the tailings.

Scenarios 1 and 2 use a slip surface suggested by WM&B (2001). Scenario 3 used the same slip surface as a starting point but the software was allowed to optimise it. In all other scenarios, a critical slip surface was searched for. Scenarios 6 and 7 assume that the tailings above the water table are not saturated and therefore not susceptible to liquefaction. Scenario 6 assumes that these non-liquefiable tailings have $\varphi' = 37^{\circ}$, whereas scenario 7 assumes they have $\varphi' = 43^{\circ}$. The resulting factors of safety for scenarios 6 and 7 are virtually identical.

As explained in Section 5.2.4, the flow failure behaviour of this case history was not correctly predicted by the Olson and Stark methodology and therefore each scenario was analysed a second time with different *YSR* and *LSR* values. For the second analysis the *YSR* and *LSR* values were calculated using the upper bound values. The scenarios corresponding to the first and second rounds of analyses are identified with the letters *a* and *b*, respectively, in Table B.9.

B.9 Dam A – Brazil, 2009

As described in Section 4.8, this case history was studied by Neto (2009) to determine whether the construction of a 3.5 m rise on the outer wall could compromise its stability. As a worst case scenario, a completely undrained loading was assumed here when modelling the slope stability of Dam A. This implies that the construction of the 3.5 m rise will generate an increase in pore water pressures (Δu) and therefore a reduction in effective stresses that could be detrimental to the stability of the Dam. It is a worst case scenario because in reality, it is possible that the tailings are coarse enough to quickly dissipate any pore water pressure build-up that could be caused by the construction of the 3.5 m rise.

The magnitude of Δu depends on the magnitudes of the increase in the total principal stresses $\Delta\sigma_1$ and $\Delta\sigma_3$, and the Skempton pore water pressure parameters A and B. To simplify the determination of $\Delta\sigma_1$ and $\Delta\sigma_3$, the geometry of the 3.5 m rise was converted into an equivalent rectangle having the same area and therefore applying the same total load on the dam (Figure 4.21). The equivalent rectangle applies a uniform strip load on the dam and therefore the increments in σ_1 and σ_3 that it generates at any point beneath the beach surface can be readily calculated from a suitable stress distribution chart. In this study, the chart 'Principal stresses under strip load' presented in Lambe and Whitman (1969) was used to determine $\Delta\sigma_1$ and $\Delta\sigma_3$ at several points on the surface of the original water table.

In the determination of Skempton parameter A, its value at failure (A_f) was calculated from the results of six undrained triaxial tests published by Neto (2009). These undrained triaxial tests had initial confinement pressures of 50 kPa and 100 kPa which compare well with the initial confinement pressures estimated for the tailings in the location of the water table which ranged approximately from 15 kPa to 90 kPa. The A_f values ranged from 0.45 to 0.65 with an average value of 0.54 which was taken here as representative of the tailings. Even though the construction of the 3.5 m rise did not load the underlying tailings to the point of failure, use of a single A_f value was deemed acceptable as a conservative simplifying assumption. Skempton parameter B was taken equal to 1 as is usually the case in saturated soils.

It is standard practice in soil mechanics to divide the total increase in pore water pressure (Δu) caused by undrained loading into two parts: The increase due to the isotropic loading (Δu_i), and the increase due to the deviator stress (Δu_d). Therefore Δu can be calculated as:

$$\Delta u = \Delta u_i + \Delta u_d \qquad \text{Eq. B.1}$$

And Δu_i and Δu_d can be calculated as:

$$\Delta u_i = \Delta\sigma_3 \cdot B = \Delta\sigma_3 \qquad \text{Eq. B.2}$$

$$\Delta u_d = (\Delta\sigma_1 - \Delta\sigma_3) \cdot A \qquad \text{Eq. B.3}$$

The total increase in pore water pressure (Δu) was modelled by increasing the height of the water table. This increase in height (Δh) was calculated as:

$$\Delta h = \frac{\Delta u}{\gamma_w} \qquad \text{Eq. B.4}$$

Where γ_w is the unit weight of water, taken as 9.81 kN/m^3. A rise in the height of the water table is only an approximate way of modelling the effect of the undrained loading that could be generated by the 3.5 m rise. By raising the water table, the exact Δu can be generated at the original location of the water table, however, pore water pressures in greater than the ones expected due to undrained loading are generated below the original location of the water table. Nonetheless, the difference between the modelled and real pore water pressures becomes less important with depth. It should also be noticed that by raising the water table, the regime of pore water pressures being generated is on the conservative side. The raised water table was used in the slope stability models of Dam A. The detailed calculations are shown in Table B.11.

Four scenarios were considered when modelling the slope stability of Dam A (Figure B.45 to Figure B.48 and Table B.10). In accordance with Neto (2009), scenarios 1, 2 and 3 assumed that all tailings deposited below the height of 1089.4 m were non-liquefiable.

However in accordance with the findings of this study (Figure 5.7), scenario 4 assumed that all deposited tailings were liquefiable. In no case was triggering of liquefaction predicted. Scenario 1 used the slip surface suggested by Neto (2009), whereas in scenarios 2, 3 and 4 the critical slip surface was searched for.

B.10 Tables and Figures

Note: For tables Table B.1 to Table B.10, FS_T = factor of safety against triggering of liquefaction and FS_F = factor of safety against flow failure.

Table B.1 Scenarios used to analyse Hokkaido Dam.

Scenario	Liquefiable tailings			Non-liquefiable tailings			Dyke material			M_w	a_{max}	q_{c1}*	Slip surface	FS_T	FS_F
	φ'	c'	γ_t	φ'	c'	γ_t	φ'	c'	γ_t	(--)	(m/s^2)	(MPa)			
1	0	24.3	19.8	30	0	19.8	Impenetrable bedrock			8	2.3	0.47	Critical slip surface was searched.	0.45	0.15
2		24.0		35										0.46	0.15
3		12.9		32.5									Slip surface is upper one suggested by Olson (2001).	0.59	0.23
4		17.9		32.5									Slip surface is lower one suggested by Olson (2001).	0.48	0.16
5		23.4		30									Critical slip surface was searched.	0.46	0.15
6		23.3		35										0.46	0.15
7		5.2		--	--	--							Slip surface taken as planar.	0.59	0.35

Table B.2 Scenarios used to analyse Mochikoshi Dyke 1

Scenario	Liquefiable tailings			Dyke material			M_w	a_{max}	q_{c1}*	Slip surface	FS_T	FS_F
	φ'	c'	γ_t	φ'	c'	γ_t	(--)	(m/s^2)	(MPa)			
1	0	30.5	17.6	35	0	16.6	7.7	2.5	0.23	Critical slip surface was searched.	0.45	0.15
2		30.5									0.46	0.15
3		19								Slip surface is upper one suggested by Olson (2001).	0.59	0.23
4		28								Slip surface is lower one suggested by Olson (2001).	0.48	0.16

Table B.3 Scenarios used to analyse Mochikoshi Dyke 2.

Scenario	Liquefiable tailings			Dyke material			M_w	a_{max}	q_{c1}*	Slip surface	FS_T	FS_F
	φ'	c'	γ_t	φ'	c'	γ_t	(--)	(m/s^2)	(MPa)			
1a	0	20.9	17.6	35	0	15.1	7.7	2.5	0.23	Critical slip surface was searched.	0.48	0.16
1b								1.75			0.68	0.30
2a		20.9						2.5			0.48	0.16
2b								1.75			0.68	0.30
3a		3.2						2.5		Slip surface is upper one suggested by Olson (2001).	0.74	0.60
3b								1.75			1.16	--
4a		11.8						2.5		Slip surface is middle one suggested by Olson (2001).	0.53	0.20
4b								1.75			0.76	0.37
5a		14.0						2.5		Slip surface is lower one suggested by Olson (2001).	0.47	0.18
5b								1.75			0.68	0.35

Table B.4 Scenarios used to analyse Dashihe Beach.

Scenario	Liquefiable tailings			Non-liquefiable tailings			Clay			M_w	a_{max}	q_{c1}*	Slip surface	FS_T	FS_F
	φ'	c'	γ_t	φ'	c'	γ_t	φ'	c'	γ_t	(--)	(m/s^2)	(MPa)			
1a	0	10.2	19.6	39	0	15.9	0	164	18.9	7.5	1.2	4.5	Critical slip surface was searched.	2.51	--
1b											1.6			1.74	--
2a		3.9									1.2		Slip surface is as suggested by Amante (1993).	1.84	--
2b											1.6			1.31	--
3a		9.4									1.2		Critical slip surface was searched.	2.31	--
3b											1.6			1.59	--
4a		2.7									1.2		Slip surface is as suggested by Amante (1993).	1.66	--
4b											1.6			1.12	--

Table B.5 Scenarios used to analyse Dashihe Outer Wall.

Scenario	Liquefiable tailings			Non-liquefiable tailings			Clay			M_w	a_{max}	q_{c1}*	Slip surface	FS_T	FS_F
	φ'	c'	γ_t	φ'	c'	γ_t	φ'	c'	γ_t	*(--)*	*(m/s^2)*	*(MPa)*			
1	0	75	19.6	39	0	15.9	0	164	18.9	7.5	1.2	5.6	Critical slip surface was searched.	1.22	--
2		0											Slip surface is as suggested by Amante (1993).	--	--
3		77.1											Critical slip surface was searched.	1.19	--
4		0											Slip surface is as suggested by Amante (1993).	--	--

Table B.6 Scenarios used to analyse Sullivan Dam.

Scenario	Liquefiable tailings			Dyke material			q_{c1}*	Slip surface	FS_T	FS_F
	φ'	c'	γ_t	φ'	c'	γ_t	*(MPa)*			
1	0	43.6	24	35	15	22.4	1.4	Critical slip surface was searched.	0.85	0.19
2		43.6		30	5				0.83	0.18
3		23.7		35	15			Slip surface was forced to intersect different portion of tailings.	0.95	0.21
4		25.3		30	5				0.89	0.20

Table B.7 Scenarios used to analyse Merriespruit Dam.

Scenario	Liquefiable tailings			Natural soil			q_{c1}*	Slip surface	FS_T	FS_F
	φ'	c'	γ_t	φ'	c'	γ_t	*(MPa)*			
1	0	83.3	20	40	40	20	0.92	Critical slip surface was searched.	0.42	0.08
2		55						Slip surface is as suggested by Jones & Wagener.	0.36	0.07
3		83.6						Critical slip surface was searched controlling entry and exit angles.	0.42	0.08
4		83		Impenetrable bedrock				Critical slip surface was searched.	0.43	0.09

Table B.8 Scenarios used to analyse GMTS Dam.

Scenario	Liquefiable tailings			Non-liquefiable tailings			Foundation Soil			q_{c1}*	Slip surface	FS_T	FS_F
	φ'	c'	γ_t	φ'	c'	γ_t	φ'	c'	γ_t	*(MPa)*			
1a	0	48	19	--	--	--	34	7	18	2.5	Slip surface is as suggested by WM&B (2001).	1.57	--
1b												1.83	--
2a		119									Slip surface is as suggested by WM&B (2001) but then optimised.	0.75	0.21
2b												0.87	0.30
3a		135		37	0	19					Critical slip surface was searched.	0.72	0.20
3b												0.84	0.29
4a		134.4		43								0.73	0.20
4b												0.85	0.29
5a		99.5		43			28	0			Slip surface was forced to intersect different portion of tailings.	0.67	0.18
5b												0.78	0.27

Table B.9 Scenarios used to analyse Mooifontein Dam.

<table>
<tr><th rowspan="2">Scenario</th><th colspan="3">Liquefiable tailings</th><th colspan="3">Non-liquefiable tailings</th><th colspan="3">Foundation Soil</th><th>q_{c1}*</th><th rowspan="2">Slip surface</th><th rowspan="2">FS_T</th><th rowspan="2">FS_F</th></tr>
<tr><th>φ'</th><th>c'</th><th>γ_t</th><th>φ'</th><th>c'</th><th>γ_t</th><th>φ'</th><th>c'</th><th>γ_t</th><th>(MPa)</th></tr>
<tr><td>1a</td><td rowspan="14">0</td><td rowspan="2">101.6</td><td rowspan="14">19</td><td rowspan="10">--</td><td rowspan="10">--</td><td rowspan="10">--</td><td rowspan="2">34</td><td rowspan="2">7</td><td rowspan="14">18</td><td rowspan="14">2.7</td><td rowspan="4">Slip surface is as suggested by WM&B (2001).</td><td>0.81</td><td>0.23</td></tr>
<tr><td>1b</td><td>0.94</td><td>0.33</td></tr>
<tr><td>2a</td><td rowspan="2">88</td><td rowspan="4">37.5</td><td rowspan="4">15</td><td>0.93</td><td>0.26</td></tr>
<tr><td>2b</td><td>1.08</td><td>--</td></tr>
<tr><td>3a</td><td rowspan="2">132</td><td rowspan="2">Slip surface is as suggested by WM&B (2001) but then optimised.</td><td>0.66</td><td>0.19</td></tr>
<tr><td>3b</td><td>0.76</td><td>0.27</td></tr>
<tr><td>4a</td><td rowspan="2">144.8</td><td rowspan="2">34</td><td rowspan="2">7</td><td rowspan="8">Critical slip surface was searched.</td><td>0.68</td><td>0.19</td></tr>
<tr><td>4b</td><td>0.79</td><td>0.27</td></tr>
<tr><td>5a</td><td rowspan="2">140</td><td rowspan="6">37.5</td><td rowspan="6">15</td><td>0.66</td><td>0.19</td></tr>
<tr><td>5b</td><td>0.77</td><td>0.27</td></tr>
<tr><td>6a</td><td rowspan="2">147.5</td><td rowspan="2">37</td><td rowspan="4">0</td><td rowspan="4">19</td><td>0.66</td><td>0.18</td></tr>
<tr><td>6b</td><td>0.76</td><td>0.27</td></tr>
<tr><td>7a</td><td rowspan="2">147.2</td><td rowspan="2">43</td><td>0.66</td><td>0.19</td></tr>
<tr><td>7b</td><td>0.77</td><td>0.27</td></tr>
</table>

Table B.10 Scenarios used to analyse Dam A.

<table>
<tr><th rowspan="2">Scenario</th><th colspan="3">Liquefiable tailings</th><th colspan="3">Non-liquefiable tailings</th><th colspan="3">Dyke material</th><th>q_{c1}*</th><th rowspan="2">Slip surface</th><th rowspan="2">FS_T</th><th rowspan="2">FS_F</th></tr>
<tr><th>φ'</th><th>c'</th><th>γ_t</th><th>φ'</th><th>c'</th><th>γ_t</th><th>φ'</th><th>c'</th><th>γ_t</th><th>(MPa)</th></tr>
<tr><td>1</td><td rowspan="4">0</td><td>17.6</td><td rowspan="4">22.8</td><td>30</td><td rowspan="3">0</td><td rowspan="3">22.8</td><td rowspan="4">30</td><td rowspan="4">20</td><td rowspan="4">17.7</td><td rowspan="4">1.3</td><td>Slip surface is as suggested by Neto (2009).</td><td>1.83</td><td>--</td></tr>
<tr><td>2</td><td>1.5</td><td>25</td><td rowspan="3">Critical slip surface was searched.</td><td>22.4</td><td>--</td></tr>
<tr><td>3</td><td>20.7</td><td>30</td><td>1.66</td><td>--</td></tr>
<tr><td>4</td><td>45.9</td><td>--</td><td>--</td><td>--</td><td>1.13</td><td>--</td></tr>
</table>

Table B.11 Calculations to account for undrained loading in Dam A.

Points on initial water table (Figure 4.21)	**Point 1**	**Point 2**	**Point 3**	**Point 4**	**Point 5**	**Point 6**	**Point 7**
X-coordinate (m)	33.0	35.7	41.1	46.4	51.8	57.1	59.8
Y-coordinate (m)	1097.9	1097.3	1096.1	1094.9	1093.7	1092.5	1091.9
Horizontal distance from center of load (m)	13.4	10.7	5.4	0	5.4	10.7	13.4
Horizontal distance from center of load (*a*)[I]	1.25	1	0.5	0	0.5	1	1.25
Depth beneath beach surface (m)	1.1	1.7	2.9	4.1	5.3	6.5	7
Depth beneath beach surface (*a*)[I]	0.1	0.2	0.3	0.4	0.5	0.6	0.7
$\Delta\sigma_1/\Delta q_s$ – From Figure B.49	0.25	0.75	0.97	0.97	0.93	0.7	0.55
$\Delta\sigma_3/\Delta q_s$ – From Figure B.49	0	0.15	0.6	0.6	0.4	0.1	0.05
$\Delta\sigma_1$ due to Δq_s = 41.9 kN/m^2 (kPa)	10.5	31.4	40.6	40.6	39	29.3	23
$\Delta\sigma_3$ due to Δq_s = 41.9 kN/m^2 (kPa)	0	6.3	25.1	25.1	16.8	4.2	2.1
$\Delta\sigma_1 - \Delta\sigma_3$ due to Δq_s = 41.9 kN/m^2 (kPa)	10.5	25.1	15.5	15.5	22.2	25.1	20.9
Skempton parameter A	0.54						
Skempton parameter B	1						
Total pore water pressure build-up (kPa)	5.7	19.9	33.5	33.5	28.7	17.8	13.4
Total pore water pressure head build-up (m)	0.6	2	3.4	3.4	2.9	1.8	1.4
Final Y-coordinate of WT (m)	1098.5	1099.3	1099.5	1098.3	1096.6	1094.3	1093.3

Note I: Figure B.49 shows definition of *a*.

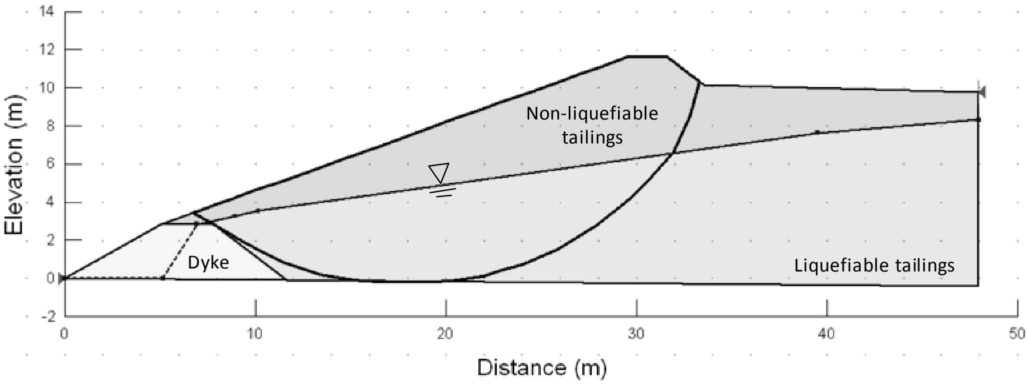

Figure B.1 Hokkaido Dam: Geometry of model used in scenario 1.

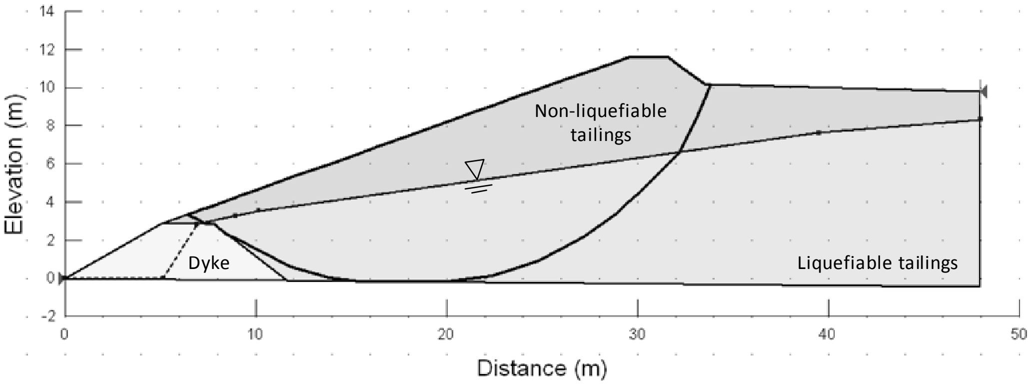

Figure B.2 Hokkaido Dam: Geometry of model used in scenario 2.

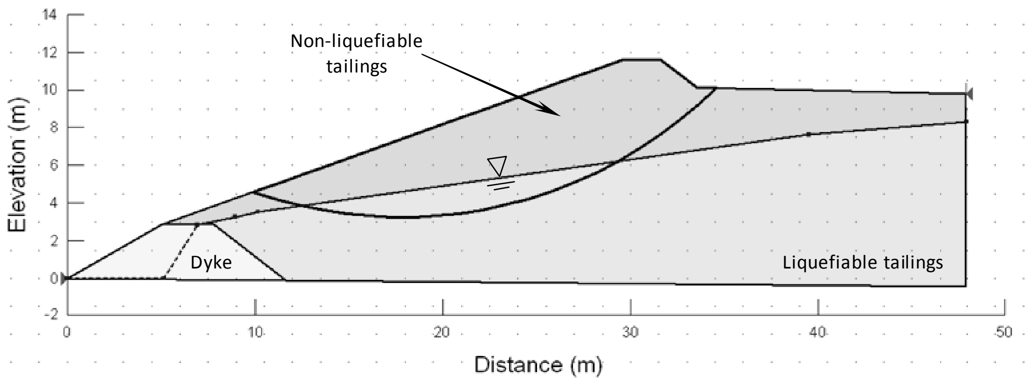

Figure B.3 Hokkaido Dam: Geometry of model used in scenario 3.

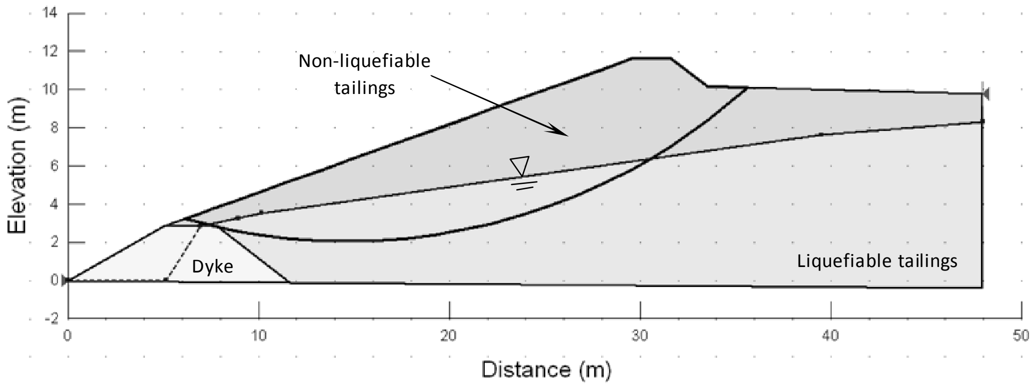

Figure B.4 Hokkaido Dam: Geometry of model used in scenario 4.

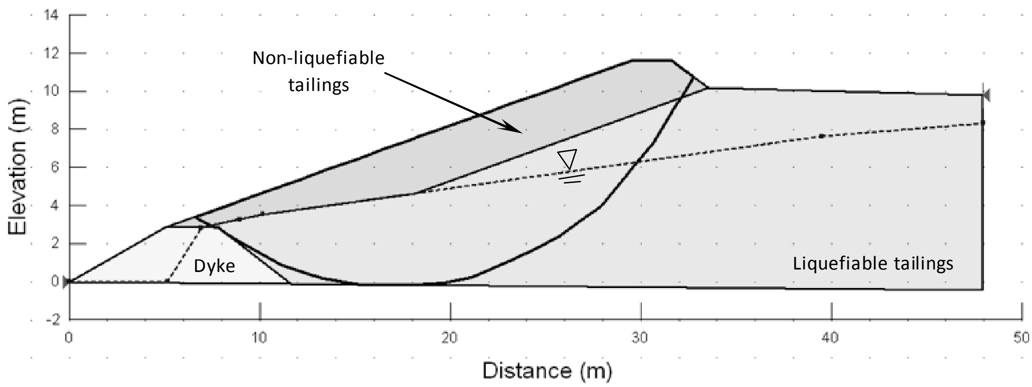

Figure B.5 Hokkaido Dam: Geometry of model used in scenario 5.

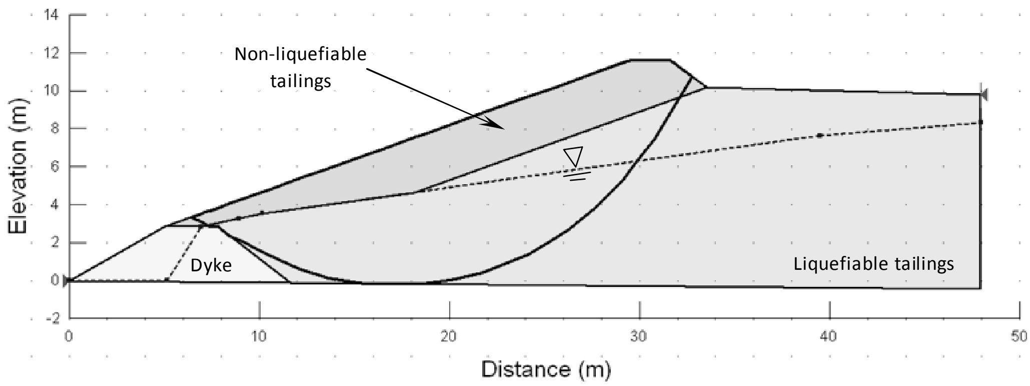

Figure B.6 Hokkaido Dam: Geometry of model used in scenario 6.

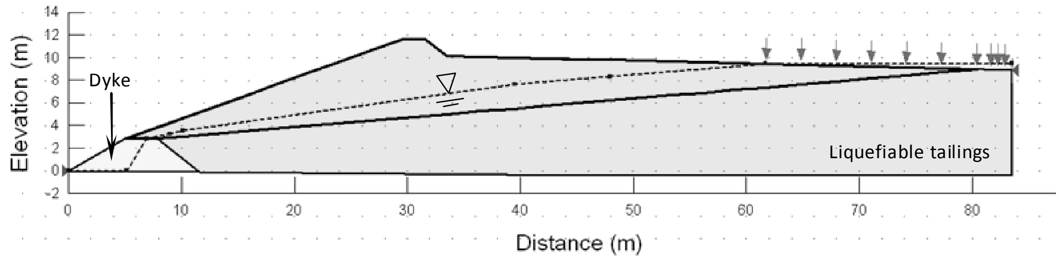

Figure B.7 Hokkaido Dam: Geometry of model used in scenario 7.

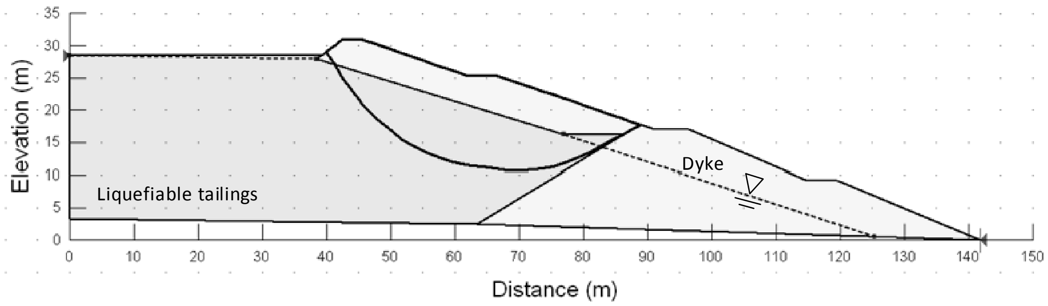

Figure B.8 Mochikoshi Dyke 1: Geometry of model used in scenario 1.

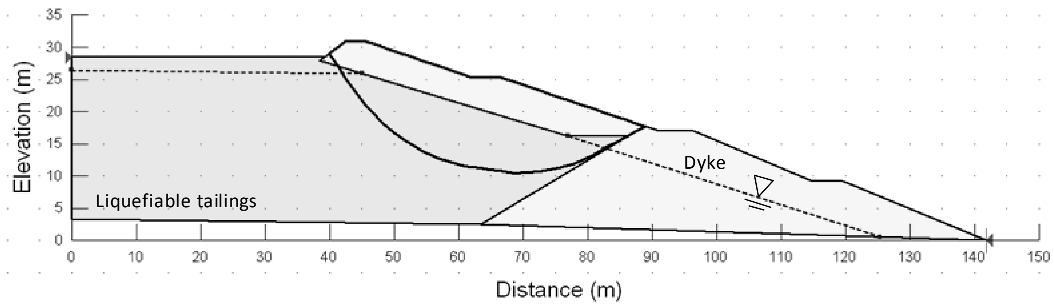

Figure B.9 Mochikoshi Dyke 1: Geometry of model used in scenario 2.

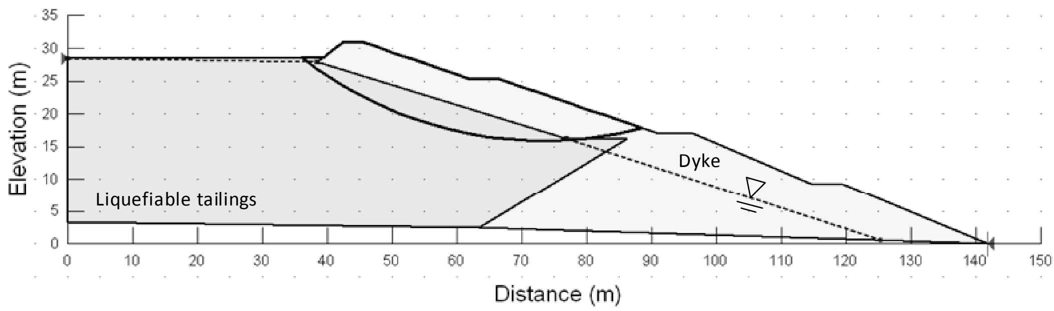

Figure B.10 Mochikoshi Dyke 1: Geometry of model used in scenario 3.

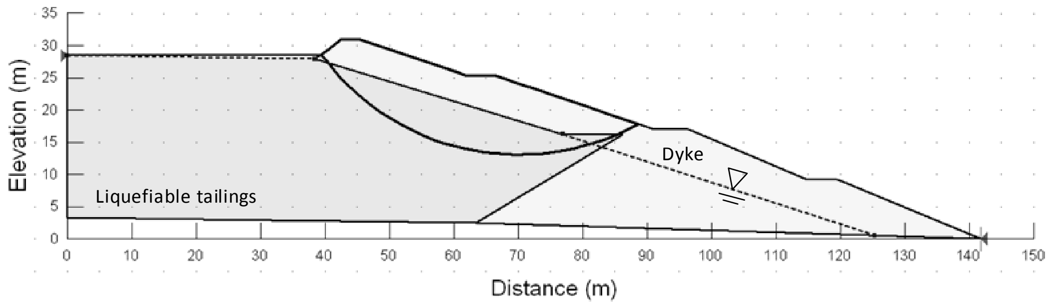

Figure B.11 Mochikoshi Dyke 1: Geometry of model used in scenario 4.

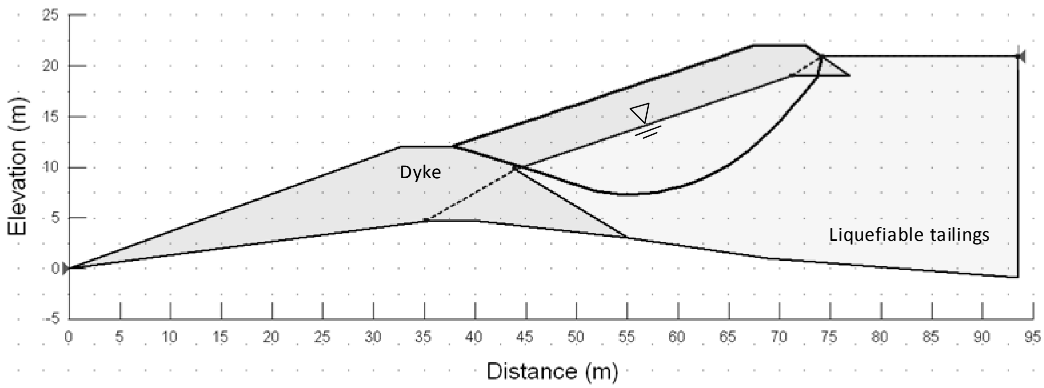

Figure B.12 Mochikoshi Dyke 2: Geometry of model used in scenarios 1a and 1b.

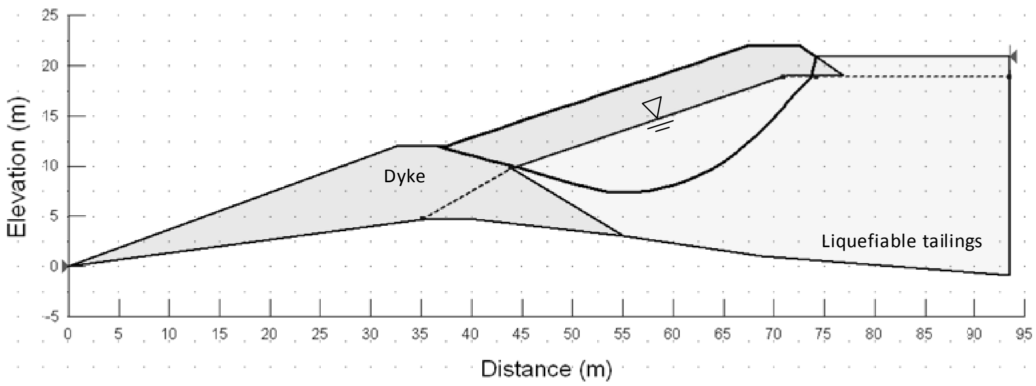

Figure B.13 Mochikoshi Dyke 2: Geometry of model used in scenarios 2a and 2b.

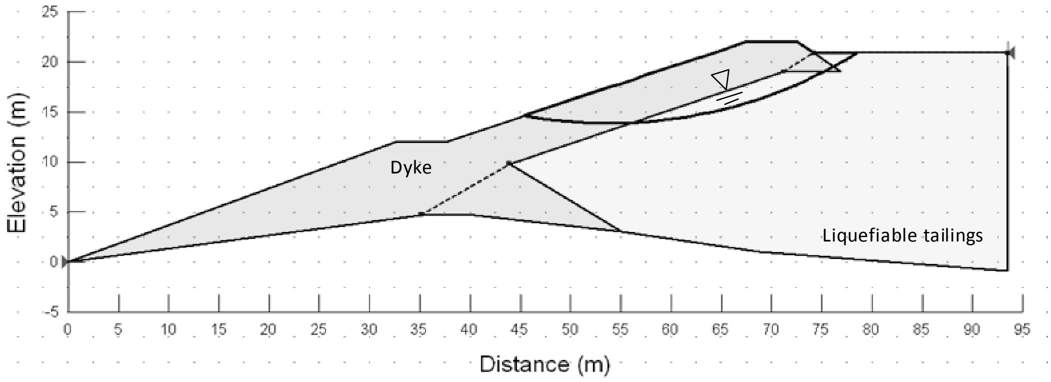

Figure B.14 Mochikoshi Dyke 2: Geometry of model used in scenarios 3a and 3b.

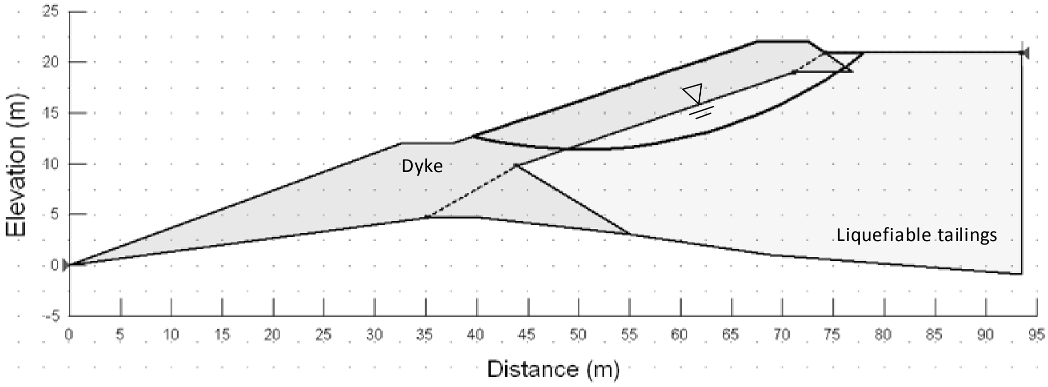

Figure B.15 Mochikoshi Dyke 2: Geometry of model used in scenarios 4a and 4b.

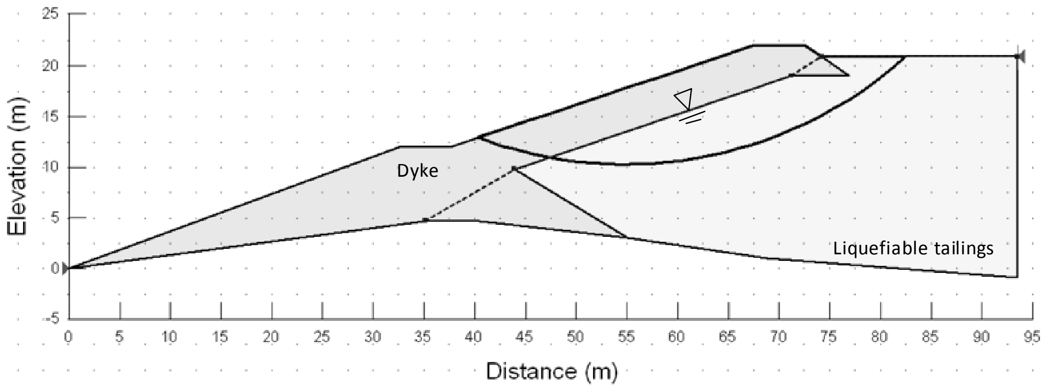

Figure B.16 Mochikoshi Dyke 2: Geometry of model used in scenarios 5a and 5b.

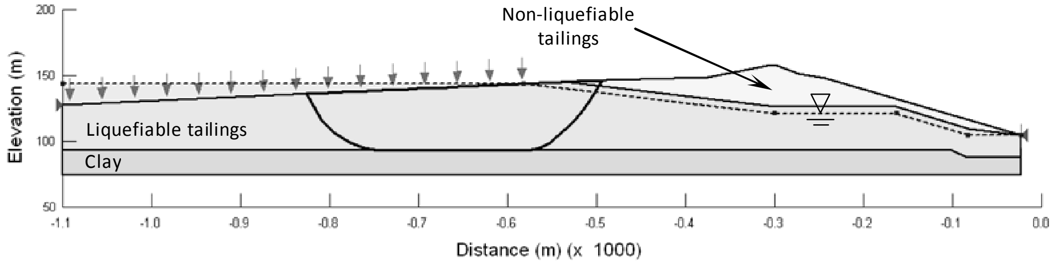

Figure B.17 Dashihe Beach: Geometry of model used in scenarios 1a and 1b.

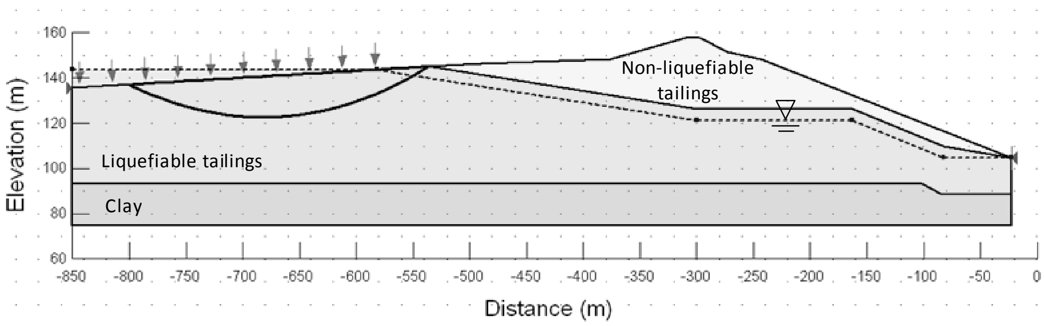

Figure B.18 Dashihe Beach: Geometry of model used in scenarios 2a and 2b.

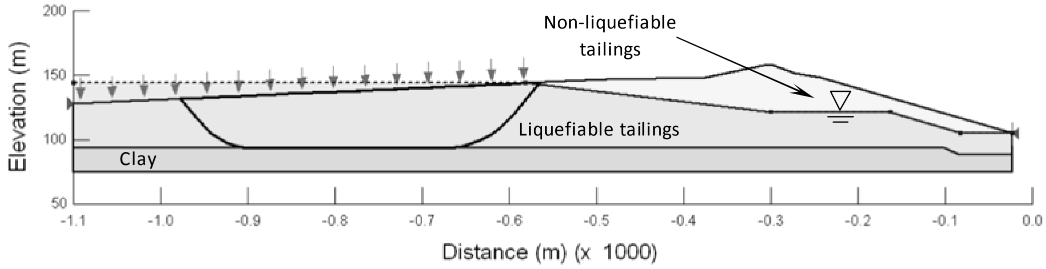

Figure B.19 Dashihe Beach: Geometry of model used in scenarios 3a and 3b.

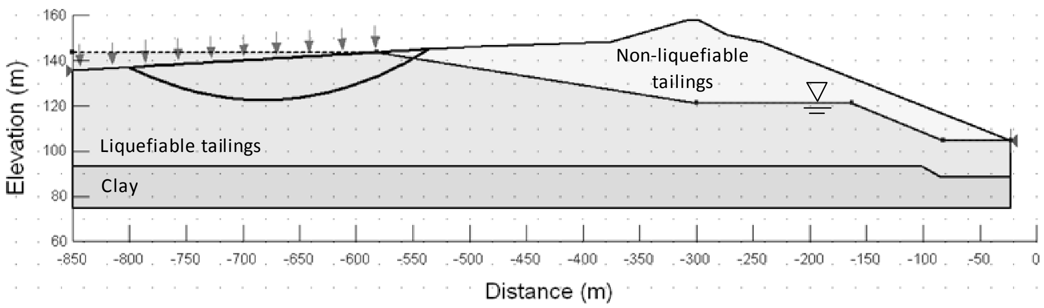

Figure B.20 Dashihe Beach: Geometry of model used in scenarios 4a and 4b.

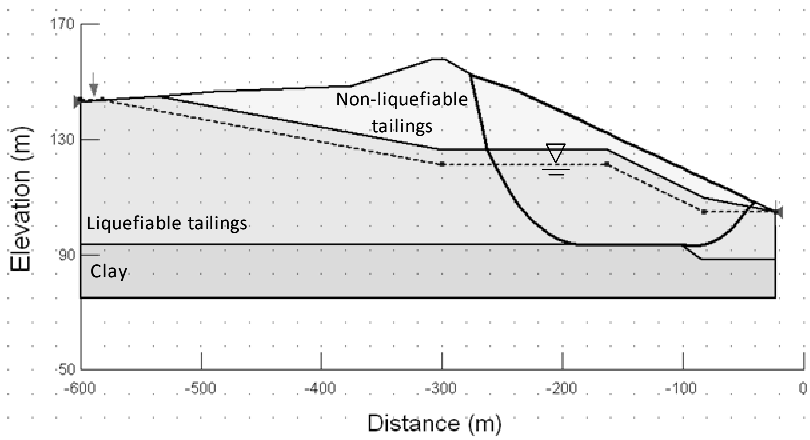

Figure B.21 Dashihe Outer Wall: Geometry of model used in scenario 1.

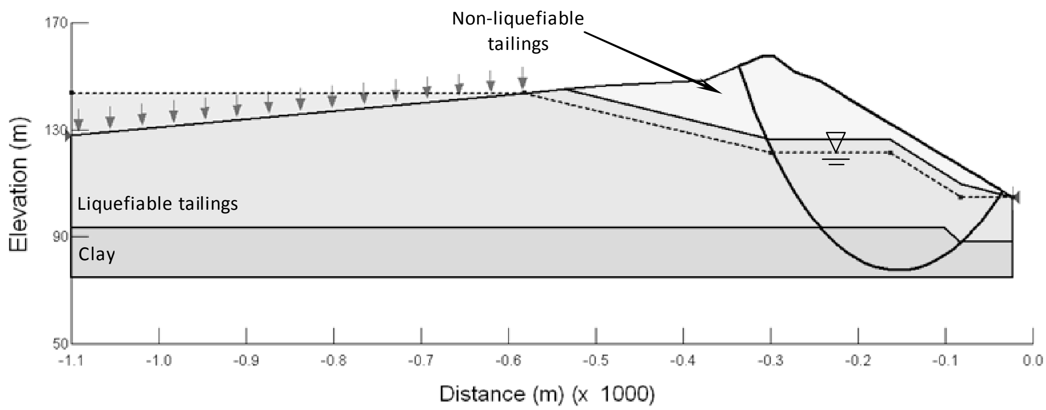

Figure B.22 Dashihe Outer Wall: Geometry of model used in scenario 2.

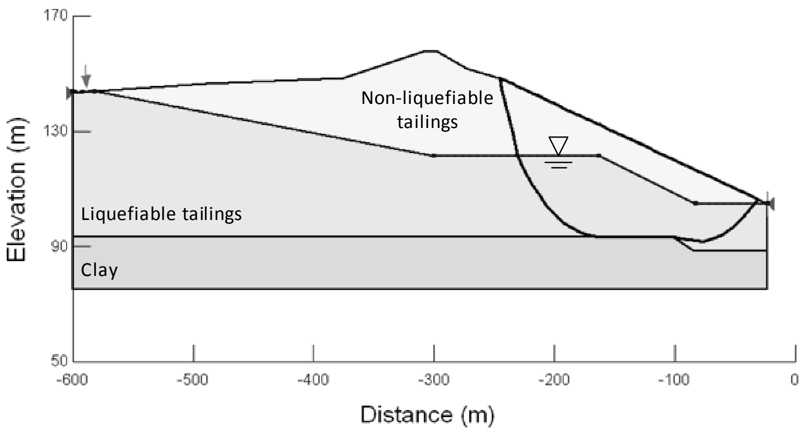

Figure B.23 Dashihe Outer Wall: Geometry of model used in scenario 3.

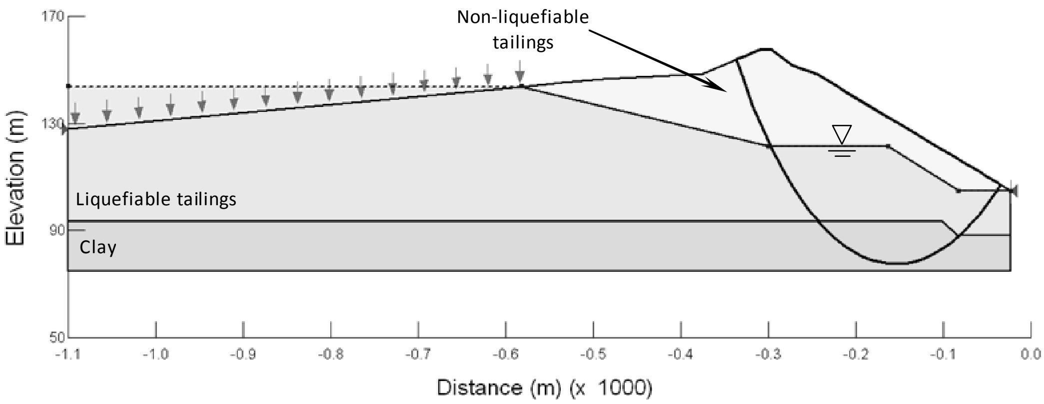

Figure B.24 Dashihe Outer Wall: Geometry of model used in scenario 4.

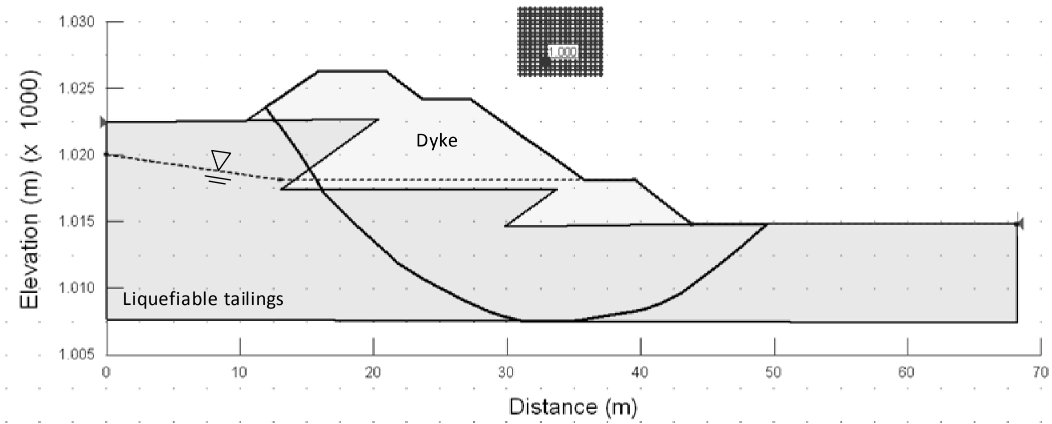

Figure B.25 Sullivan Dam: Geometry of model used in scenario 1.

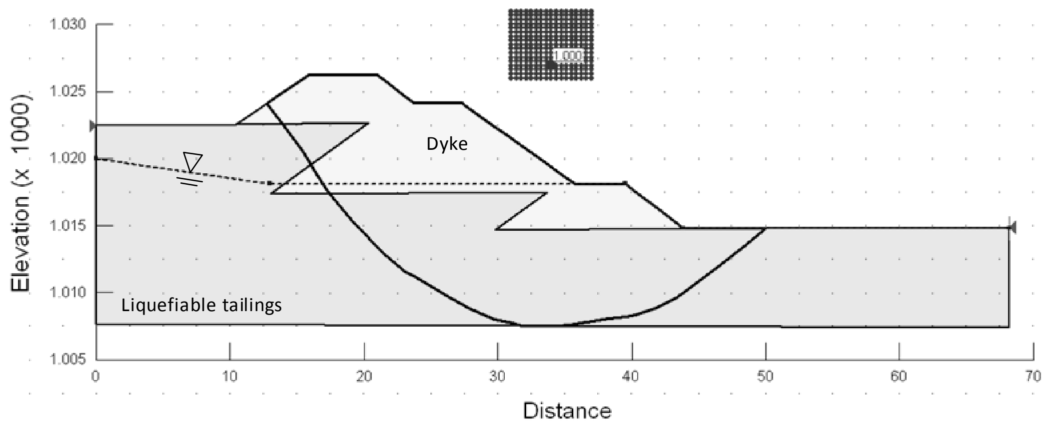

Figure B.26 Sullivan Dam: Geometry of model used in scenario 2.

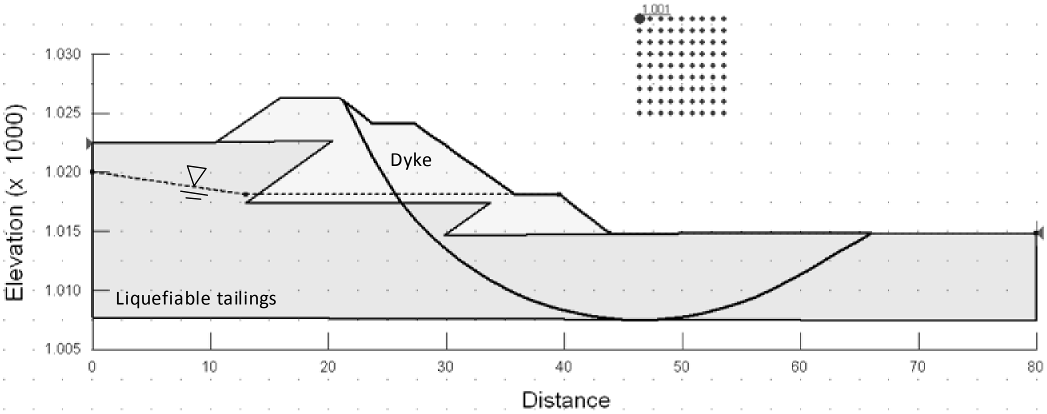

Figure B.27 Sullivan Dam: Geometry of model used in scenario 3.

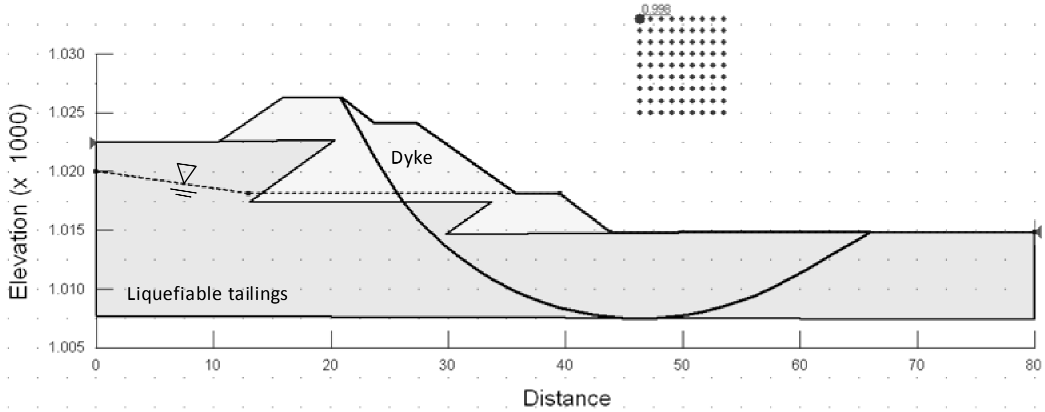

Figure B.28 Sullivan Dam: Geometry of model used in scenario 4.

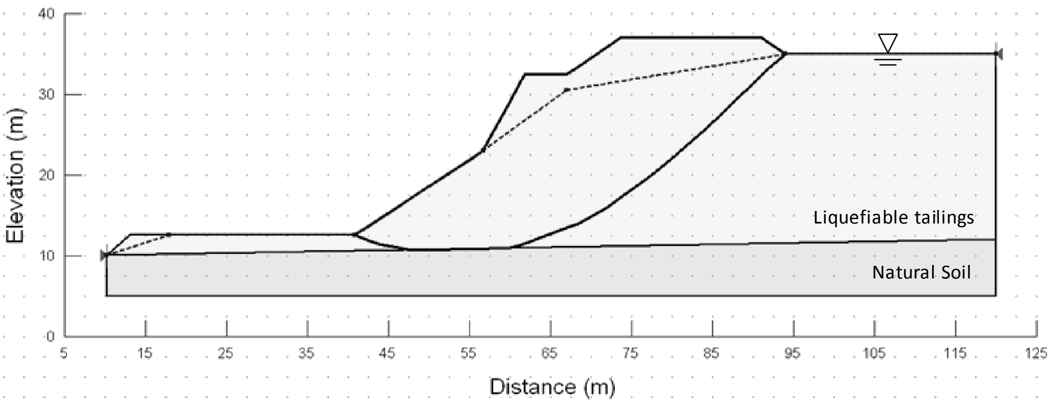

Figure B.29 Merriespruit Dam: Geometry of model used in scenario 1.

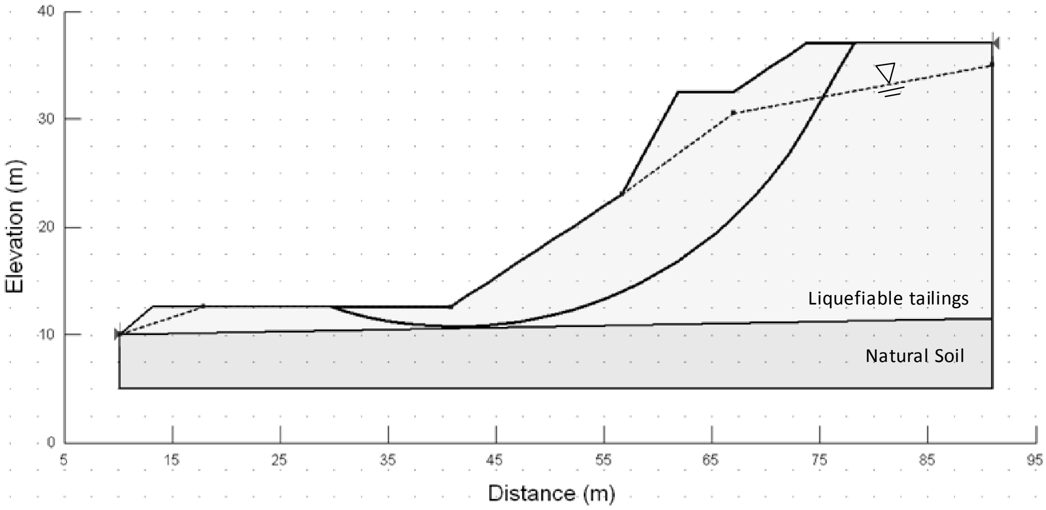

Figure B.30 Merriespruit Dam: Geometry of model used in scenario 2.

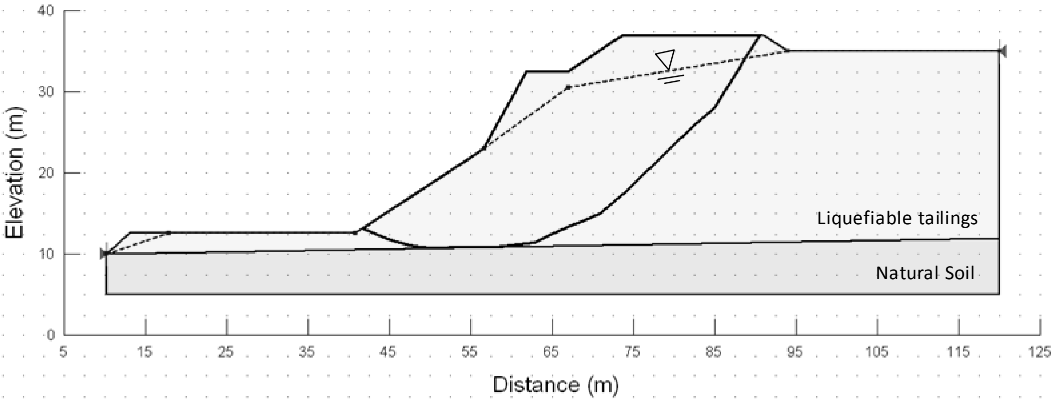

Figure B.31 Merriespruit Dam: Geometry of model used in scenario 3.

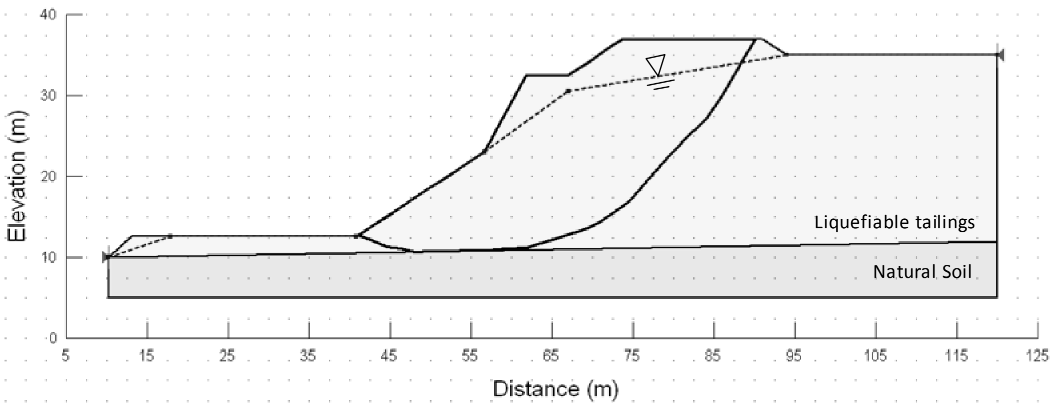

Figure B.32 Merriespruit Dam: Geometry of model used in scenario 4.

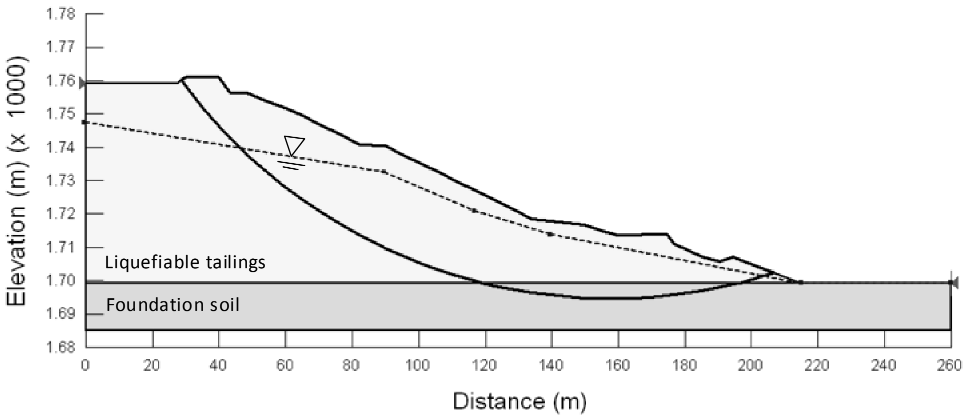

Figure B.33 GMTS Dam: Geometry of model used in scenarios 1a and 1b.

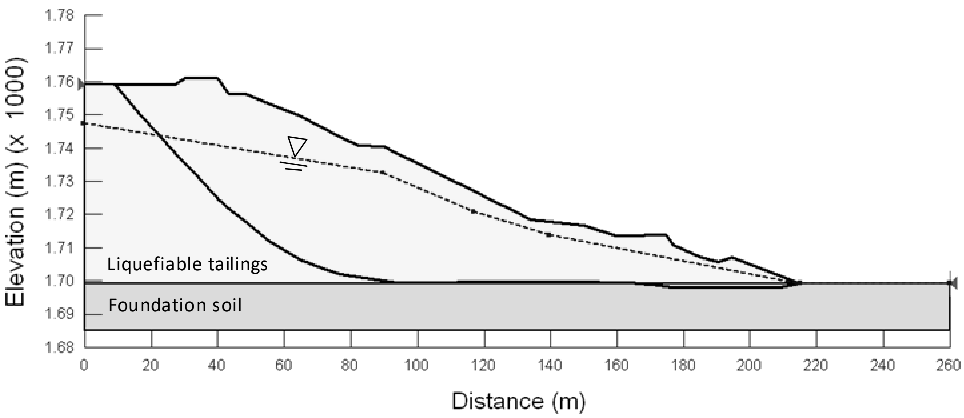

Figure B.34 GMTS Dam: Geometry of model used in scenarios 2a and 2b.

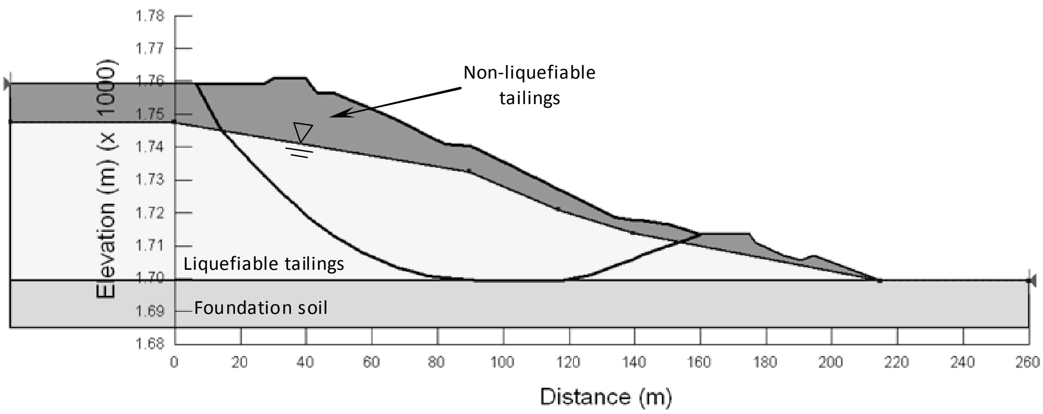

Figure B.35 GMTS Dam: Geometry of model used in scenarios 3a and 3b.

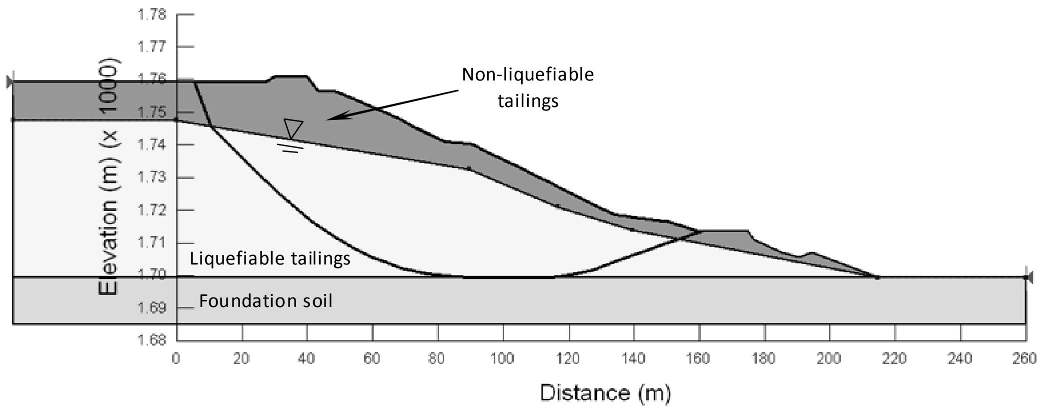

Figure B.36 GMTS Dam: Geometry of model used in scenarios 4a and 4b.

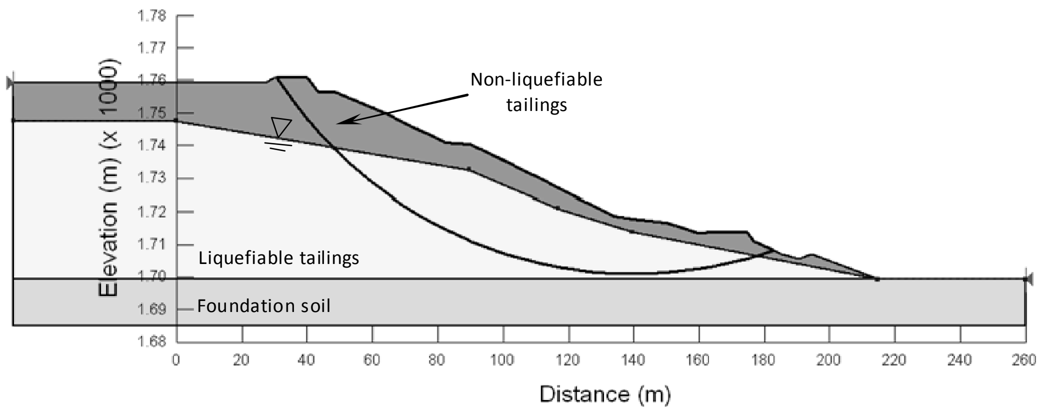

Figure B.37 GMTS Dam: Geometry of model used in scenarios 5a and 5b.

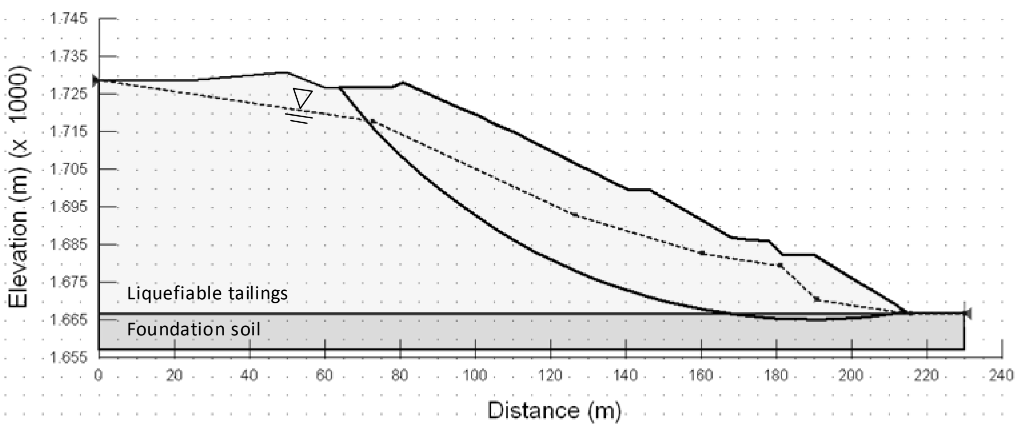

Figure B.38 Mooifontein Dam: Geometry of model used in scenarios 1a and 1b.

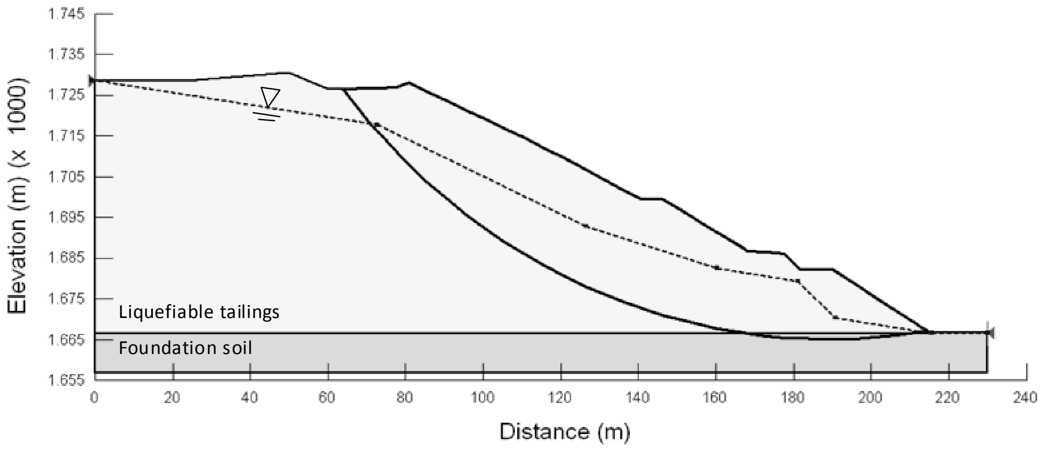

Figure B.39 Mooifontein Dam: Geometry of model used in scenarios 2a and 2b.

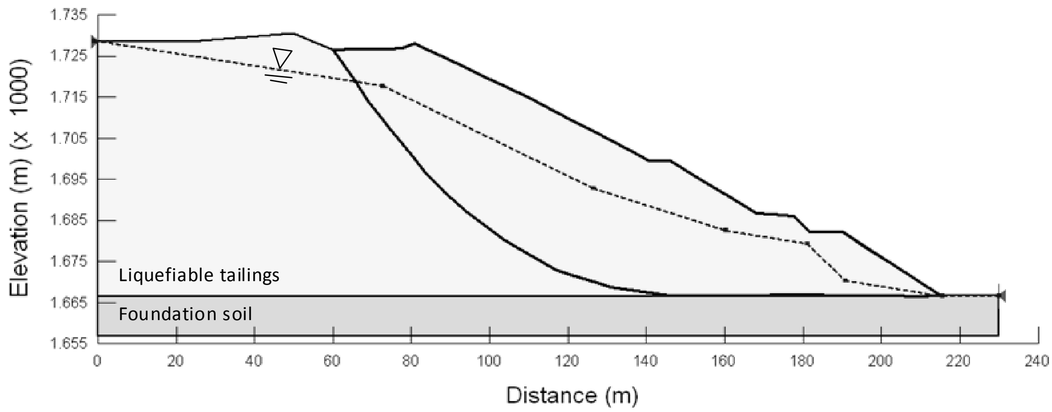

Figure B.40 Mooifontein Dam: Geometry of model used in scenarios 3a and 3b.

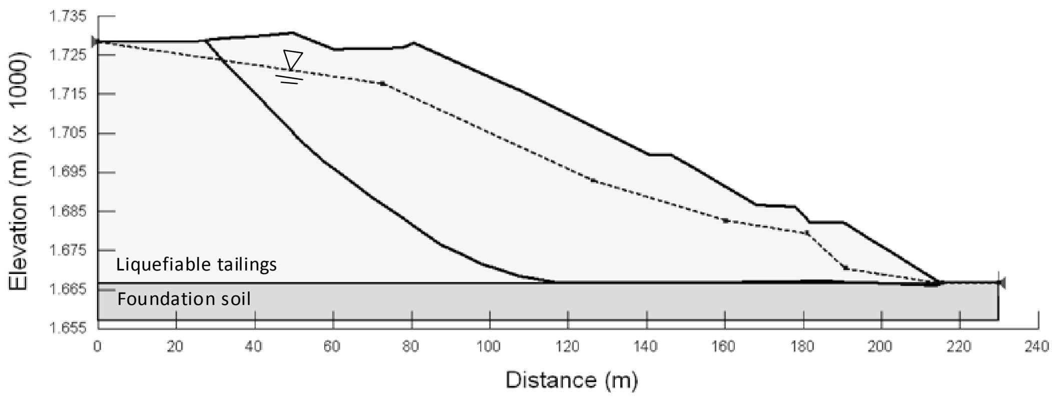

Figure B.41 Mooifontein Dam: Geometry of model used in scenarios 4a and 4b.

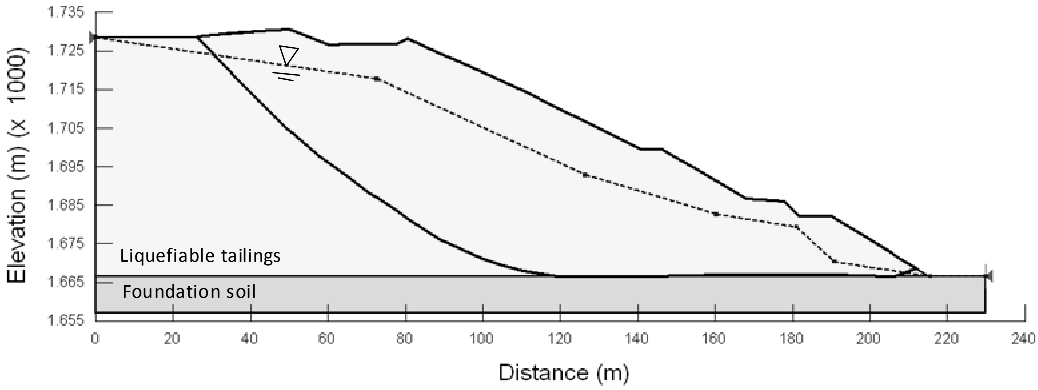

Figure B.42 Mooifontein Dam: Geometry of model used in scenarios 5a and 5b.

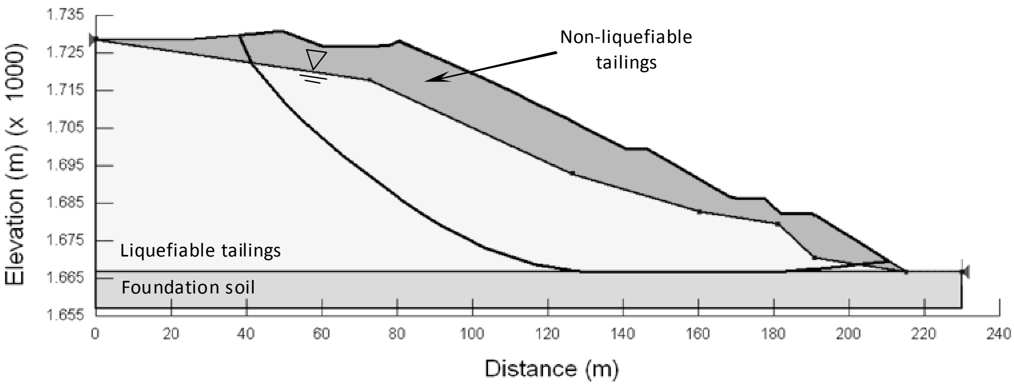

Figure B.43 Mooifontein Dam: Geometry of model used in scenarios 6a and 6b.

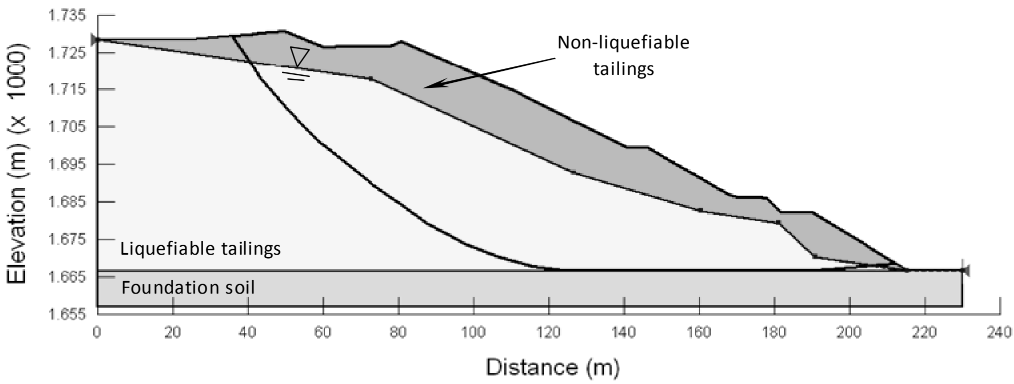

Figure B.44 Mooifontein Dam: Geometry of model used in scenarios 7a and 7b.

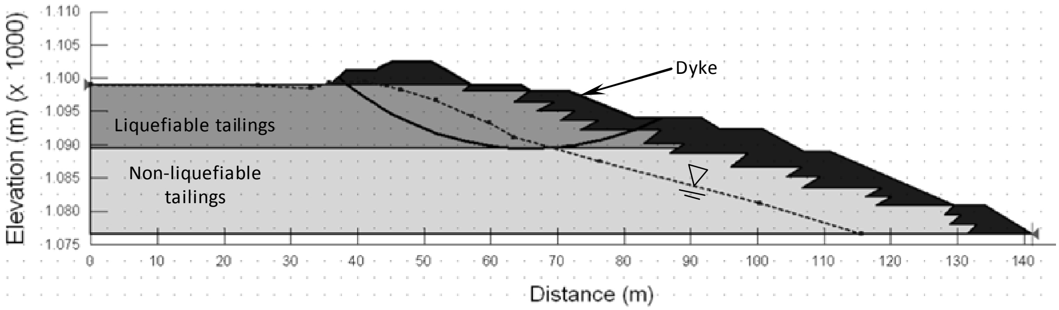

Figure B.45 Dam A: Geometry of model used in scenario 1.

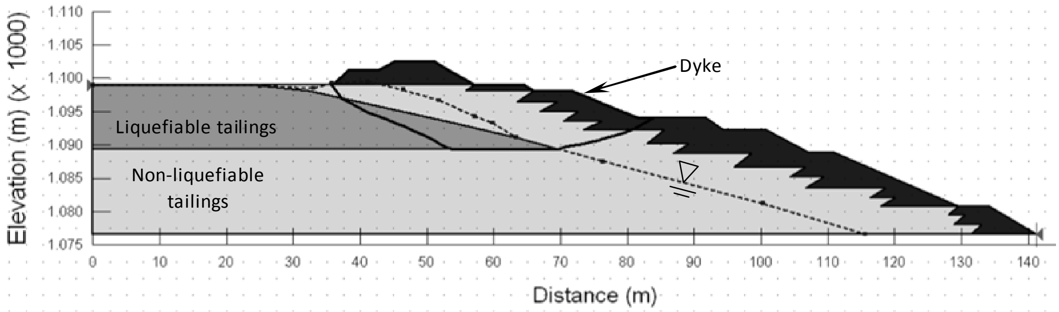

Figure B.46 Dam A: Geometry of model used in scenario 2.

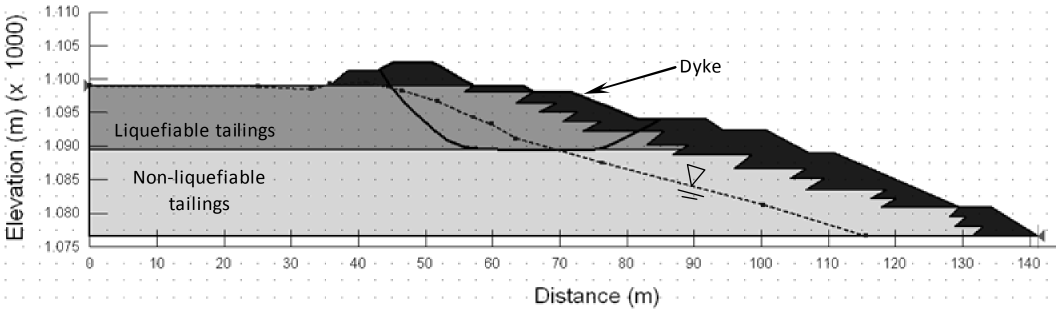

Figure B.47 Dam A: Geometry of model used in scenario 3.

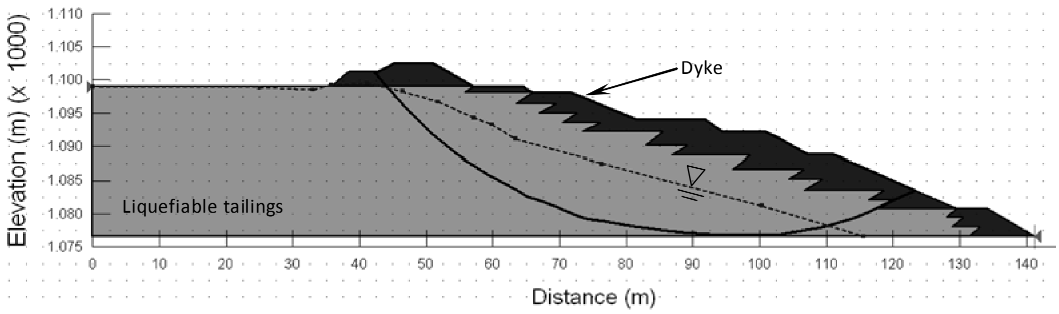

Figure B.48 Dam A: Geometry of model used in scenario 4.

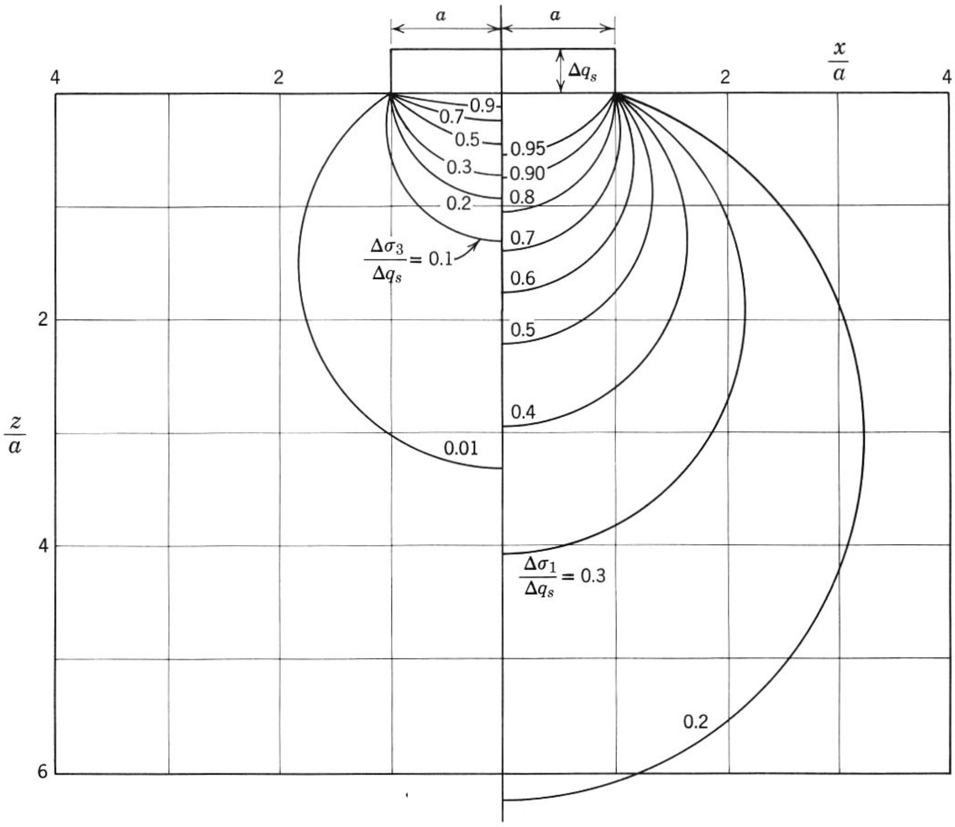

Figure B.49 Principal stresses under strip load (from Lambe and Whitman 1969).